

Multimodal Fusion of US and MR images for Twin to Twin Transfusion Syndrome fetal surgeries

Elena Monfort Sánchez



Universitat
Pompeu Fabra
Barcelona

Multimodal Fusion of US and MR images for Twin to Twin Transfusion Syndrome fetal surgeries

Elena Monfort Sánchez

BACHELOR THESIS UPF / 2019

THESIS SUPERVISOR(S)

Dr. Mario Ceresa

DEPARTMENT Departament de Tecnologies de la Informació i la Comunicació



Acknowledgments

I would like to express my gratitude to my supervisor (Mario Ceresa), to Miguel Angel González, Gemma Piella and Elisenda Eixarch, to Jordina, Enric and Dra. Brenda Valenzuela-Alcalaz for helping me to develop and evaluate some aspect from the project and, especially to Rocío Lopez for teaching me and supporting me during the hole project.

Abstract

Around 15% of all monochorionic pregnancies are affected by Twin to Twin Transfusion Syndrome. It involves chronic transfusion between donor twin to recipient twin, leading to an unbalanced growth of fetus due to unequal sharing of the placental blood volume. There are also other associated issues. The donor is at high risk of kidney problems related to not having enough blood flow. The extra blood flow that the recipient twin receives can put a strain on the heart leading to heart failure or developmental problems. Both twins can also have neurodevelopmental difficulties due to inadequate oxygen and nutrients as a result of blood transfusion. For untreated cases, the mortality of twins increases by around 90%. In treated cases, intrauterine surgery tries to stop blood transfusion by which some vascular connections are coagulated. Before the intervention takes place, surgeons have to plan it to ensure the correct localization of the placental vessel. Magnetic resonance (MR) is used to visualize the intrauterine structures, but the Ultrasound (US) technique is used to localize vessels because it gives accurate knowledge about vascularization.

The aim of this study is to develop a multimodal registration algorithm to combine MR and US information. Three different registration strategies were developed, so placentas for both modalities can be aligned automatically. To do so, free deformable and rigid transformations were used in combination with different input data, such as medical images, segmentation or image distance maps. Then, algorithms were tested on ten different patients from Hospital de la Maternitat, and results were visually and quantitatively assessed. For visual evaluation, MITK software is used to compare the overlapping between US and MR placentas, before and after registration. Algorithms are also verified by some quantitative metrics (Dice, Volume Similarity, Hausdorff distance, and umbilical cord insertion distances) that measure the overlapping and surface distances between registered placentas. Some limitations regarding provided images and data have been taken into account after registration.

Results obtained suggest that a high level of deformation is produced when free deformable strategies and segmentations were used. As a result, vessels morphology can be lost in some cases. When greater preservation of the shape is needed distance map images in combination with rigid strategies should be implemented. Beside intrinsic variations, developed strategies have shown considerable advances in the registration process, thus being potential tools for improving the pre-clinical planning of the TTTS intervention.

Keywords

Twin to Twin Transfusion Syndrome, Magnetic Resonance, Ultrasound, Multimodal Registration, SimpleElastix, MITK, Fetal Surgery, Distance Map.

Contents

List of Figures

List of Tables

1 INTRODUCTION

1.1. Twin to Twin Transfusion Syndrome.....	1
1.2. Image modalities for TTTS	2
1.3. Computational tools in TTTS	2
1.4. Contribution of this project.....	4

2 METHODS

2.1. Programming Environment.....	5
2.1.1. Registration libraries	5
2.1.2. Open Source Toolkits	5
2.2. Registration Method.....	6
2.2.1. Data analysis.....	9
2.2.1.A. Data set.....	9
2.2.1.B. Image pre-processing.....	9
2.2.2. Registration Strategy.....	12
2.2.3. Experiment definition	16
2.2.3.A. Identification of the optimal Registration Strategy	16
2.2.3.B. Synthetic experiment for placenta vascular reconstruction	19
2.3. Validation	20

3 RESULTS & DISCUSSION

3.1. Registration Strategies	23
3.2. Vascular Placenta Parametrization	25
3.3. Validation	25

4. CONCLUSION AND FUTURE WORK

BIBLIOGRAPHY

A. SUPPLEMENTARY INFORMATION

A.1. Image Modalities for TTTS37

A.2. B-spline parameter influence39

A.3. Vascular graphs.....40

A.4. Developed MITK Plugin.....48

A.5. Registration results from all patients.....49

List of Figures

Figure 1. Fetoscopy laser coagulation procedure for TTTS: (left) intrauterine environment, and (right) monochorionic placenta with coagulated vascular connections located on the surface (hemisphere) after laser ablation.	1
Figure 2. Modules of our TTTS preoperative planning and simulation framework. The first, second and third modules automatically segment and fuse the anatomical structures on MRI and 3D US. The fourth module provides features to plan the insertion point of the fetoscope. Finally, the fifth module mainly simulates the fetoscope movements, camera and trajectory.	3
Figure 3. Illustration of ITK, VTK and Qt toolkits relation with MITK. ITK and VTK are directly linked with MITK, but Qt is implemented through Qmitk.....	6
Figure 4. Illustration of the image Registration steps: moving initial pixels are mapped to the fixed image domain (initial interpolation) and they are modified during registration. Subsequent Interpolator, Metric and Optimizer valuations during registration produce the transformation.	7
Figure 5. Illustration of fixed and moving points correspondence after transformation.	9
Figure 6. General diagram of the Registration workflow implemented.	9
Figure 7. Input Data used for developing and testing registration algorithms. MR vessels are not provided, so they cannot be used for the registration process.....	10
Figure 8. Visual comparison of original MR and US image sizes: (left) MR segmented placenta and (right) US segmented placenta, before registration.	12
Figure 9. Illustration of the characteristics of the implemented Strategies.	13
Figure 10. (a) Illustration of a B-spline local deformation example with control points represented in white and connections between them in red: A. initial conformation; B. Control point localization; C. B-spline local deformation. (b) Different mesh resolutions, from large to small spacing between control points.	14

Figure 11. (a) Basis B-spline function of a cubic B-spline transformation; (b) Example of basis functions for three control points and a cubic B-spline; (c) Control point contribution on their basis function at $t = t'$; (d) $S(t)$ transformation in grey.	14
Figure 12. Multiresolution Registration schedule.	15
Figure 13. Pipeline of the Strategies: (left) Strategies 1 and 2 and (right) Strategy 3.	16
Figure 14. Graphs used for the experiment: (left) Graph 0 (Ground truth); (middle) Graph 1 (oriented network) and (right) Graph 2 (pruned network). Bigger images can be seen on SI-Figure 25.....	19
Figure 15. Results from Registration Strategy 1 (patient 1). US registered placenta is coloured in pink and MR placenta in white. (a)Original conformation of US and MR placentas; (b) Original conformation of shrinked US and MR placenta; (c) Strategy Results. Bigger images can be seen on SI-Table 5.....	23
Figure 16. Registration Strategies applied to US vessels. MR placenta, US placenta and US vessels are differentiated by colours (white, pink and red, respectively). Bigger images can be seen on SI-Table 6.....	24
Figure 17. Developed MITK Plugin for measuring the umbilical cord insertion distances. Bigger image can be seen on SI-Figure 28.....	26
Figure 18. Selecting point procedure from medical images: (left) Select points Button; (middle) Variable Point Selection where point coordinates are saved; (right) Representation of the selected points on the US registered image.....	27
Figure 19. Draw a line and point information procedure: (a)Draw a Line and Info buttons; (b) Line between selected points created to calculate the distance between them; (c) Points information where coordinates and distance can be seen on the screen.	27
Figure 20. US registered placenta in pink and MR placenta in white, and umbilical cord insertions can be shown: US insertion (green point) and MR insertion (yellow point). (left) US placenta registered using a B-spline transformation (Strategy 1c); (right) US placenta	

registered using an Affine transformation (Strategy 2c). Umbilical cord insertion from B-spline US registered placenta is far (70.089 pixels) from the MR insertion and this is due to the strong deformation applied on it.30

Figure 21. States of water protons from rest anatomical state to magnetic field application: (a) Intrinsic rotation of water protons in anatomical state; (b) Proton spine alignment due to magnetic field effect; (c) Water protons respond when radio-frequency pulse turn on and equilibrium is broken; (d) Realignment of water protons when radio-frequency pulse turn off.....37

Figure 22. Characteristics of US transducer used for imaging: (left) illustration of convex transducer, where piezoelectric elements can be seen on the front of the US transducer, and (right) reflected sound waves, echoes, that will be detected by piezoelectric elements.38

Figure 23. Bone structure, ribs, produce shadows that prevent from seeing the behind tissue on an US image (left). However, this technique is good on imaging blood flow when Doppler is used (right).....39

Figure 24. Results from Registration Strategy 1 with different maximum iteration values: **A:** 50 maximum iterations; **B:** 256 maximum iterations (default); **C:** 400 maximum iterations.39

Figure 25. Bigger images of vascular graphs used for placental vascular reconstruction. **A:** Ground truth; **B:** Oriented graph (Graph 1); **C:** Pruned graph (Graph 2).....41

Figure 26. Structural differences between ground truth in grey and deformed graphs: (left) Graph 1 in blue and ground truth comparison and (right) Graph 2 in orange and ground truth comparison. On Graph 2 some non-connected edges can be seen on red circles.42

Figure 27. Structural differences between Graph 1 (bleu) and Graph 2 (orange)43

Figure 28. Bigger image of the developed MITK Plugin for measuring the umbilical cord insertion distances. My Plugin is the workspace created for measuring distances between selected points. There are other functions (Smoothing Region Growing, Cone points and Cone) that were used for understanding how MTIK programming works.....48

List of Tables

Table 1. Sub-strategies 1 characteristics.....	18
Table 2. Sub-strategies 2 characteristics.	18
Table 3. Sub-strategies 3 characteristics.	18
Table 4. Validation results extracted from averaging results from each patient and strategy used. Validation results extracted from averaging results from each patient and strategy used. In blue, numerical values of the non-registered structures (original conformation) in red the numerical values for the highest GS values and in green the numerical values for the lowest GS values.....	28
Table 5. Placenta results from all patient after applying each Registration Strategy (transformed US placenta in pink and MR placenta in grey). There are 10 patients, and each one of them has the initial information about the conformation of US and MR placentas and results from each Strategy and Sub-strategy.....	49
Table 6. Vessels results from all patient after applying each Registration Strategy (transformed US placenta in pink, MR placenta in grey and vessels in red). There are 10 patients, and each one of them has the initial information about the conformation of US placenta and vessels and results from each Strategy and Sub-strategy.....	69
Table 7. Validation results from all patient. 40 percentiles for DC, VS, HD, ASD and UCID have been calculated for each Registration Strategy. Maximum distance is also used to transform HD into weighted Hausdorff Distance (wHD). In blue, numerical values of the non-registered structures, (original conformation), in red the higher values and in green the lowest values. ^[1] Some UCID could not be calculated because insertions were no appreciable due to image resolution, so real GS will be higher than GS calculated. Moreover, non-registered images have very high distances between US and MR placentas (outside possible region), so in cases where UCID or other metric were not possible to calculate, ^[2] GS can't have a numerical value.	89

1 INTRODUCTION

1.1. Twin to Twin Transfusion Syndrome

About 30% of monochorionic twin pregnancies can suffer from one (or more) complications, where TTTS is included [1]. Twin to Twin Transfusion Syndrome (TTTS) is characterized by the presence of vascular anastomoses and unequal sharing of the placental blood volume between monochorionic twins, resulting in unbalanced growth and severe nervous and cardiac damages also characterized by a poor urinary output of the donor causing little amniotic liquid. On the contrary, the recipient twin has blood overloaded (producing heart failure) and too amniotic liquid (Figure 1). TTTS is a progressive disease in which complications of the pregnancy can lead to the death of twins. In single fetal death cases, the survivor twin is more likely to manifest neurological and vascular problems due to the inefficient blood supply during the pregnancy and the complication of severe prematurity [2].

The diagnosis of monochorionic twins should be done as soon as multiple pregnancy is detected. It is commonly based on MR and US imaging, to see the structure of the placenta and also the blood flow of both twins. When intertwin vascular connections are diagnosed, intrauterine surgery is required by which some vascular connections are coagulated to stop blood flow transfusion between twins. Fetoscopy laser photocoagulation technique is the intervention that has shown better results [3(2),4].

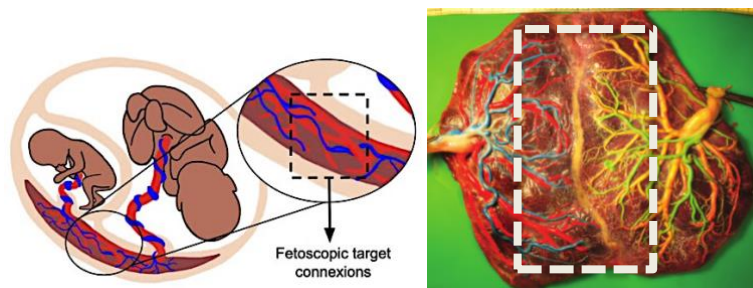


Figure 1. Fetoscopy laser coagulation procedure for TTTS: (left) intrauterine environment, and (right)¹ monochorionic placenta with coagulated vascular connections located on the surface (hemisphere) after laser ablation.

¹ Image from: Hillman, Sarah & Dhillon, R & Morris, R. Katie & Kilby, Mark. PFM.22 Fetoscopic laser coagulation for twin to twin transfusion syndrome – selective versus Solomon technique: a systematic review and meta-analysis. (2014) Archives of disease in childhood. Fetal and neonatal edition. 99. A89. doi: [10.1136/archdischild-2014-306576.254](https://doi.org/10.1136/archdischild-2014-306576.254).

When performing the intervention, surgeons have to localize the vessels that must be coagulated. For surgeons, one of the problems is to localize the optimal maternal abdominal entry perforation, because a re-entry can increase the mortality of twins [5]. This entry will depend on how the placenta and vessels are located and oriented. Therefore, planning ahead the surgery will allow surgeons to simulate different abdominal entries and evaluate the optimal solution. This will be essential for decreasing complications and for targeting and treating vessels in a more efficient and effective way.

1.2. Image modalities for TTTS

Information about some intrauterine structures such as placenta, uterus, vessels and umbilical cords is essential for planning the intervention. They are visualized by following two imaging techniques: Magnetic Resonance (MR) and Ultrasound (US). They don't produce radiation that can affect both, the mother and the fetus and they have different characteristics because the way of acquiring the images is based on different sources, such as magnetic fields for MR or sound waves for US ([SI-Image Modalities](#)). Because of that, MR and US provide different information. MR gives knowledge about how intrauterine structures are localized inside the maternal abdominal cavity. It produces images with good spatial resolution. In contrast, US provides in real time information about vessels localization, but with poor spatial resolution. However, from both imaging techniques three-dimensional (3D) volumes of the intrauterine structures can be extracted, and together with vessels information and computational techniques, they can be used for planning the TTTS intervention.

1.3. Computational tools in TTTS

Computer-assisted technology is a potential tool to overcome some intrauterine fetal surgery challenges. It has shown promising approaches to detecting ablation during TTTS interventions [6], as well as, improving the understanding of fetal anatomy complexity for fetal surgery planning [7]. Therefore, following the need of planning the TTTS intervention to localize and treat vessels successfully, Symbiosis group of UPF started a project based on computer-assisted technology to create the first TTTS planning application together with CELLEX and HSJD². The aim of it is to give experts a virtual platform where abdominal

² Refers to Hospital Sant Joan de Déu, Barcelona.

cavity and internal structures are simulated specifically for each patient, allowing to plan, simulate and make clinical decisions about the TTTS intervention before the surgery. It is a patient-specific preoperative planning that is divided into five different modules, which can be shown in Figure 2.

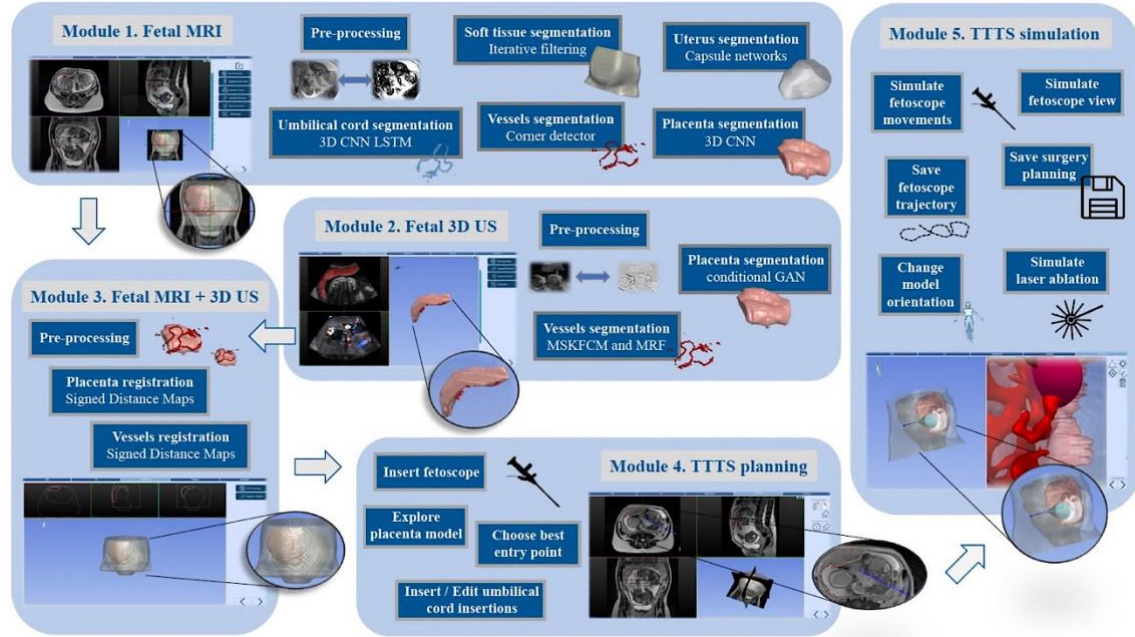


Figure 2. Modules of our TTTS preoperative planning and simulation framework³. The first, second and third modules automatically segment and fuse the anatomical structures on MRI and 3D US. The fourth module provides features to plan the insertion point of the fetoscope. Finally, the fifth module mainly simulates the fetoscope movements, camera and trajectory.

The Registration Module is based on the idea that it has been demonstrated that the fusion of US with other techniques, such as CT [8] or MR, has a variety of clinical applications because it allows to transfer and combine different information of the same target structures. Most of the registration methods, which use US and MR information, are focused on other structures, such as the liver or heart [9, 10]. Other registration methods are more related with fetal conditions [11, 12]. In that case, intrauterine vessels are the target structures in these procedures, hence proper identification of them in presurgical phases is extremely useful for medical planning. As it has been mentioned, US images gives a lot of information about the vascularization, so it would be a good approach to combine the structural information of the MR images with the blood flow information of the US images. However, any Registration method previously developed is focused specifically on combining US and MR intrauterine

³ Image provided by the Symbiosis group from Universitat Pompeu Fabra, together with CELEX and HSJD.

information, such as placentas or vessels. One of the reasons is that the 3D/3D registration of fetal MRI and 3D US is challenging. These two modalities have non-correlated intensities, but neither their resolution and field-of-view. Consequently, a new Registration method has to be developed, so TITS-GPS app can truly contribute to plan the TITS intervention.

1.4. Contribution of this project

The objective of this project is to investigate novel registration techniques for the pre-operative fusion of multimodal images in fetal surgeries to develop an MR-US Registration Method. Proper registration of US images to MRI is of paramount importance in fetal surgeries because the treatment is focused on targeting the vascular connections, so adding the US information to the 3D MR model will increase the success of the planning and thus, the intervention.

In addition to developing a new Multimodal registration method, a MITK based plugin will be also created to visualize 3D intrauterine structures (MR and US placentas and vessels) and to calculate distances between both umbilical cord insertions to evaluate the performance of the developed algorithm, before and after registration.

2 METHODS

4.1. Programming Environment

2.1.1. Registration libraries

In order to create a registration algorithm, SimpleElastix [13] has been used. It is an extension of SimpleITK and thus can be scripted in Python. SimpleElastix allows the user to compute registration (or compare different registration methods) quickly in an easy way, without losing robustness. Another library also included in SimpleITK, the SimpleTransformix, was also used. It allows to apply the transform parameters done in previous SimpleElastix registration to a higher set of images in a subsequence process.

2.1.2. Open Source Toolkits

A MITK workspace is developed for further validation processes. It is based on the framework provided by some toolkits for medical image processing, such as Qt, Insight Toolkit (ITK), Visualization Toolkit (VTK) and Medical Imaging Interaction Toolkit (MITK).

Qt [14] is a free open-source widget toolkit used for developing graphical user interfaces (GUIs) and multi-platform applications compatible with various destock platforms, such as Linus, Windows or macOS. Using this toolkit we can create buttons, scroll bars or containers for other widgets (taps) with which users will interact with through direct manipulation. They are graphical elements used to build the interface of a program. They can be enable or disable, so when widgets are linked with the application software the enable components have the capacity to respond to events, such as mouse actions, making the application more interactive for the user.

ITK [15] provides us powerful algorithms for registering and segmenting multidimensional data. In other words, it was designed to collect independent tools, the Image Filters, which many of them can be used to solve similar problems in different ways. There is a certain usable redundancy on their filters when offering different implementation for solving the same problem. However, it is an adaptable and versatile feature of ITK, because it allows us to use a large collection of combinable image processing filters.

The other toolkit that is also going to be used is VTK [16]. VTK is an open-source toolkit for data processing, visualization and analysis. It has many sophisticated visualization algorithms with a huge range of applications. In this project, it has been used to visualize the results obtained from the registration process.

However, none of the toolkits explained before offer the features to develop a high-level interactive, clinical useful medical imaging software, so a new toolkit is used, the Medical Imaging Interaction Toolkit (MITK) [17]. It is a free open-source software that combines the ITK algorithms with the VTK visualizations and an extension of these two toolkits with features outside the scope of both in an application framework. MITK allows us to create and evaluate new developed interactive applications for medical image analysis, such as image-guided therapy planning and/or it can be used within existing softwares.

The principles of MITK is to re-use as much as possible of already existing the most successful designs and implementations of ITK and VTK. For that reason, MITK is also an object-oriented, cross-platform library implemented in C++, where most of the MITK classes are derived from the ITK and VTK classes are used but not derived from. The Qt is also linked with MITK, which is independent of the GUI library because, currently, Qt implements it using Qmitk (Figure 3).

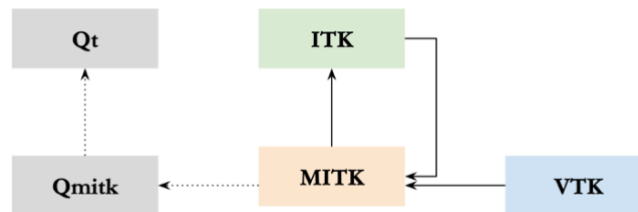


Figure 3. Illustration⁴ of ITK, VTK and Qt toolkits relation with MITK. ITK and VTK are directly linked with MITK, but Qt is implemented through Qmitk.

2.2. Registration Method

Image registration is an optimization process aiming at finding the geometric transform T that will allow to align the moving image (m) to the reference image (f) by minimizing the distance (S) between the transformed moving ($m \circ T$) image and the fixed image. Because it

⁴ Version of an Illustration from: Wolf, Ivo & Nolden, Marco & Boettger, Thomas & Wegner, Ingmar & Schoebinger, Max & Hastenteufel, Mark & Heimann, Tobias & Meinzer, Hans-Peter & Vetter, Marcus. (2005). The MITK Approach. <https://www.researchgate.net/publication/28358596>

is an iterative process, the final transformation T is extracted from the ensemble of transformations (E) created during the process.

$$\hat{T} = \min_{T \in E} S(f, m \circ T) \quad (\text{Equation 1})$$

In this case, the fixed and the moving images are MR and US images respectively. On the iterative process of finding the geometrical transformation (Figure 4), there are many options to create an efficient and effective registration method to align medical images. Each method is based on the same components, which together define the registration instance. These main components are: Transformation, Similarity Metric, Optimizer and Interpolator.

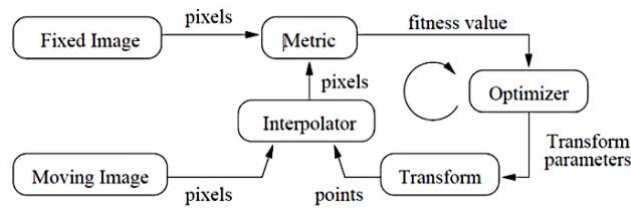


Figure 4. Illustration⁵ of the image Registration steps: moving initial pixels are mapped to the fixed image domain (initial interpolation) and they are modified during registration. Subsequent Interpolator, Metric and Optimizer valuations during registration produce the transformation.

This registration method can be done using different criteria, such as *landmark-based*, *segmentation-based* or *intensity-based* registration, which follow the same Registration framework but with slight differences.

Landmark-based registration uses the landmarks selected by the user to align the images in a faster computation method. Because of the landmarks selection is done by a human criterion the method is not as consistent and reproducible as the other two, and so, final registration precision is undermining.

Segmentation-based registration is based on aligning segmented structures of both images, but, even though it is also a fast method, the final registration performance depends on the accuracy of the pre-processing step.

One slower, but automatic criteria is the *intensity-based* segmentation method. It uses the image intensity to align both images without modifying the data. The alignment is based on

⁵ Image from ITK software guide book Chapter 3 - Registration.
<https://itk.org/ITKSoftwareGuide/html/Book2/ITKSoftwareGuide-Book2ch3.html>

minimizing the intensity difference between points corresponding of both images. For that reason, it is slower than the previous criteria, especially for 3D images and also when images have been acquired with different imaging modalities (as in our case).

Even though there are different criteria for registering images, components inside the framework can also vary. One component to take into account when performing a registration method is the type of spatial *transformation*, which defines the mapping between the images. Some of them are *rigid*, *affine* or *deformable*. When the transformation of some image points to the other image map only implies rotation and translation, we will be working with a *rigid* transformation. *Affine* transformation is applied when the alignment relies also on skewing and scaling. And if we have a more complex registration, the *deformable* transformation allows us to map points from one image to the other in a freer way.

The aim of the registration is to map each voxel of the moving image to its correspondence voxel in the fixed image, therefore the parameters produced by the spatial transformation will try to maximize the similarity metric between both images. There are lots of *similarity metrics* to measure the similarity between the images, such as mutual information, correlation ratio or least squares. Each one of them has different features that will influence the transformation, as well as the computational cost of our registration method. And thus, the result of the algorithm.

As it has been mentioned before, one of the goals of this project is to obtain an efficient and effective registration method. This method has to have an optimizing way of obtaining a transformation map to align the coordinate system of one image (the moving image) into the coordinate system of the other image (the fixed one). The iterative process for obtaining the perfect match, and therefore a higher similarity value, will be based on an *optimizer*. This optimizer will search in each interaction for the best transform parameters., so that, the desired alignment is achieved when the moving image is interpolated with those parameters.

When transformation is applied to the moving image, their pixels are moved to the moving space to the space where fixed image is. And when this happens, some points will most likely not correspond to a point of the fixed image, meaning that they could be between two points of the fixed image (Figure 5). The intensity at the coincidence point is computed by

interpolation. The *interpolation* is a step needed for image generation and processing, such as compression and resampling, and can impact the results. Some common interpolation algorithms are the nearest neighbour, linear interpolation, quadratic, cubic or Gaussian interpolation [18, 19].

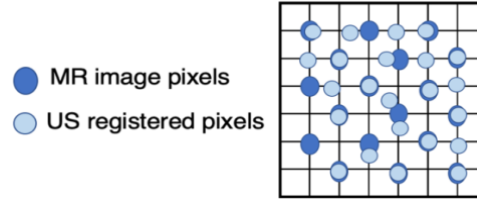


Figure 5. Illustration of fixed and moving points correspondence after transformation.

Using these general features and the information from 10 different patients, a new registration method to align fetal images (MRI and US) is proposed in this project. Then, it could be incorporated in the TTTS-GPS application (Figure 2) to improve planning, simulation and clinical decisions.

2.2.1. Data analysis

2.2.1.A. Data set

In that project, information from 10 different patients, from Hospital de la Maternitat (in Barcelona), have been used to compare the algorithms and to calculate their robustness and accuracy. As it has been explained before, US provides precise information about vessels, so combining the structural information of the MR images with the blood flow information of the US images will increase the success of the interventional planning. From each patient, US, MR and Doppler images from the abdominal cavity are used to extract intrauterine structures, such as placenta and vessels (Figure 7).

2.2.1.B. Image pre-processing



Figure 6. General diagram of the Registration workflow implemented.

The aim of the project is to investigate novel registration techniques and develop an improved method using the libraries and the data mentioned before. The implemented workflow (Figure 6) proposes an Image pre-processing before registration takes place. It is done to extract structures, such as placentas and vessels, that will be used as input data (Figure 7) on the Registration algorithms. Pre-processed Original images and the US vascular segmentations (vessel masks) have been provided by the hospital and the research group, respectively. Something to take into account is that US images do not correspond to the overall placenta of the patient. They have captured only a portion of it during the image acquisition, therefore the information of the overall placentas is not provided. In the same way, MR vessels masks are also not given.

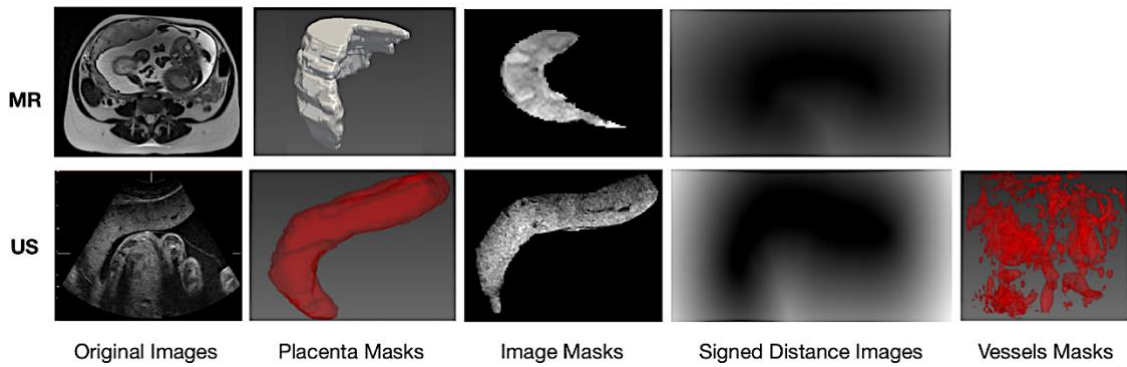


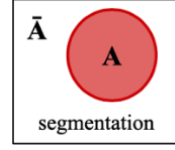
Figure 7. Input Data used for developing and testing registration algorithms. MR vessels are not provided, so they cannot be used for the registration process.

The Placenta masks have been acquired using the MITK segmentation tool, which allows to manually segment the structure of the placentas (US and MR). Image Masking function also belongs to MITK segmentation utilities and it is used to create Image masks. Using this tool the grey value image (Original Image) can be masked with an existing segmentation. The result is an image containing only the pixels that are cover by the respective mask, so we have the information about the intensity of each pixel and the shape of the placenta. Regarding the vessel segmentation, only the vascularization of the US images was provided.

The signed distance images (Figure 7) have been created following the idea of the Distance maps. They are commonly used in image processing for several purposes [20, 21], such as sampling or skeletonizing structures. They are an alternative to pure binary shrinking in binary images (such as masks) because distance maps are based on gradients that work better with gradient-based optimizers. These type of images contain two sets of pixels:

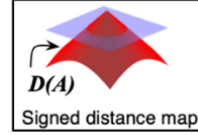
$$A = \text{pixels with value 1 (object)}$$

$$\bar{A} = \text{pixels with value 0 (background)}$$



The distance map of the object, $D(A)$, encompass values that indicates, for each pixel (p) in A , the shortest distance to the nearest background pixel (q) in \bar{A} . This means that there is a corresponding pixel in $D(A)$ where:

$$D(A) = \min\{ \text{dist}(p, q), q \in \bar{A} \}$$



(Equation 2)

The computational procedure ($D: A \rightarrow D(A)$) is called distance map. In this case, the distance map metric used is the Euclidean distance transformation. It is defined as the length of the line \overline{PQ} that connects this two points (p, q) in the image (Equation 3).

$$\text{dist}(p, q) = \sqrt{\sum_{i=1}^n (q_i - p_i)^2} \quad (\text{Equation 3})$$

To compute approximations of the Euclidean distance transformation, the Danielsson mapping [22] is used. It computes the signed distance field for the placenta output masks in MRI and 3D US. Because it creates the Danielsson distance field, these types of images are from now, called **ddf**. The transformations were done using a code from the research group and, as well as the Shrinking algorithm, it is run from the same bash file (Do_Reg.sh). When it is run, the filter returns three files: 1) a signed distance map with the approximation to the Euclidean distance, 2) a Voronoi partition, and 3) a vector map relating the current voxel with the closest point of the closest object to this voxel.

The aim of the project is to develop a registration method to align vessels from both modalities. However, MR vascular information is not available for this project (Figure 7), so they cannot be used for the registration process.

A part from manipulating the data set from each patient to obtain the input data for the registration algorithms, another image processing step (Shrinking) has been carried out only in the obtained US input images from Figure 7. As we can see on Figure 8, the size of the US images is larger than the MR images.

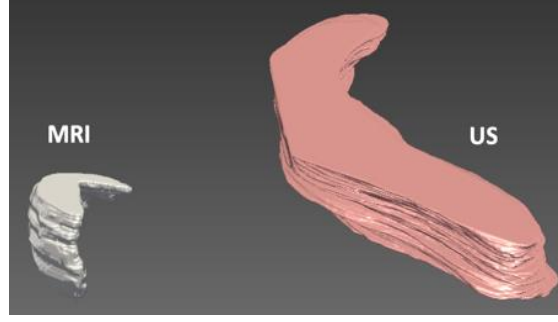


Figure 8. Visual comparison of original MR and US image sizes: (left) MR segmented placenta and (right) US segmented placenta, before registration.

In order to speed up the registration process, the US images (US image, US segmented placenta and vessels) are resampled by a factor f_{shrink} to be closer to the MR image dimension. The final value s_{output} for each dimension is given by Equation 4. To do this pre-processing, an algorithm called (ShrinkImage.cxx) is used.

$$s_{output} = \max(\text{floor}(\frac{s_{input}}{f_{shrink}}, 1) \quad (\text{Equation 4})$$

This algorithm applies the resampling procedure explained before. 3D US images, US segmented structures and the Shrinking parameters (f_{shrink} for each dimension) are the inputs of this algorithm. It returns the input images and segmented structures rescaled in each dimension by the f_{shrink} factor. Because the inputs are subsampled, the spacing between voxels has to be also changed to keep the correlation between them. Therefore, the spacing of the outputs is set to 0.75 in each dimension.

Because the developed registration method may be implemented in an application, the process has to be as automatic as possible. However, due to the fact that each patient image set is different from the rest, the resampling is done specifically for the 10 cases.

2.2.2. Registration Strategy

After pre-processing patient images, different types of registration strategies have been carried out (Figure 6). They can be classified depending on the type of resolution level, transformation and input images used (Figure 9).

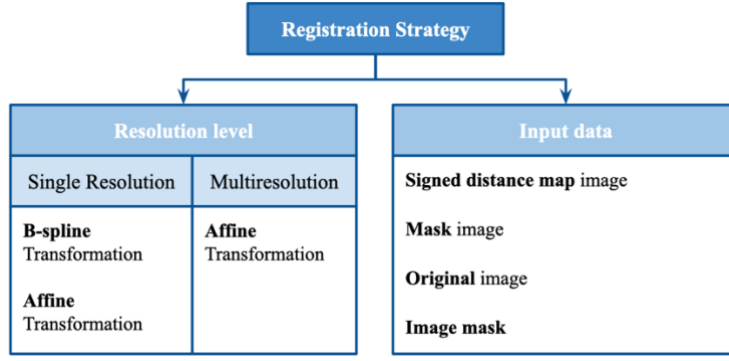


Figure 9. Illustration of the characteristics of the implemented Strategies.

Regarding the **type of transformations**, they will map points in the moving space to points in the fixed space: $(x', y', z') = f(x, y, z)$. These transformations (f) can be simple, as in the case of the Affine Transformation, or more complex, such as the B-spline.

The Affine Transformation [23] preserves collinearity (i.e., all points lying on a line initially still lie on a line after transformation) and ratios of distances (e.g., the midpoint of a line segment remains the midpoint after transformation), but it does not necessarily preserve the angles. Its geometrical transformations include translation, scaling, rotation and shearing, and their combinations. Because we are working with 3D images, the Affine Transformation is represented by a 4x4 matrix:

$$\begin{bmatrix} x' \\ y' \\ z' \\ 1 \end{bmatrix} = \begin{bmatrix} a_{11} & a_{12} & a_{13} & a_{14} \\ a_{21} & a_{22} & a_{23} & a_{24} \\ a_{31} & a_{32} & a_{33} & a_{34} \\ 0 & 0 & 0 & 1 \end{bmatrix} \cdot \begin{bmatrix} x \\ y \\ z \\ 1 \end{bmatrix}, \text{ where } a_{nn} \text{ is the parameter of the geometrical affine transformation.}$$

When the Registration Strategy uses an Affine Transformation, each voxel (x, y, z) from the moving image is multiplied by a 4x4 matrix and is transformed to the fixed coordinate system (x', y', z') .

In general, the Affine Transformations only captures the global image motion. More complex transformations, such as B-spline [24], can be used to simulate the local image deformations (Figure 10a). However, this type of transformation is relatively difficult to use because local features of medical images change with different patients and ages. This means that some parameters of the transformation have to be tuned manually. The general idea is to deform an object or an image by manipulating a regular grid of control points distributed across the image at an arbitrary mesh resolution (Figure 10b). Control points are moved by

the transformation and the position of individual pixels between the control points is computed from the positions of the surrounding control points.

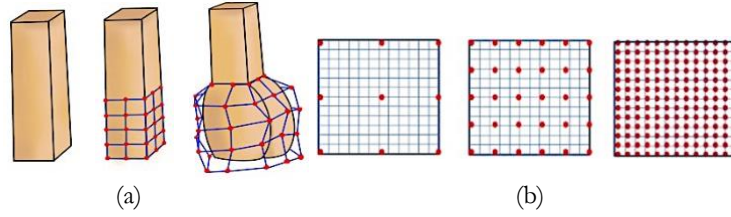


Figure 10. (a) Illustration of a B-spline local deformation example with control points represented in white and connections between them in red: **A.** initial conformation; **B.** Control point localization; **C.** B-spline local deformation. (b) Different mesh resolutions, from large to small spacing between control points.

$$S(t) = \sum_{i=0}^{m-1} p_i b_{i,3}(t) \quad (\text{Equation 5})$$

The most used B-spline transformation is the cubic B-splines (degree $D=3$) (Figure 11a). The transformation function $S(t)$ (Equation 5) is a linear combination of basis B-splines $b_i(t)$, for each control point (i), that have the same shape and are shifted versions of each other. They show how to blend the points. The function $S(t)$ on each global parameter t depend on the sum of the contributions of each control point (p_i) on its basis at this t . Let's imagine the next situation where there are three control points distributed in the space. We have three basis functions (Figure 11b). On $t = t'$, each point has a contribution on the basis function (Figure 11c) and the transformation follows the $S(t)$ equation (Figure 11d)

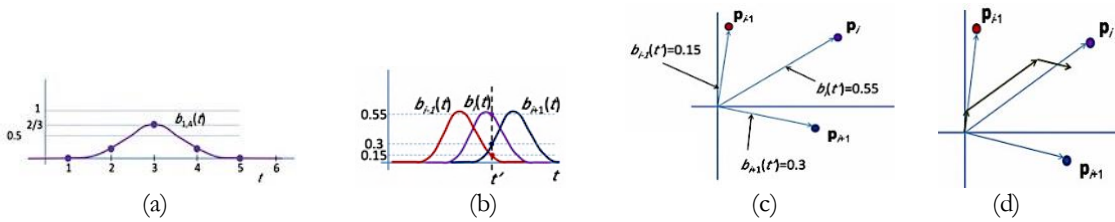


Figure 11.⁶ (a) Basis B-spline function of a cubic B-spline transformation; (b) Example of basis functions for three control points and a cubic B-spline; (c) Control point contribution on their basis function at $t = t'$; (d) $S(t)$ transformation in grey.

The spacing between control points also determines the type of deformation applied to the object. For a smoother global shape, a relatively larger spacing between control points is preferred, while a small spacing is more suitable in local non-rigid deformations.

⁶ Images extracted from: Splines IV – B-spline curves. SlidePlayer. <https://slideplayer.com/slide/2488748/>

Regarding the **level of resolution**, one Registration Strategy is based on Multiresolution. It is based on building two pyramids by down sampling and aligning the images on each level (Figure 12). It starts by reducing in size and resolution the fixed and moving images. Level 0 corresponds to the smallest and blurriest images, while Level 4 stands for original images. This multiresolution procedure starts by registering Level 0 and applying the output parameter map to the input images of the Level 1. Then, this level is registered again and, as before, the output transformation is applied to the input images of the next level. All the pyramid works in the same way. The last output transformation is the final result.

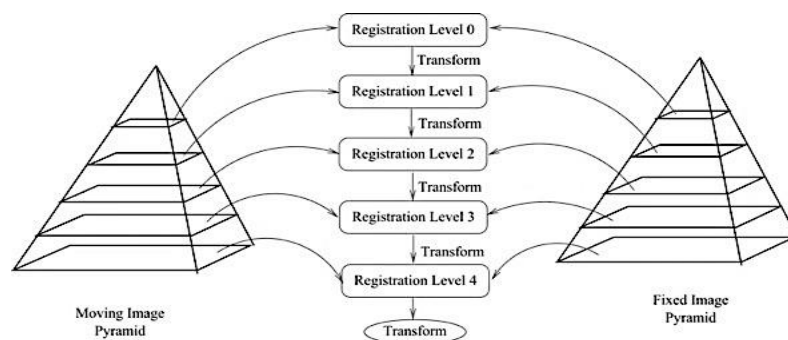


Figure 12. Multiresolution Registration schedule⁷.

Regarding the **type of Input Data** (Figure 7), the Registration Strategies uses the images from the Data set explained before.

As it has been mentioned in the introduction. The registration process needs to define some type of components, such as the type of Interpolator, Optimizer and Metric, that will define the behaviour of the algorithm and thus, the results.

- Interpolator

The interpolator used is the default, the Linear Interpolator, because it gives good results.

- Optimizer

The optimizer used is the Advanced Stochastic Gradient Descent because Simple Elastix documentation suggests to use it as there aren't any immediate preferences and this Optimizer requires less parameters to be set and tends to be more robust.

⁷ Image from ITK software guide book Chapter 3 - Registration.
<https://itk.org/ITKSoftwareGuide/html/Book2/ITKSoftwareGuide-Book2ch3.html>

- Metric

The Similarity metric objective is to evaluate quantitatively the similarity between the moving image and the fixed image. It is a crucial element of the registration process and it should be chosen with care depending on the type of problem to solve (image type and similarity criteria (contours or grey level). We are working with images from different modalities, this means that the relationship between the grey levels and the structures varies from one system to the other. We therefore assumed that the images contained different intensities information and used the multimodal metric named *Mutual Information*. It measures the mutual dependence between the fixed and the moving image, that is, it measures the amount of information that one of the images has over the other.

2.2.3. Experiment definition

The aim of the project is to develop a Registration method by investigating novel registration techniques for the pre-operative fusion of multimodal images in fetal surgeries. To achieve the objective, two experiments have been carried out.

2.2.3.A. Identification of the optimal Registration Strategy

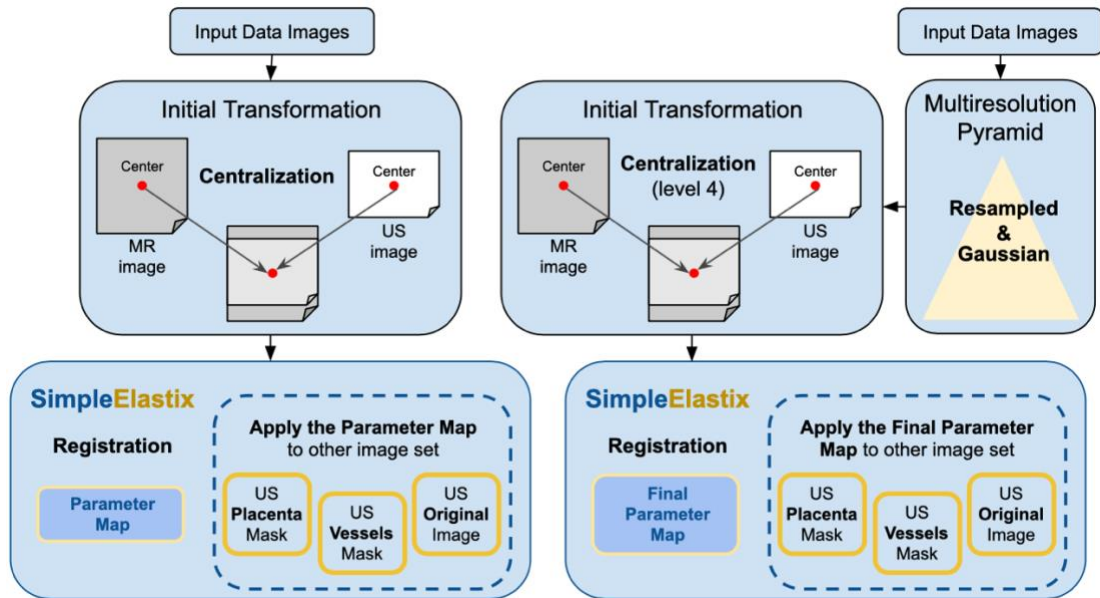


Figure 13.. Pipeline of the Strategies: (left) Strategies 1 and 2 and (right) Strategy 3.

On this experiment, some Registration algorithms have been developed to align US and MR information, specially placentas from both modalities. They have been created by combining

all the information (type of input data, transformations and resolution levels) and Python libraries explained before. There are three general Strategies where different transformations and techniques have been implemented (Figure 13). Moreover, depending on the type of input data used, each Strategy encompasses different sub-strategies.

Strategy 1 contains the Registration algorithms that use a B-spline transformation. The Strategy 1 has the sub-strategies shown on Table 1. As it has been explained before, local features of medical images change with different patients, so some parameter of this transformation have to be tuned to adapt the registration to the target structures.

- Maximum iterations.

This parameter defines the number of iterations that the Registration loop does. It is related with the convergence of the algorithm. On SimpleElastix, the convergence value of the “B-spline Transformation” cannot be modified. Therefore, the b-spline algorithm can be stopped before convergence reaches their value by decreasing the maximum number of iterations. Here two type of deformations are classified: (1) free deformable and (2) preserved deformation. The first deformation allows registration to deform the US placenta freely. Only mask and image masking input data use this deformation. The second one enables local deformations but it does not deform completely the US placenta, preserving the original shape as much as possible. These two deformations are used because higher iterations values for original and ddf input data lead to incorrect deformations, as they can be seen on SI-Figure 24. For that reason, the value for maximum iterations is set to 400 for mask input data, 256 (default) for image masking input data and to 20 for original and ddf input data.

- Control Points Spacing

As it has been explained before, B-spline transformation allows to create local deformations. The type of deformation applied to the object can be also controlled by modifying the Spacing between control points. A large spacing is used to ensure that the surface of the object is deformed without losing its smoothness. The default value is 8, but it is set to 50 for all types of input data.

- Bending Energy Penalty

It is an explicit regularization that has been used in other registration methods [25] and it constraints unrealistic deformations. To follow the same idea and to avoid that the lowest volume of the US placenta exceeds the MR placenta, a Bending Energy Penalty is applied. By default, the Mutual Information and Penalty Metrics have the same weight (value of 1), but on these Strategies the weights are changed to 0.1 and 0.9 respectively.

Strategy	Strategy 1a	Strategy 1b	Strategy 1c	Strategy 1d
Transformation	B-spline	B-spline	B-spline	B-spline
Input Data	Ddf	Mask	Original Image	Image Mask
Resolution level	Single	Single	Single	Single

Table 1. Sub-strategies 1 characteristics.

The **Strategy 2** corresponds to the Registration algorithms that use an Affine Transformation. As in Strategy 2, there are different sub-strategies 2 depending on the type of input used (Table 2).

Strategy	Strategy 2a	Strategy 2b	Strategy 2c	Strategy 2d
Transformation	Affine	Affine	Affine	Affine
Input Data	Ddf	Mask	Original Image	Image Mask
Resolution level	Single	Single	Single	Single

Table 2. Sub-strategies 2 characteristics.

The **Strategy 3** encompasses the Registration algorithms that uses an Affine transformation with Multiresolution method (Table 3).

Strategy 3	Strategy 3a	Strategy 3b
Transformation	Affine	Affine
Input Data	Original Image	Image Mask
Resolution level	Multiresolution	Multiresolution

Table 3. Sub-strategies 3 characteristics.

Despite the type of input data and the type of transformation used, Strategy 1 and 2 follow the same pipeline (Figure 13 left). In the case of the Strategy 3, due to the fact that it follows a Multiresolution method, the pipeline is different from Strategies 1 and 2. However, sub-strategies 3 have the same pipeline (Figure 13 right).

2.2.3.B. Synthetic experiment for placenta vascular reconstruction

Due to the fact that MR vascularization is not provided, a synthetic experiment has been carried out to test if vascular networks can be reconstructed by registering uncompleted and deformed versions. The vascular networks are graphs that have three components: (1) edges; (2) connexions and (3) bifurcations. In this experiment, ground truth is provided, and it represents a completed vascular network. Then, the deformed versions are created modifying some features of the ground truth. The code tries to create similar structures as original graph, so it create different versions: Graph 1 and Graph 2. Figure 14 shows graph frontal views, but for better understanding of their differences see SI-Figure 25, 26 and 27.

Graph 1 is the orientated vascular network. It is different from the ground truth because some edges have different orientation (SI-Figure 26). It is de default structure that the code produces.

Graph 2 is the pruned vascular network. It is a graph in which some connections have been deleted (probability to disconnect each branch: 0.05), but it is also different from Graph 1 and ground truth (SI-Figure 26).

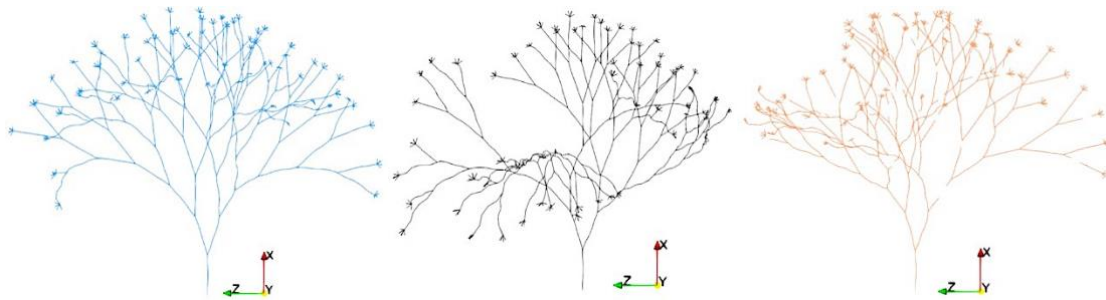


Figure 14. Graphs used for the experiment: (left) Graph 0 (Ground truth); (middle) Graph 1 (oriented network) and (right) Graph 2 (pruned network). Bigger images can be seen on SI-Figure 25.

Once the reconstructed graph is created, it has to be compared with the ground truth. To do so, two probabilistic rules are used to calculate similarity between them: (1) Rule 1: edge probability increases if its connections are similar from the ground truth; (2) Rule 2: edge

probability decreases if its connections are different from the ground truth. At the end, the reconstructed graph will only include those edge with higher probability.

2.3. Validation

The Registration methods and results obtained has an important influence on the medical decision making process and on surgical actions, because the registration method may has an important impact on the performance of the TTTTS intervention. Therefore, high quality and accuracy are expected. In image processing there are numerous of uncertainties related with different factors. Some are related with biology variability. Other are related to the image acquisition process, such as the limited spatial resolution or those related to the intrinsic data variability (e.g., patient movement during acquisition). Certain errors are common to any type of modality whereas others are specific to the type of modality.

On this field, the validation process is required to understand the features and behaviour of the Registration method, to evaluate the performance and limitations. Consequently, a validation process gives us the information about the potential clinical application that the method may serve. Even if the method does not gives us a perfect alignment of the placentas, it may have a significant clinical value if it can reduce the time it takes for clinicians to take a decision. However, there are some validation issues concerning the number of validations that can be done. In this case, the validation has to follow a clinically relevant criteria. Proper validated methods are more likely to receive clinical acceptance and the eventual clinical use of these methods is the one that provides the final test of their ability to impact patient treatment and care.

Dice similarity coefficient, Volume similarity, Hausdorff distance, average surface distance and umbilical cord insertion distances were used as five metrics to evaluate the accuracy of US and MR placenta registration. The fourth first metrics have been previously used to validate other registration methods [26]. Finally, a global score is calculated to ranked all Strategies.

A. Dice Similarity coefficient (DC)

This metric (Equation 6) computes the number of pixels that overlap between the two placentas and normalizes it by the half the sum of the number of nonzero pixels in the two placentas. The result is a value between 0 (no overlap) and 1 (perfect overlap)

$$DC = \frac{2 \cdot |A \cap B|}{|A| + |B|} \quad (\text{Equation 6})$$

,where A is the MR segmented placenta, and B is the registered US placenta. The metric is symmetric and is sensitive to both differences in scale and position.

B. Volume Similarity (VS)

VS (Equation 7) is defined as $1 - VD$ where VD is the volumetric distance [27]. VD is the absolute volume difference divided by the sum of the compared volumes and V_N is the volume for segmentation N .

$$VS = 1 - \frac{||V_B| - |V_A||}{|V_B| + |V_A|} \quad (\text{Equation 7})$$

While volume overlap is a good indicator of mismatch, it is a poor indicator of shape since is not a measure of distance and, hence, the following metrics are also evaluated to assess the overall accuracy.

C. Weighted Hausdorff Distance (wHD)

The Hausdorff distance[28] (Equation 8) measures the degree of mismatch between two sets and behaves like a metric over the set of all closed bounded sets - with properties of identity, symmetry and triangle inequality. It is defined as the maximum of the closest distance between two volumes (i.e., it is the greatest of all the distances from a point x in one non-zero pixel set (X) to the closest point y in the other non-zero pixel set (Y)).

$$HD(X, Y) = \max \{ \max_{x \in X} \min_{y \in Y} d(x, y), \max_{y \in Y} \min_{x \in X} d(y, x) \} \quad (\text{Equation 8})$$

, where \max represents the maximum and \min the minimum. This metric is sensitive to outliers since the most mismatched point is the sole determining criteria of the distance. HD values are weighted using the maximum distance between points of X and Y .

D. Average surface distance (*ASD*)

This metric (Equation 9) mitigates the outlier problem exhibited by the Hausdorff distance. The metric is the average of the absolute distance from each surface pixel in one image to its closest point on the other image.

$$ASD(X,Y) = \max \{ \max_{x \in X} \frac{1}{N} \sum_{y \in Y} \min d(x,y) , \max_{y \in Y} \frac{1}{N} \sum_{x \in X} \min d(y,x) \} \quad (\text{Equation 9})$$

E. Umbilical Cord Insertion Distance (*UCID*)

As it has been explained in the Introduction, the TTTS is produced by an unequal sharing of the maternal blood flow due to the fact that twins vascularization is connected between them. Therefore, blood flows from the donor to the recipient, producing side effects in both twins. The intervention is focus on stop these connections. The umbilical cords are some tangible structures that are always present.. The objective of the Registration Algorithm is to align the segmented placentas and thus, the US vascularization. Therefore, umbilical cords insertions can be used as fixed points to measure the distances between placentas after the registration.

F. Global Score (*GS*)

To encompass all the validation information in a single variable, a Global Score has been calculated. It follows the idea that:

- (1) Results from validation metrics whose optimal value is 0 will be subtracted to the global score. These validation metric are: VS, wHD, ASD.
- (2) Results from validation metrics, whose optimal value is 1 will be added to the global score. This validation measure is DC.

Therefore, Global Score is calculated as follow, and the optimal value for GS is 1:

$$GS = DC - VS - wHD - ASD \quad (\text{Equation 10})$$

The UCID measurements have not been used to calculate the GS. However, they are useful for visually analysing, the registration results because Umbilical cord insertions are fixed structures and can give information about the transformation of the placentas.

1 RESULTS AND DISCUSSION

In this project, the Registration Strategies developed are evaluated in ten different patients. For that purpose, the validation metrics explained before are applied to each Strategy and patient.

3.1. Registration Strategies

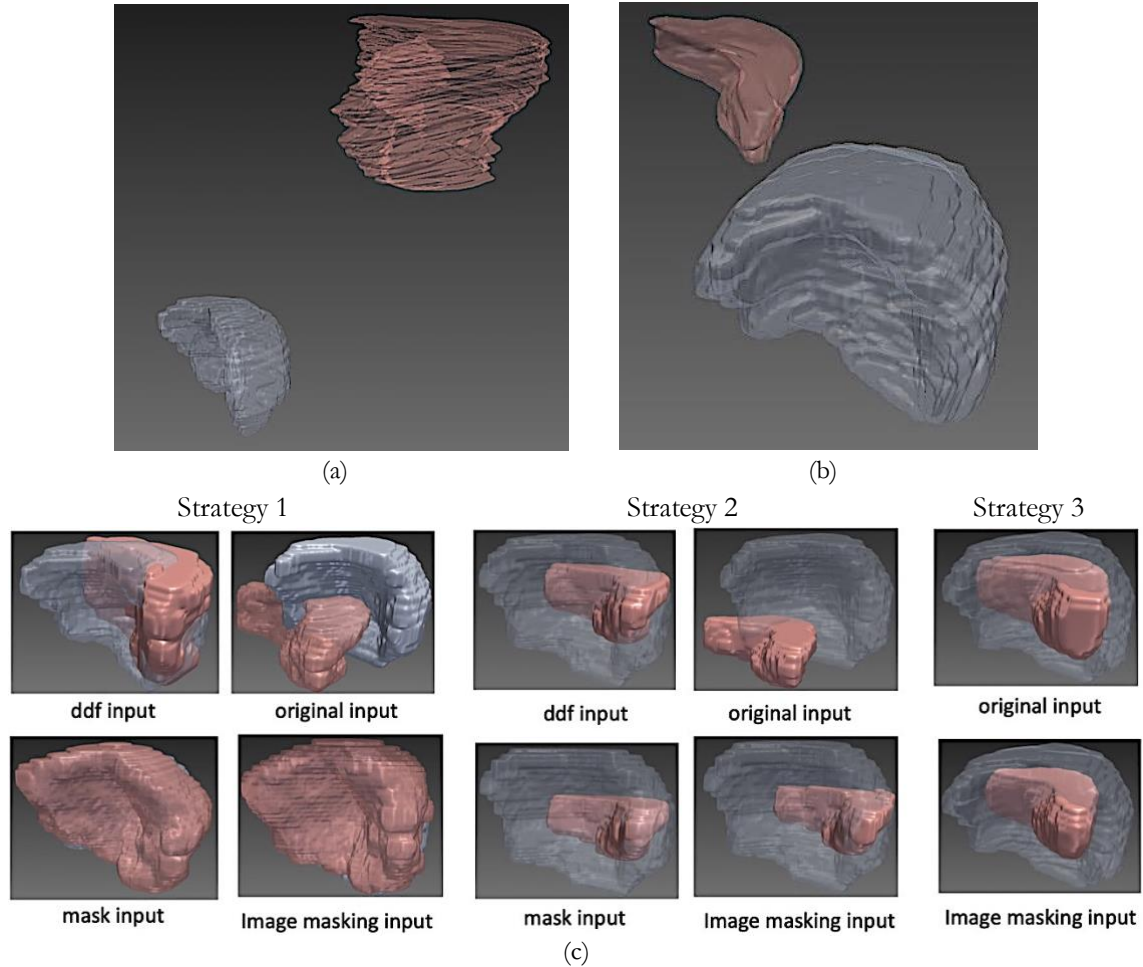


Figure 15. Results from Registration Strategy 1 (patient 1). US registered placenta is coloured in pink and MR placenta in white. (a) Original conformation of US and MR placentas; (b) Original conformation of shrunk US and MR placenta; (c) Strategy Results. Bigger images can be seen on [SI-Table 5](#).

Once the Registration Strategies are fully developed, they are run on each patient data set. As it can be seen on [Figure 15](#), Registration Strategy 1 results show the biggest difference when comparing the overall results. In the image registration smoothness of the registration result is so important, with the B-spline transformation, high smoothness can be obtained, however, the preservation of topology is not guaranteed. It is due to the fact that it uses a

free deformable method (B-spline), so the US placenta mask is fully adapted to the MR placenta mask in Strategy 1, when input data are directly the segmented placenta (mask input) or the image masking input. When input data is ddf or original images, pixel spacing and iteration have different values, so results from these input data preserve the general structure of the original US placenta shape. Same happened with results from Strategies 2 and 3, but in these cases it is due to the fact that they use a rigid transformation, so no local deformations are created and original shape is preserved.

Visually, original input from Strategies 1 and 2 do not show good alignments with MR placentas because the US placenta, even though they have been transformed from the original conformation, they are not adapted to the MR structure. The rest of results show better alignments because the US volume conformations is located in places that can be potentially correct. On SI-Table 5 and 6 results for each Strategy and patient can be seen. Same overall behaviour explained before happened for each registration strategy tested.

Due to the fact that each Strategy is based on different input data, transformation and resolution level, they have produced different results (Figure 15). As it has been mentioned in the Data Set Section, US images do not encompass the structure of the overall placenta, while MR images do. This will difficult the Registration procedure because US and MR placentas will not share the general structure and alignment errors can appear more frequently.

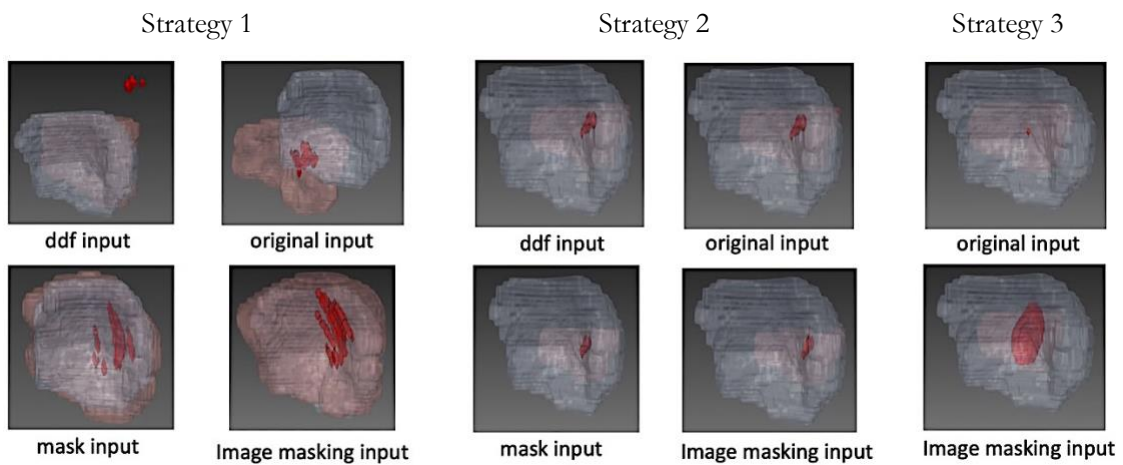


Figure 16. Registration Strategies applied to US vessels. MR placenta, US placenta and US vessels are differentiated by colours (white, pink and red, respectively). Bigger images can be seen on SI-Table 6.

The objective of the project is focus on developing a Registration method that will align US and MR placentas, so US vascular information can be added to the MR improving the planification process. Therefore, registration algorithms are also applied to US vessels (Figure 16). Same behaviour as in placental Registration can be seen. Strategies where free deformable algorithm has been applied (Strategy 1) show higher level of vessel deformation. However, non-realistic vessel transformations can be seen on Strategy 3 results. The reason of that is because Strategy 3 is based on multiresolution pyramid that varies the intensity of the images. The borders between the placenta and the background are more defined than vessel margins. Consequently, when resolution decreases during the registration process the vascular information is lost and final conformation is not realistic. Moreover, comparisons between US and MR vascularization after registration cannot be established because MR vessels are not provided.

It is shown on Figure 15, Figure 16, SI-Table 5 and SI-Table 6 that there are differences between Strategies and sub-Strategies. These differences cannot be assessed only by visual inspection. Therefore, some metric have been used to quantify the accuracy of the algorithm and also the differences between each strategy.

3.2. Vascular Placenta Parametrization

As it has been mentioned before, MR vascularization is not provided, so a synthetic experiment is carried out to analyse if it is possible to reconstruct vascular networks from deformable networks. However, because of a matter of time, final graph couldn't be created and it will be considered for further work.

3.3. Validation

Results from each Registration Strategy haven been quantitatively tested using the metrics explained before: Dice, Volume Similarity, Hausdorff distance, Average surface distance and Umbilical cord insertions distances.

Regarding the results from each measurement used for validate the Strategies, average results from each patient are described and discussed. The units are in pixels because we do not have the original pixel spacing to convert them to millimetres (mm). The reasons are:

- (1) MR images are pre-processed by a neuronal network to extract the segmentations of other structures such as: mother soft tissue or uterus, that are used for another project. Therefore, these images are transformed and the original spacing is changed to 0.75 for each dimension. And the original spacing is not known.
- (2) US images are acquired through a video (.avi) and then pre-processed to change the slice dimension. So, the original spacing is not known.

For quantifying the distances between umbilical cord insertions, a MITK based plugin has been developed (Figure 17). The graphical user interface has been customized using Qt5 Designer. It includes a window, where the user can load the medical images, select two points from each image and calculate and see the distance between them.

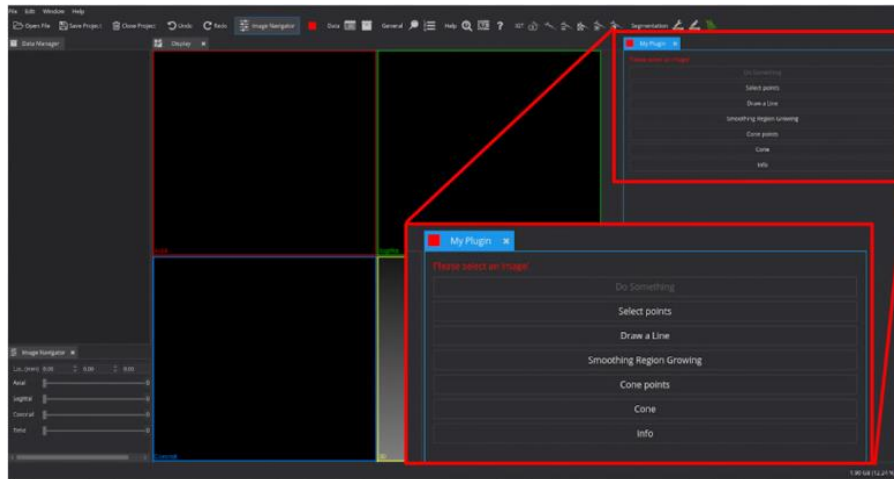


Figure 17.. Developed MITK Plugin for measuring the umbilical cord insertion distances. Bigger image can be seen on SI-Figure 28.

- Select points button.

After loading the medical images (.nii), the user can select one point from each image (Figure 18). They are saved on a variable called *Point Selection*. The order of selecting the point is important to calculate the distances. Therefore, the US umbilical cord insertion should be selected before the MR insertion.

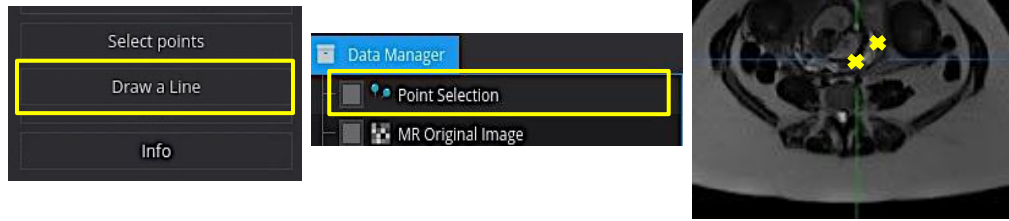


Figure 18. Selecting point procedure from medical images: (left) Select points Button; (middle) Variable Point Selection where point coordinates are saved; (right) Representation of the selected points on the US registered image.

- Draw a Line button.

Once points are selected, the user can press the “Draw a Line” button to draw a red line between points. This line can be seen on the 3D window (Figure 19).

- Points information button.

Finally, the user can press the “Information” button to calculate the distance between points that is shown on the interface, shortly after the “Information” button (Figure 19c).

The results is the Euclidean distance between both umbilical cord insertions (Figure 19b).

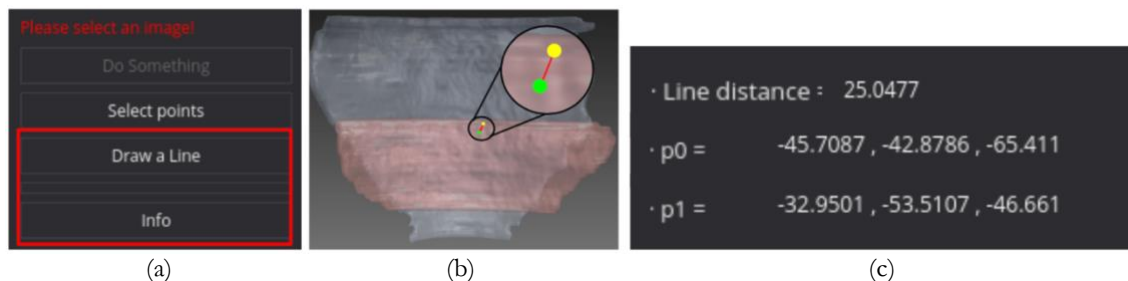


Figure 19. Draw a line and point information procedure: (a) Draw a Line and Info buttons; (b) Line between selected points created to calculate the distance between them; (c) Points information where coordinates and distance can be seen on the screen.

On Table 4 quantitative results from each validated metric is shown. Values are correlated with images shown on Figure 15. On one hand, initial conformations do not overlap (DC and VS are zero) and wHD and ASD could not be measured because their distance exceeds from the largest possible region. On the other hand, volumetric measurements (DC and VS) from registered structures (Strategy 1,2 and 3) show an increment with respect to original conformation, meaning that there is overlapping between placentas.. This alignment is also described by the decrement of the distance measurements, with respect to original

conformation. Same behaviour can be seen on Table SI-Table 7, where volumetric and distance measurements from all patients from Hospital de la Maternitat are shown.

Table 4. Validation results extracted from averaging results from each patient and strategy used. Validation results extracted from averaging results from each patient and strategy used. In blue, numerical values of the non-registered structures (original conformation) in red the numerical values for the highest GS values and in green the numerical values for the lowest GS values.

	DC	VS	wHD	ASD	UCID	Global Score
Original conformation						
	0,0000	0,0000	Outside region	Outside region	180,2143	> 180,2143
Strategy 1						
1a. ddf	0,3667	0,5406	0,0067	6,78626	50,7145	-6,9669
1b. Image	0,1193	0,6986	0,0169	15,9084	72,5617	-16,5048
1c. Mask	0,771	-0,3012	0,0046	1,9729	49,7307	-0,9043
1d. Cut	0,6709	-0,4038	0,0111	6,9746	75,7991	-5,9108
Strategy 2						
2a. ddf	0.2754	1.0089	0,0080	7.2334	22,4076	-7,9749
2b. Image	0.0969	1.0385	0,0090	19.7485	68,8826	-20,6991
2c. Mask	0.3440	0.9680	0,0162	8.1560	29,0902	-8,7963
2d. Cut	0.3238	1.0318	0,0079	11.8947	32,9895	-12,6107
Strategy 3						
3a. Image	0.2907	0.9044	0,0073	8.0612	65,3512	-8,6820
3b. Cut	0.2858	1.1338	0,0066	9.2606	44,3938	-10,1152

By observing the quantitative results, DICE and Volume similarity values from Strategy 1, in general, agree with results from Figure 15. They show a high value of adjustment between US and MR placenta (0.70 and - 0.33 respectively). Cases where Volume similarity has negative values means that US placenta has exceed the MR placenta limits. From Strategy 1, the sub-strategy that shown best results in terms of volume ,but also for surface distance metrics , is the one that uses the mask images as input (Strategy 1c).

Regarding Strategy 2, sub-strategy 2c shows better volume results (0.3442 for Dice and 0.96806 for VS) than the result of sub-strategies 2. However, sub-strategy 2a, which uses ddf images as input, has also good volume results (0.27548 for Dice and 1.008967 for VS) and better surface distance results (78.23992 for HD and 7.23346 for ASD) than the rest of sub-strategy 2. Therefore, sub-strategy 2a is in general better than the rest of sub-strategies 2. Regarding Strategy 3, sub-strategy 2a has more accurate values than the sub-strategy 3b. At this point, the algorithm that better aligns US and MR placentas, and thus US vessels, should be chosen.

As it has been explained, one of the metrics used to validate the methods is the distance between umbilical cord insertions (from US to MR). The points of the insertions were localized by experts using the developed MITK based plugin. However, some insertions were not able to be located for all patients. In some cases, insertions were covered by part of the fetus that avoid experts to detect them, while in other cases the resolution on the US images was not good enough to see them. Moreover, all insertions are represented as points, which do not restrict the US placenta transformation. This means that, placenta transformation could have been rotated about the umbilical cord insertion and even though the calculated distances (UCID) are close to zero, the conformation of the US registered placenta may not be correct. For these reasons, results obtained by this parameter are not totally decisive because the correctness of the placenta (and thus, US vessels) is not guarantee. Therefore, a correlation between umbilical cord insertion distances and correct registration cannot be established. However, they are used for visual validation.

Something to take into account is that US placentas do not represent the overall volume due to the acquisition technique. Therefore, a strong deformation (as in Strategies 1c and 1d) does not produce such as realistic conformations as those strategies that preserve the original shape of the placenta. The reason is that some structures, such as umbilical cord insertion, or more important structures, such as vessels, can be improperly disfigured. And this happens when US placentas are excessively deformed to perfectly mimic the shape of the MR placentas, as it can be shown [Figure 20](#). This problem represents an algorithm restriction. Just in cases where US images fully represent the overall volume of the placenta, the algorithm could apply stronger and more complex transformations, such as local deformations.

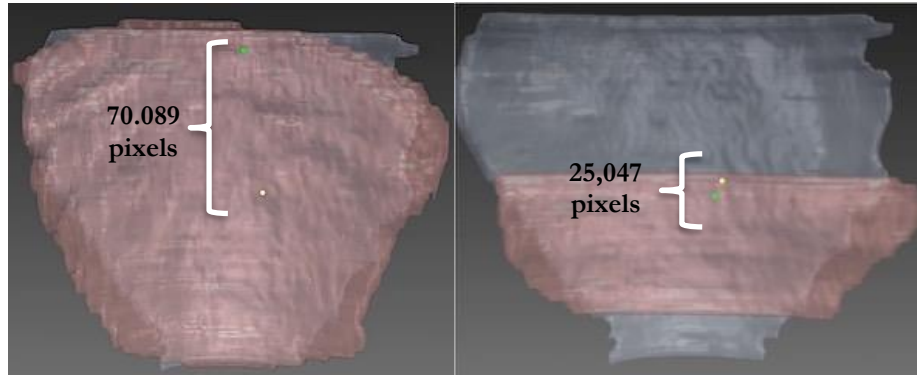


Figure 20.. US registered placenta in pink and MR placenta in white, and umbilical cord insertions can be shown: US insertion (green point) and MR insertion (yellow point). (left) US placenta registered using a B-spline transformation (Strategy 1c); (right) US placenta registered using an Affine transformation (Strategy 2c). Umbilical cord insertion from B-spline US registered placenta is far (70.089 pixels) from the MR insertion and this is due to the strong deformation applied on it.

Following the objective of the project, different Multimodal Registration methods have been implemented. By one side, some Registration Strategy, such as Strategy 1 and 3 preserve the structure of the placentas and show good volumetric and distance results. However, they do not show satisfying volumetric and distance results, and neither Global score. Strategy 1, and especially Strategy 1c, has the more positive GS (Table 4). Unfortunately, more adaptative results could mean an increase in umbilical cord insertion distances and undesired transformations of intrinsic structures, such as vessels. These will influence the planning of the intervention, leading to inaccurate and fatal results. Therefore, more restrictive transformations (rigid transformations) are desired to use when working with images that only represent sections of the placenta.

Consequently, the best Registration Strategy will depend on the images and the information that is extracted from them. If US and MR placenta volumes are fully acquired, more free deformable transformations, such as Strategies 1c or 1d, can be used. However, if US or MR placentas are not completely collected, more restrictive transformations, such as Strategy 1a, 2a or 3a, should be used. Registration strategies will be improved if a tracking system is used to trace the US probe in the surgery room [29]. It is based on the idea of registering the target 3D volume and its temporal evolution in the same coordinate system, while the US probe can be moved freely. This follow-up can be done by different tracking systems, such as optical or electromagnetic trackers. In that way, information from the US scan can be transferred to another coordinate frame, so detailed and more realistic 3D models can be built.

4. CONCLUSION AND FUTURE WORK

In this Project, different registration algorithms have been developed to align segmented structures, such as placentas, from both techniques. After this process, target structures (vessels) are registered using the resulted parameter maps. Among this study, different patients were studied. The placental morphology and acquired quantity were different from each patient. This second characteristic limited some registration aspects, such as type of transformation (B-spline or Affine), type of input data (images, segmentations, image masks or distance maps) or intrinsic transform parameters (maximum iterations, spacing or penalty).

By one side, free transformations (B-spline) and specific input data, such as masks or image masks, allow a high level of US placenta adaptation to MR placenta morphology. By the other side, more rigid transformations produce greater preservation of the original US placenta shape. However, in all registration cases, distances between MR and US structures have decreased, getting minimum surface distances of 1,9729 pixels, in comparison with initial conformations. In terms of volumetric features, only in some cases (Strategy 1b and Strategy 2b) overlapping between structures have not been improved.

Regarding validation, a MITK based plugin was developed to calculate distances between umbilical cord insertions, before and after registration. These points were not accessible in all patient images because of the low resolution of US images, so they could not be used as a quantitative measure of the registration correctness. Moreover, distances between surfaces from the original conformations could not be obtained due to limitations in some functions (Hausdorff and Average Surface distances). However, all results were able to be analysed visually in MITK, suggesting overlapping and approaching between registered structures.

Concerning target structures (vessels), each strategy transformation was applied and similar conclusions were obtained. Rigid registrations preserve original vessel conformations, while free registrations produce disfigured vascular shapes. In these last cases, alteration of the vessels morphology can lead to incorrect localization. There are two factors that determine the success of vessel registration: (1) not overall placenta could be used for registration,

leading to excessive deformations, and (2) absence of MR vessels to evaluate the correctness of the registered vessels.

To avoid image restrictions, it would be a good decision to establish an image acquisition protocol to provide fully placenta information. In that case, a freer deformable registration method, such as Strategy 1c or 1d can be applied to align multimodal information. Moreover, vascular MR information is needed for the evaluation of US registered vessels.

In conclusion, developed algorithms show considerable improvements with respect to original conformations. These results give valuable information for planning the intervention because the knowledge from both techniques is combined. Although algorithms are not very accurate, they can be used as a starting point for further improved versions. Regarding synthetic vascular restoration, further work is needed to do to develop a reconstructive algorithm.

Future directions are focused on algorithm optimization to obtain a method that: (1) aligns placental structures correctly and (2) is not be sensitive to possible volumetric limitations of input structures. For the first characteristic, intrinsic registration parameters can be tuned to obtain optimum values for validation metrics and visible correct alignments. For the second feature, in the case that overall placenta volume could not be acquired, the algorithm can restrict the registration. This condition may penalize those areas where the level of deformation of the moving structure is excessively high, indicating that the structure does not belong to that position. Moreover, some US tracking experiments should be done to improve these registration strategies.

BIBLIOGRAPHY

1. Lewi L, Gucciardo L, Van Mieghem T, de Koninck P, Beck V, Medek H, Van Schoubroeck D, Devlieger R, De Catte L, Deprest J (2010): *Monochorionic Diamniotic Twin Pregnancies: Natural History and Risk Stratification*. Fetal Diagn Ther; 27:121-133. doi: <https://doi.org/10.1159/000313300>
2. Daniel W. Skupski. Twin-to-Twin Transfusion Syndrome (2013) JP Medical Ltd, 186 pp., ISBN 978-93-509-351-3. doi: <https://doi.org/10.1017/thg.2014.24>
3. Haruhiko Sago, Keisuke Ishii, Rika Sugibayashi, Katsusuke Ozawa, Masahiro Sumie and Seiji Wada (2018): *Fetoscopic laser photocoagulation for twin-twin transfusion syndrome*. J Obstet Gynaecol Res; vol. 44 (5): 831-839. doi: <https://doi.org/10.1111/jog.13600>
4. Robert D, Neilson JP, Kilby MD, Gates S: *Interventions for the treatment of twin-twin transfusion syndrome* (2014) Cochrane Database Syst Rev.; vol. 30 (1). doi: [10.1002/14651858.CD002073.pub3](https://doi.org/10.1002/14651858.CD002073.pub3).
5. R. Papanna, L. K. Mann, K. J. M. Jr., T. Kyriakides, A. Johnson, E. Garcia, C. S. Buhimschi, I. A. Buhimschi, *Histologic changes of the fetal membranes after fetoscopic laser surgery for twin-twin transfusion syndrome* (2015), Pediatric Research vol. 78 pp.: 247–255. doi: [10.1038/pr.2015.105](https://doi.org/10.1038/pr.2015.105).
6. Francisco Vasconcelos, Patrick Brandão, Tom Vercauteren, Sebastien Ourselin, Jan Deprest, Donald Peebles, and Danail Stoyanov: *Towards computer-assisted TTTS: Laser ablation detection for workflow segmentation from fetoscopic video* (2018) Int J Comput Assist Radiol Surg.; vol. 13 (10): 1661-1670. doi: [10.1007/s11548-018-1813-8](https://doi.org/10.1007/s11548-018-1813-8)
7. R. Pratt, J. Deprest, T. Vercauteren, S. Ourselin, A. L. David, *Computer-assisted surgical planning and intraoperative guidance in fetal surgery: asystematic review*, (2015) Prenatal Diagnosis 35 pp.: 1159–1166. doi: [10.1002/pd.4660](https://doi.org/10.1002/pd.4660)

8. Wolfgang Wein, Shelby Brunke, Ali Khamene Matthew R.Callstrom, Nassir Navab. *Automatic CT-ultrasound registration for diagnostic imaging and image-guided intervention* (2008) Medical Image Analysis, vol. 12 (5), pp. 577-585. doi: [10.1016/j.media.2008.06.006](https://doi.org/10.1016/j.media.2008.06.006)
9. G.P.Penney, J.M.Blackall, M.S.Hamady, T.Sabharwal, A.Adam, D.J.Hawkes. *Registration of freehand 3D ultrasound and magnetic resonance liver images* (2004) Medical Image Analysis, vol. 8 (1), pp. 81-91. doi: [10.1016/j.media.2003.07.003](https://doi.org/10.1016/j.media.2003.07.003)
10. Huang X., Hill N.A., Ren J., Guiraudon G., Boughner D., Peters T.M. (2005) *Dynamic 3D Ultrasound and MR Image Registration of the Beating Heart* (2005) In: Duncan J.S., Gerig G. (eds) Medical Image Computing and Computer-Assisted Intervention – MICCAI. Lecture Notes in Computer Science, vol. 3750. Springer, Berlin, Heidelberg. doi: [10.1007/11566489_22](https://doi.org/10.1007/11566489_22)
11. François Rousseau, Orit Glenn, Bistra Iordanova, Claudia Rodriguez-Carranza, Dan Vigneron, et al.. *Registration-based Approach for Reconstruction of High Resolution In Utero Fetal MR Brain Images* (2006) Academic Radiology, Elsevier, vol. 13 (9), pp.1072-1081. doi: [10.1016/j.acra.2006.05.003](https://doi.org/10.1016/j.acra.2006.05.003).
12. Maria Kuklisova-Murgasova, Amalia Cifor, Raffaele Napolitano, Aris Papageorgiou, Gerardine Quaghebeur, Mary A. Rutherford, Joseph V. Hajnal, J. Alison Noble, Julia A. Schnabel. *Registration of 3D fetal neurosonography and MRI* (2013) Medical Image Analysis, vol. 17 (8), pp. 1137–1150. doi: [10.1016/j.media.2013.07.004](https://doi.org/10.1016/j.media.2013.07.004)
13. Kasper Marstal. *SimpleElastix Documentation*.Release 1.0. Dec 14, 2018.
<https://media.readthedocs.org/pdf/simpleelastix/latest/simpleelastix.pdf>
14. Qt: <https://www.qt.io>
15. ITK: <https://itk.org>
16. VTK: <https://vtk.org/about/#history>
17. Ivo Wolf, Marcus Vetter, Ingmar Wegner, Marco Nolden, Thomas Böttger, Mark Hastenteufel, Max Schöbinger, Tobias Kunert, Hans-Peter Meinzer. *The Medical Imaging Interaction Toolkit (MITK) – a toolkit facilitating the creation of interactive software by extending*

- VTK and ITK* (2004) SPIE 5367, Medical Imaging: Visualization, Image-Guided Procedures, and Display. doi: <https://doi.org/10.1117/12.535112>
18. Juenlin Leng, Gualiang Xu and Yongjie Zhang: *Medical image Interpolation Based on multi-resolution registration* (2013) Computers and Mathematics with Applications, vol. 66, no. 1, pp. 1-18. doi: <http://dx.doi.org/10.1016/j.camwa.2013.04.026>
 19. Thomas M. Lehman, Member, IEEE, Claudia Gönner and Klaus Spitz: *Survey: Interpolation Methods in Medical Image Processing*. (1999) IEEE Transactions on Medical Imagin, vol. 18, No. 11. <http://www.cs.tau.ac.il/~turkel/imagepapers/interpolation-medical.PDF>
 20. H.S.Wong, N.R.Buenfeld. *Euclidean Distance Mapping for computing microstructural gradients at interfaces in composite materials*. (2006)Cement and Concrete Research, vol. 36 (6), pp. 1091-1097. doi: <doi.org/10.1016/j.cemconres.2005.10.003>
 21. Mille, J., Leborgne, A. & Tougne. *Euclidean Distance-Based Skeletons: A Few Notes on Average Outward Flux and Ridgeness*. (2018) Journal of Mathematical Imaging and Vision, pp 1–21. doi: <doi.org/10.1007/s10851-018-0836-7>
 22. P.-E. Danielsson, *Euclidean distance mapping*, (1980) Computer Graphics and Image Processing, vol. 14 (3), pp. 227–248. doi: [https://doi.org/10.1016/0146-664X\(80\)90054-4](https://doi.org/10.1016/0146-664X(80)90054-4)
 23. Narayan Paniphi, Smite Tripathy. *Image Registration using Polynomial Affine Transformation*. (2002) Defence Science Journal. 52. doi: <doi.org/10.14429/dsj.52.2180>.
 24. D. Rueckert, P. Aljabar, R. A. Heckemann, J. V. Hajnal, A. Hammers. *Diffeomorphic registration using b-splines*, (2006) in: Proc. of the 9th International Conference on Medical Image Computing and Computer-Assisted Intervention, pp. 702–709. doi: 10.1007/11866763_86
 25. Kanai, Takayuki et al. *Evaluation of accuracy of B-spline transformation-based deformable image registration with different parameter settings for thoracic images*. (2014) Journal of radiation research, vol. 55 (6), pp.: 1163-70, doi:<10.1093/jrr/rru062>

26. Eric Poulin, Karim Boudam, Csaba Pinter, Samuel Kadoury, Andras Lasso, Gabor Fichtinger, Cynthia Ménard, *Validation of MRI to TRUS registration for high-dose-rate prostate brachytherapy*, (2018) Brachytherapy, vol. 17 (2), pp. 283-290, ISSN 1538-4721, doi: [10.1016/j.brachy.2017.04.093](https://doi.org/10.1016/j.brachy.2017.04.093)
27. Taha AA, Hanbury A. *Metrics for evaluating 3D medical image segmentation: analysis, selection, and tool*. (2015) BMC Med Imaging, vol. 15:29. Published 2015 Aug 12. doi: <https://doi.org/10.1186/s12880-015-0068-x>
28. Henrikson, Jeff. *Completeness and total boundedness of the Hausdorff metric*. MIT (2002) Undergraduate Journal of Mathematics, pp. 69–80. <http://citeseerx.ist.psu.edu/viewdoc/download?doi=10.1.1.353.633&rep=rep1&type=pdf>
29. Vasconcelos, F., Peebles, D., Ourselin, S. et al. Int J CARS (2016) International Journal of Computer Assisted Radiology and Surgery. Vol. 11 (6), pp.: 1091-1099. doi: doi.org/10.1007/s11548-016-1392-5

A. SUPPLEMENTARY INFORMATION

A.1. Image Modalities for TTTs

Magnetic Resonance (*MR*)

Magnetic Resonance Imaging consists of a non-invasive technology which does not use ionizing radiation to generate three-dimensional anatomical images. To produce these images, the body's own molecules, in particular water protons, are excited by the system and, at the same time, the system detects the change in the direction of the rotational axis of these protons.

To do this, powerful magnets are used. They create a strong magnetic field so protons are forced to align with it. Anatomically, these protons rotate intrinsically on different axis (Figure 21a), but when the MR system applies a magnetic field, they align with it to achieve an equilibrium (Figure 21b). After this, a radio-frequency current is pulsed through the patient and protons are stimulated. This excitation forces the protons to go against the pull of the magnetic field, breaking the equilibrium (Figure 21c).

When the radio-frequency field is turned off, the protons realign with the magnetic field. On that state, the MRI sensors are able to detect the energy released as the protons recover the equilibrium (Figure 21d). The time it takes, as well as the amount of energy released, changes depending on the surrounding tissue (environment) and the chemical nature of the molecules (type of tissue). The faster the protons realign with the main magnetic field, the brighter the image. Therefore, MR can produce images showing various differentiated tissues, based on these magnetic properties..

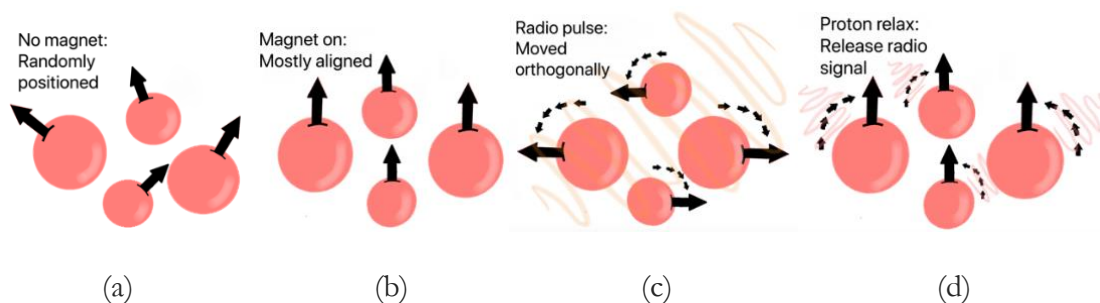


Figure 21. States of water protons from rest anatomical state to magnetic field application: (a) Intrinsic rotation of water protons in anatomical state; (b) Proton spine alignment due to magnetic field effect; (c) Water protons respond when radio-frequency pulse turn on and equilibrium is broken; (d) Realignment of water protons when radio-frequency pulse turn off.

To obtain a MRI image, the patient, placed inside a large magnet, must remain very still during the imaging process in order not to blur the image. Then, the system moves a magnetic ring across the desired zone of the patient body and three dimensional anatomical images are produced. These images are not three dimensional on the sense that MRI system produces a volume of the zone, but the image slices have the information of the three anatomical planes (Axial/Transverse, Sagittal and Coronal). The number of slices produced depends on the spacing between each MRI detection (e.g. on the imaging equipment limitations). And this proportion will also determine the resolution of the images, which used to be high in comparison with other techniques such as US.

Ultrasound (US)

In the case of Ultrasound, it is also a non-invasive technique because it uses sound waves. These sound waves have frequencies above the threshold of human hearing (around megahertz (MHz) range). The main structures of the US system are the transducers (Figure 22a). They produce sound waves and detect the echoes reflected back by the different tissues. This process of producing and detecting waves is based on the piezoelectric material properties of the transducers. When electric field is applied to them, they are able to create sound waves. In addition, they can also produce electric field when sound waves (echoes) hit them (Figure 22b). Therefore, because of each type of tissue reflects sound waves in different ways, we are able to detect boundaries such as fluid and tissues or tissue and bone.

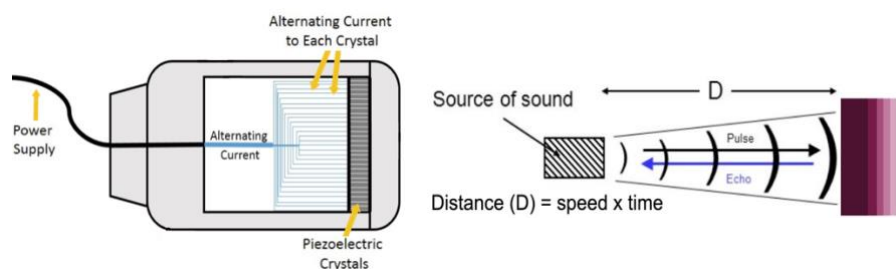


Figure 22. Characteristics of US transducer used for imaging: (left)⁸ illustration of convex transducer, where piezoelectric elements can be seen on the front of the US transducer, and (right)⁹ reflected sound waves, echoes, that will be detected by piezoelectric elements.

Using the speed of sound produced and the time of each echo's return, another part of the US system, the scanner, calculates the distance between the transducers and the tissue

⁸ Image from: [Basic Physic of Ultrasound](#), Dr Jaime Robinson - Department of Nuclear Cardiology, Intensive care society.

⁹ Image from: The physics of Diagnostic Ultrasound – Mark Wilson - <https://slideplayer.com/slide/4383886/>

boundary. Then, two-dimensional slices are created, but three-dimensional and four-dimensional images can be also done.

Because US is based on how tissues reflect sound waves, it is not very good for imaging tissues that are enclosed inside bones structures because bones reflect all sound waves (Figure 23a). However, Ultrasound is very useful for monitoring the growth and development of the fetus, but also for imaging vessels (Figure 23b).



Figure 23¹⁰. Bone structure, ribs, produce shadows that prevent from seeing the behind tissue on an US image (left). However, this technique is good on imaging blood flow when Doppler is used (right).

A.2. B-spline parameter influence

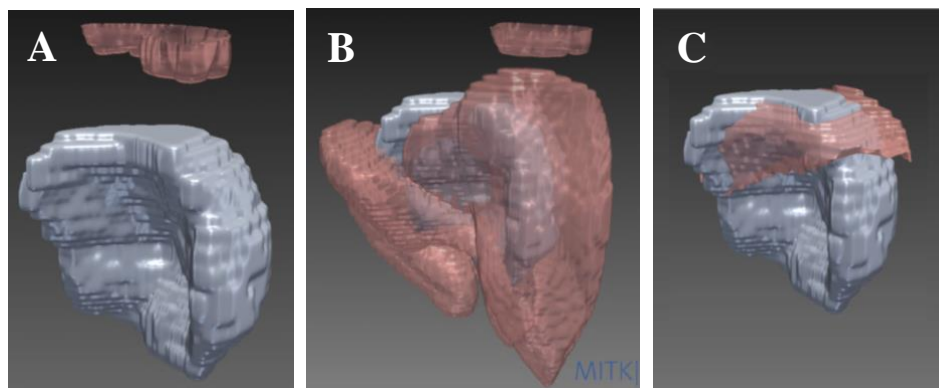
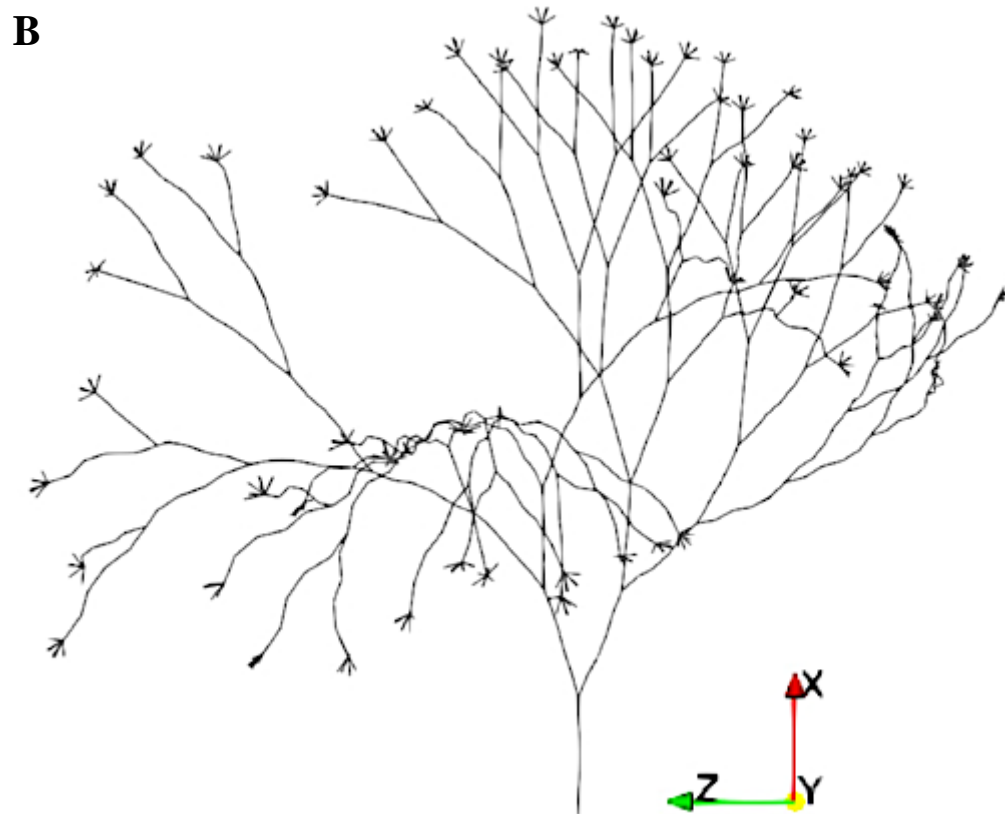
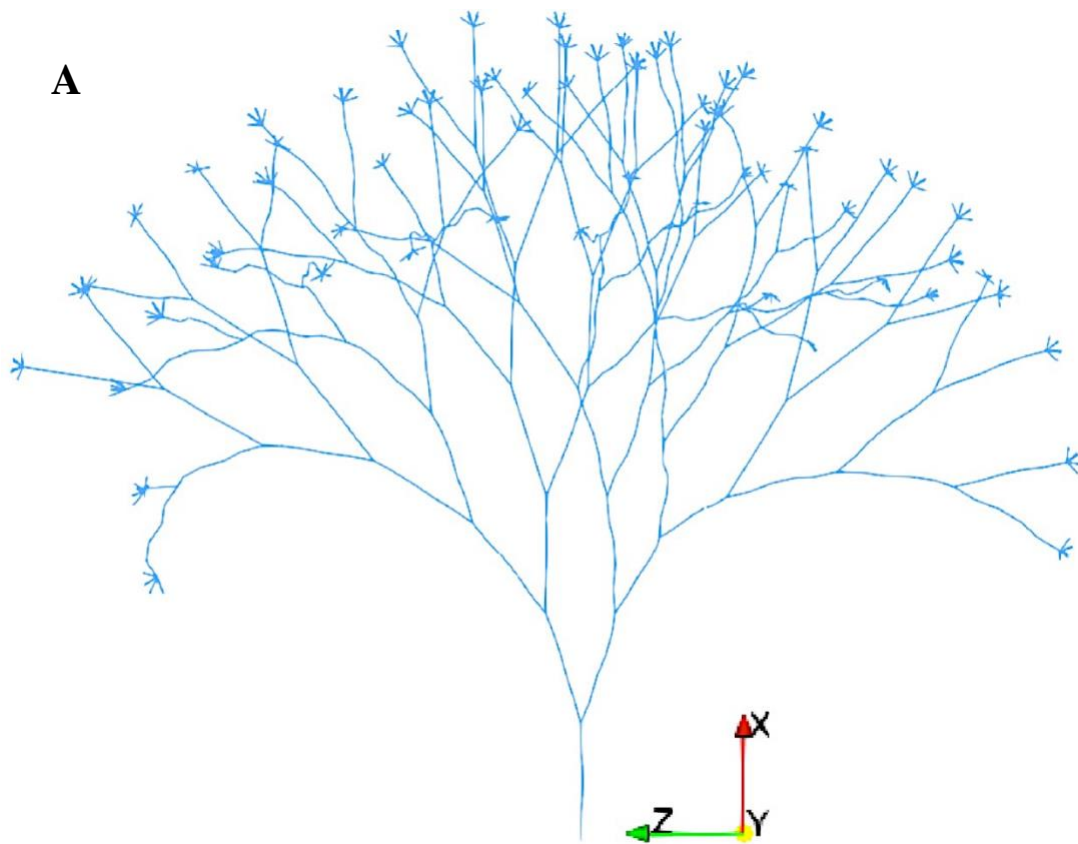


Figure 24. Results from Registration Strategy 1 with different maximum iteration values: A: 50 maximum iterations; B: 256 maximum iterations (default); C: 400 maximum iterations.

¹⁰ Images from: (left) Ihnatsenka B, Boezaart AP. *Ultrasound: Basic understanding and learning the language*. Int J Shoulder Surg 2010; vol. 4, pp.: 55-62 - <http://www.internationalshoulderjournal.org/text.asp?2010/4/3/55/76960> and (right) Start radiology – Ultrasound Technique - <http://www.startradiology.com/the-basics/ultrasound-technique/>

A.3. Vascular graphs



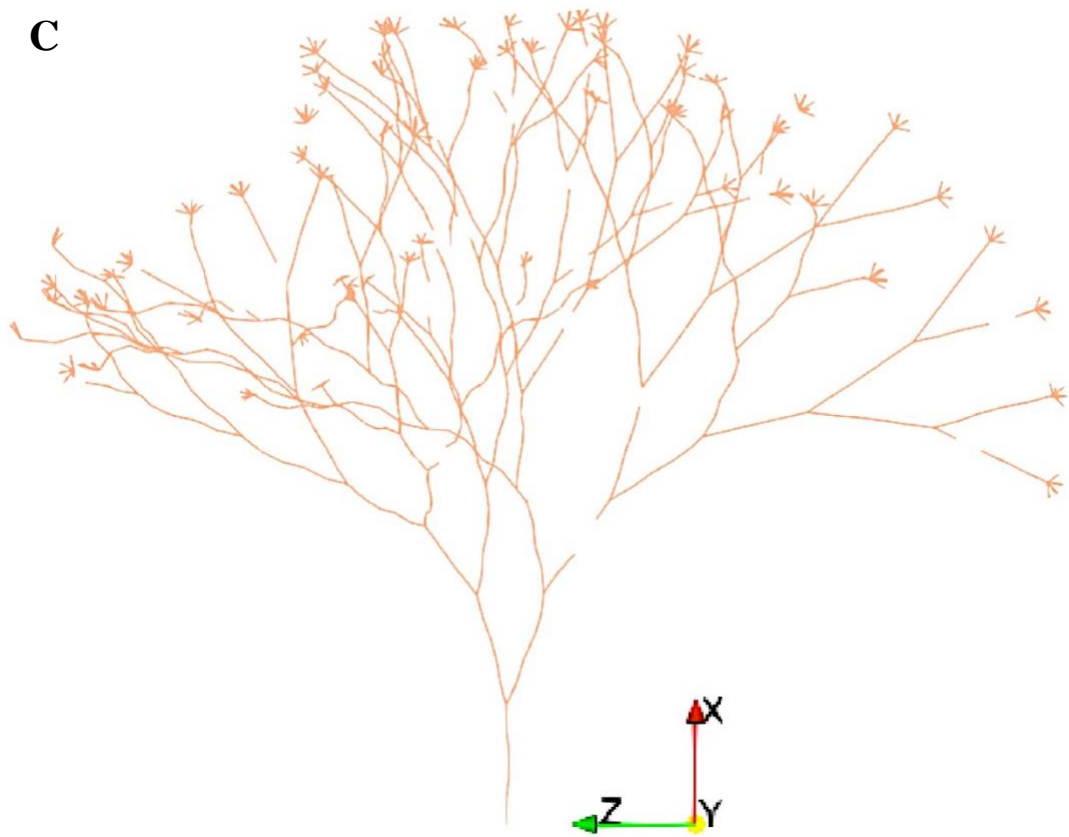


Figure 25. Bigger images of vascular graphs used for placental vascular reconstruction. A: Ground truth; B: Oriented graph (Graph 1); C: Pruned graph (Graph 2).

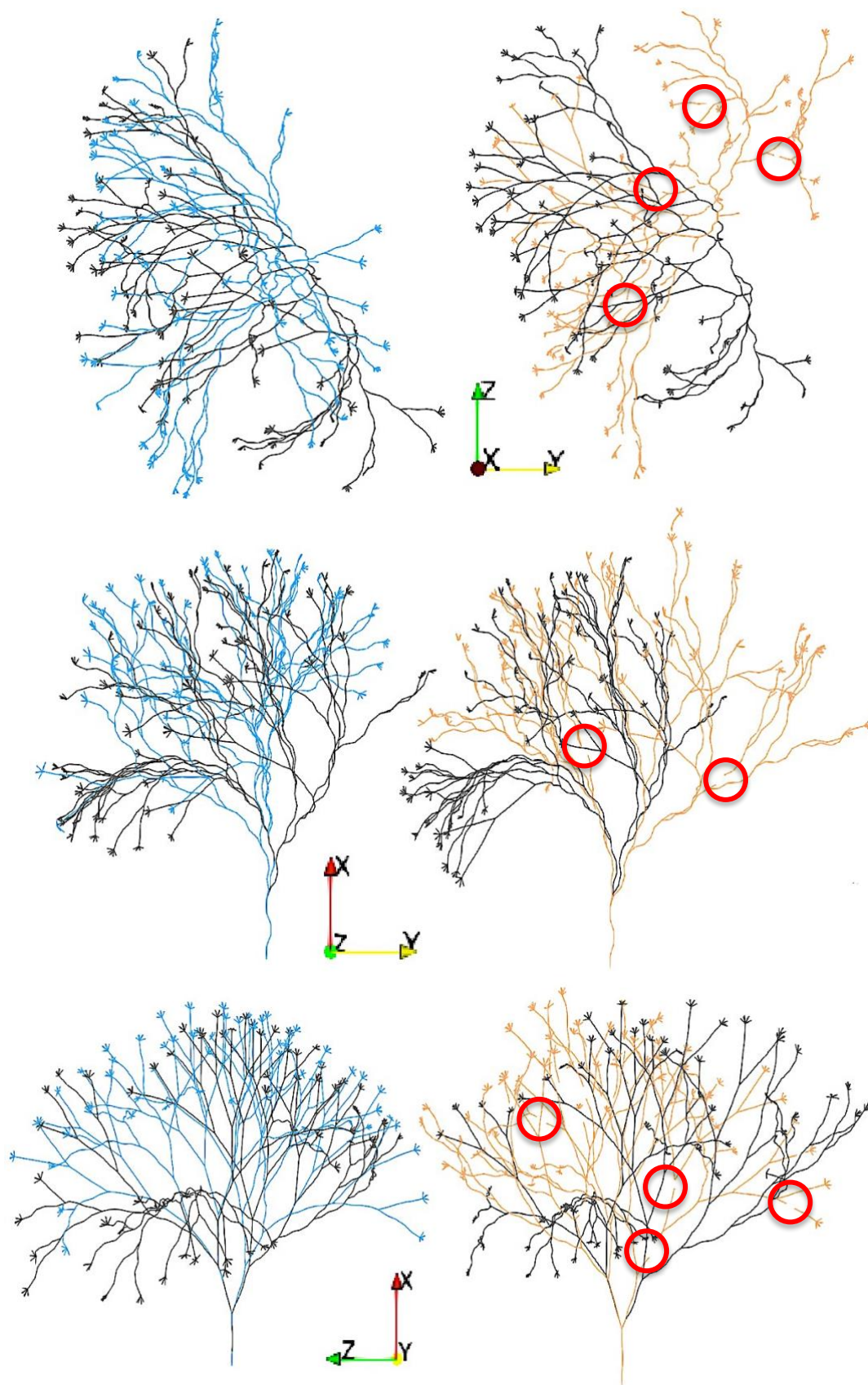


Figure 26. Structural differences between ground truth in grey and deformed graphs: (left) Graph 1 in blue and ground truth comparison and (right) Graph 2 in orange and ground truth comparison. On Graph 2 some non-connected edges can be seen on red circles.

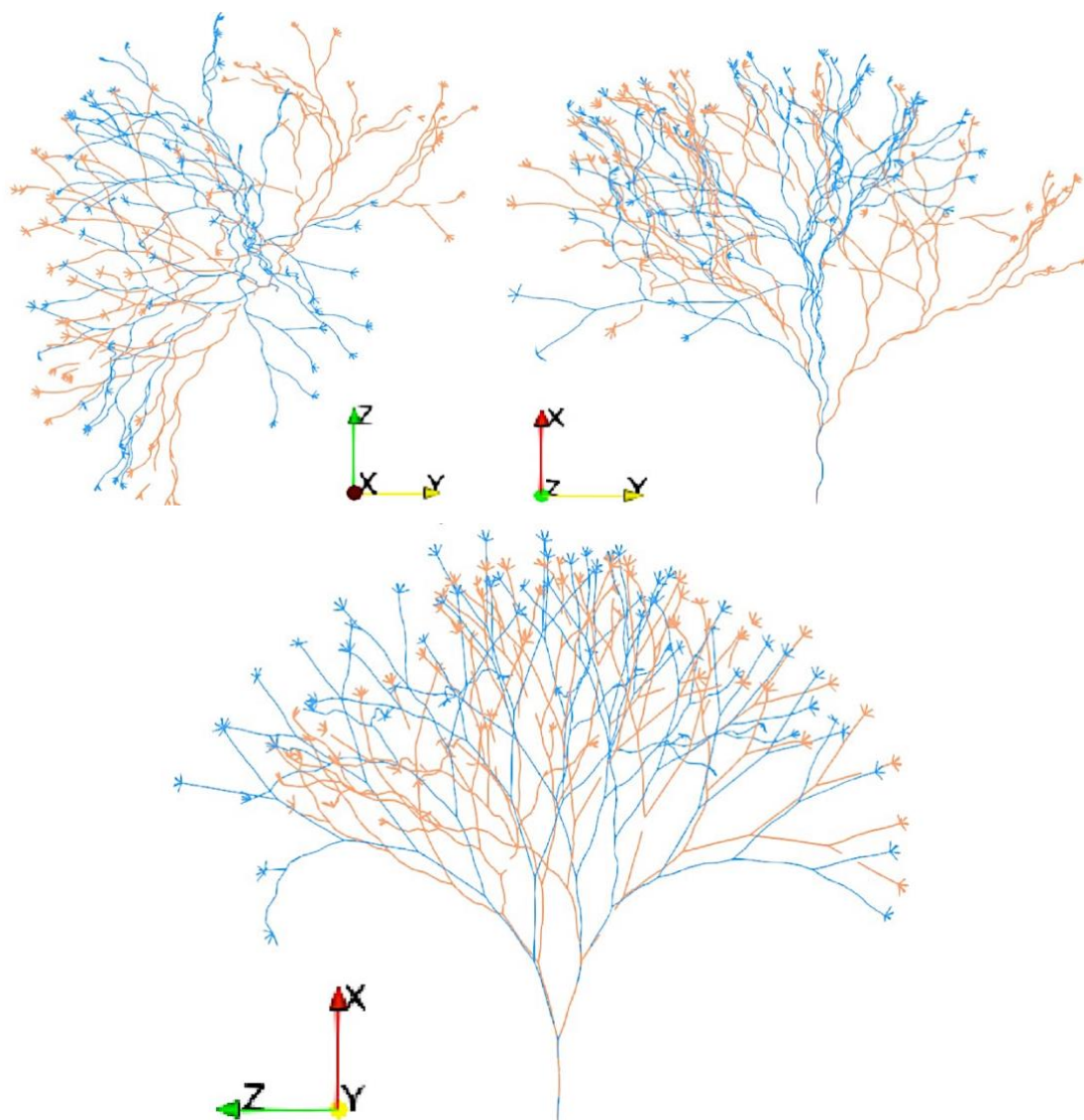


Figure 27. Structural differences between Graph 1 (bleu) and Graph 2 (orange)

A.4. Developed MITK Plugin

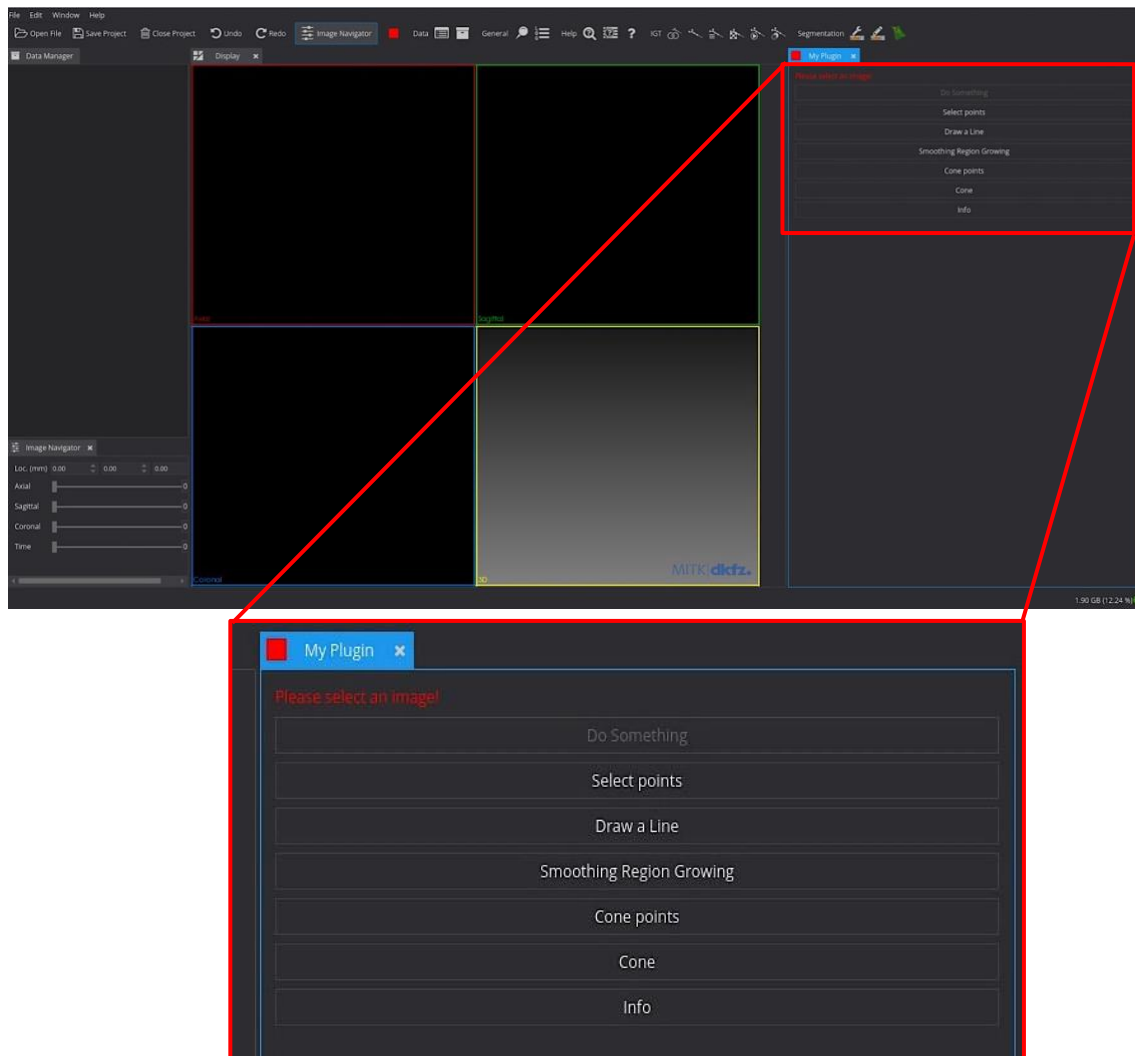
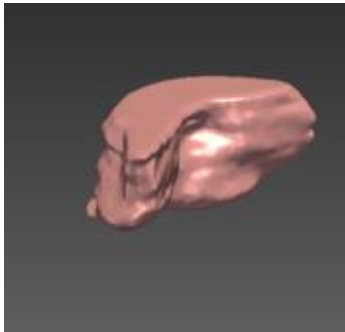
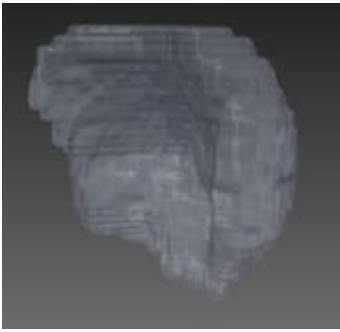
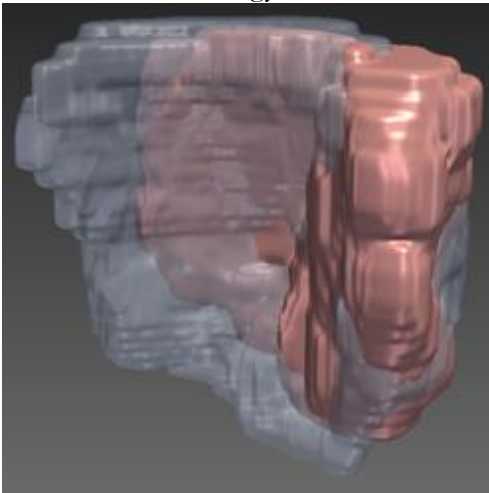
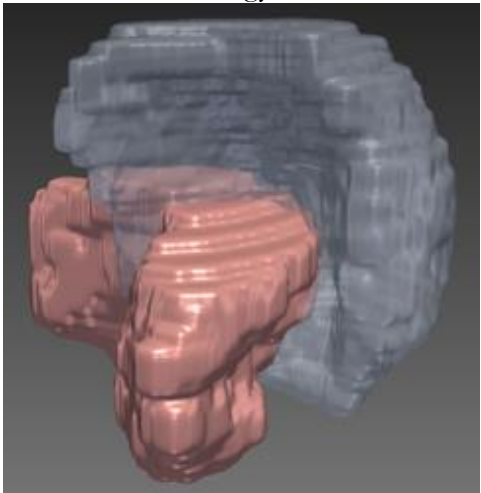
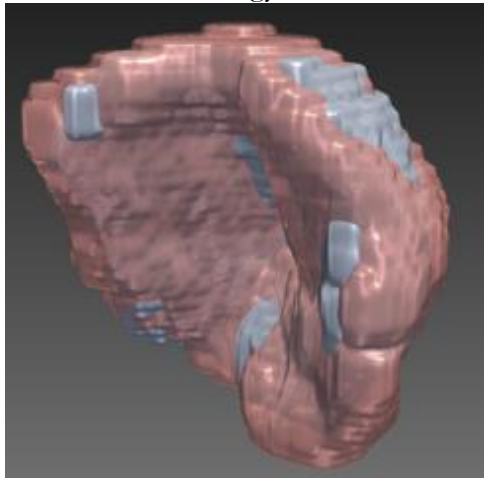
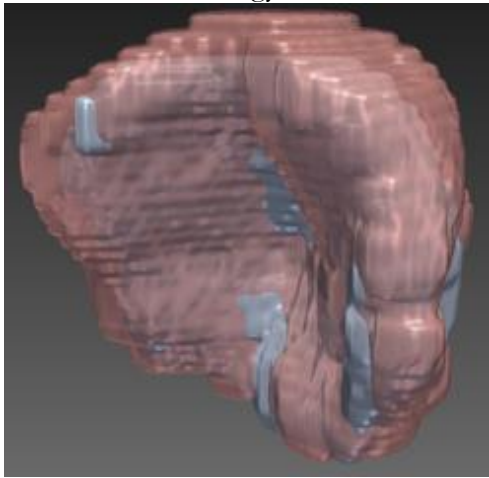


Figure 28. Bigger image of the developed MITK Plugin for measuring the umbilical cord insertion distances. My Plugin is the workspace created for measuring distances between selected points. There are other functions (Smoothing Region Growing, Cone points and Cone) that were used for understanding how MITK programming works.

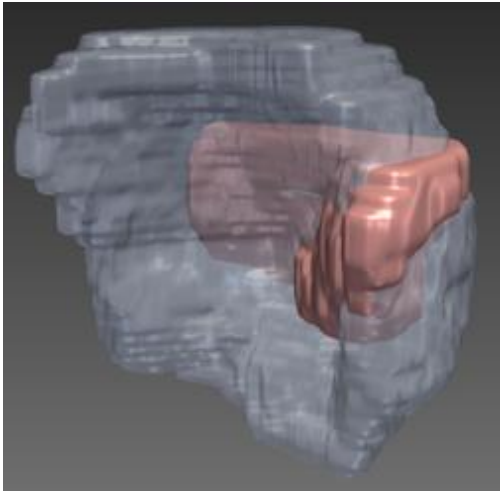
A.5. Registration results from all patients

Table 5. Placenta results from all patient after applying each Registration Strategy (transformed US placenta in pink and MR placenta in grey). There are 10 patients, and each one of them has the initial information about the conformation of US and MR placentas and results from each Strategy and Sub-strategy.

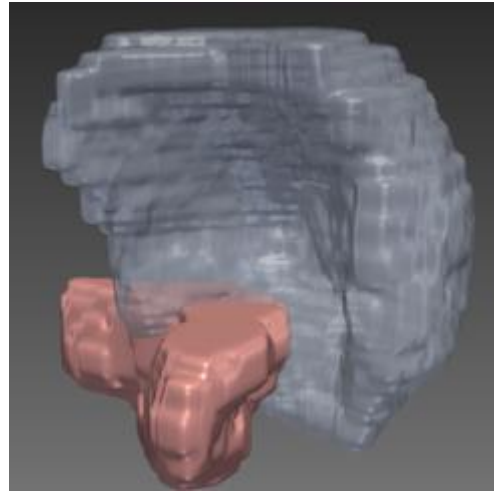
PATIENTS	
Patient 1	
Initial US 	Initial MR 
Strategy 1	
Strategy 1a 	Strategy 1b 
Strategy 1c 	Strategy 1c 

Strategy 2

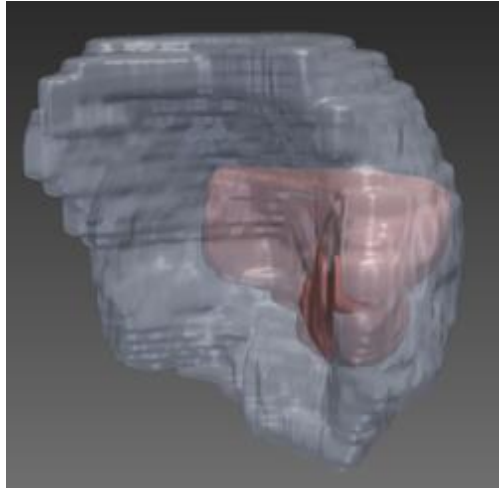
Strategy 2a



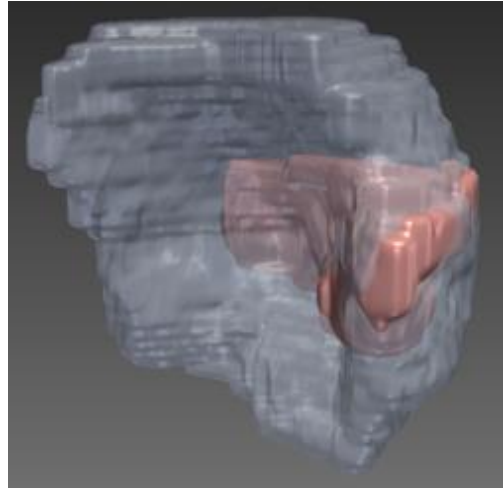
Strategy 2b



Strategy 2c

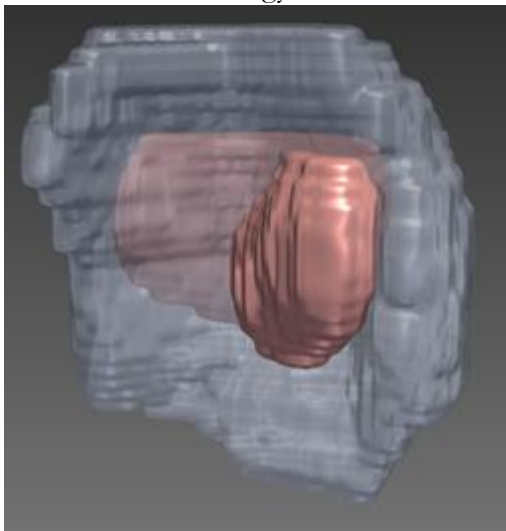


Strategy 2d

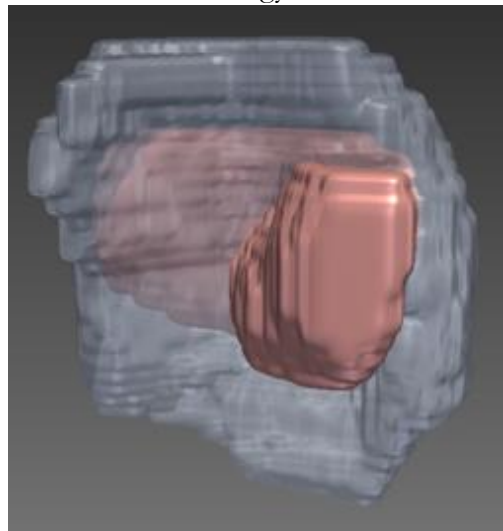


Strategy 3

Strategy 3a



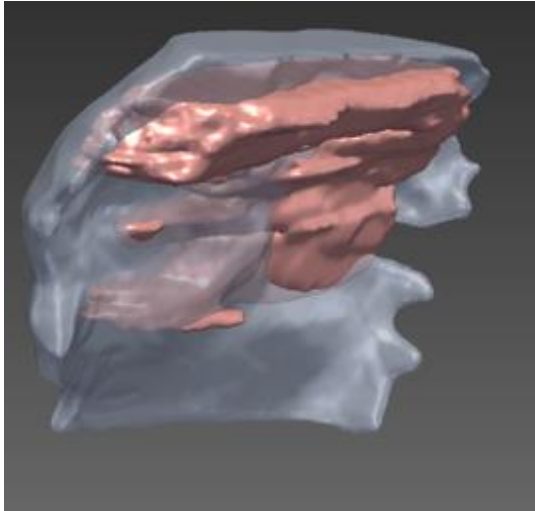
Strategy 3b



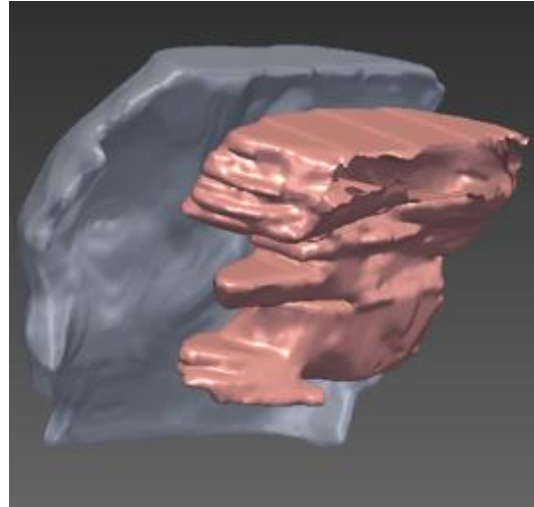
Patient 2	
Initial US	Initial MR
Strategy 1	
Strategy 1a	Strategy 1b
Strategy 1c	Strategy 1c

Strategy 2

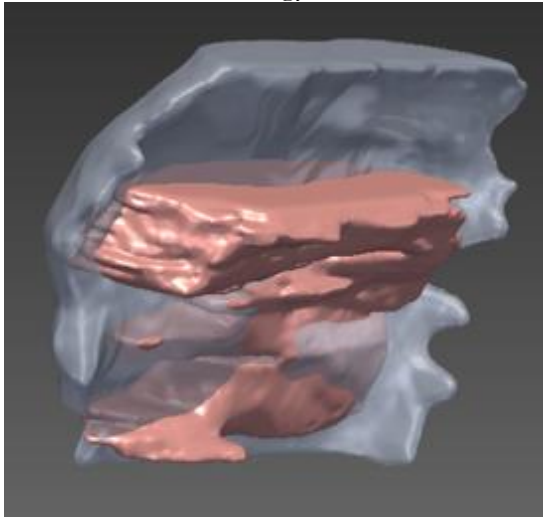
Strategy 2a



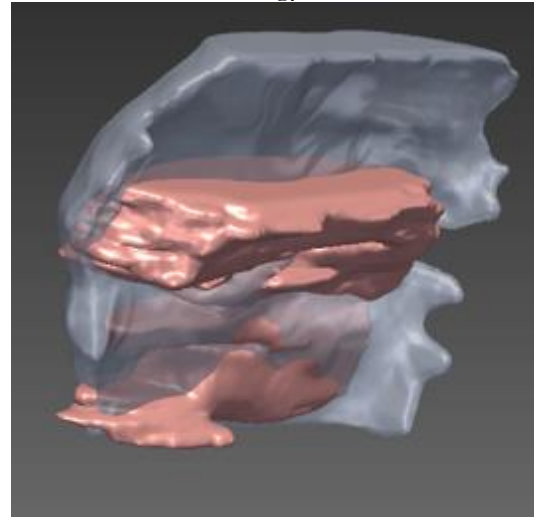
Strategy 2b



Strategy 2c

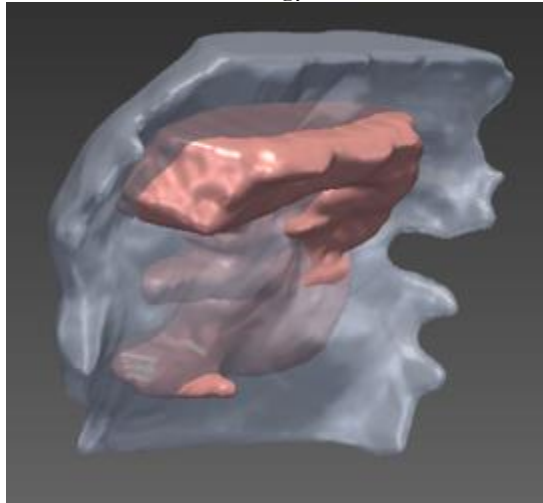


Strategy 2d

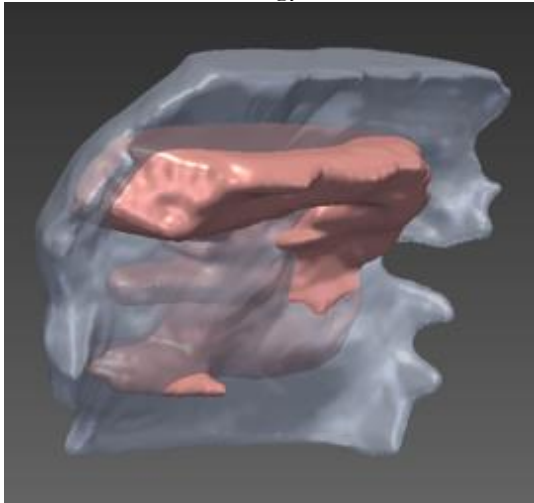


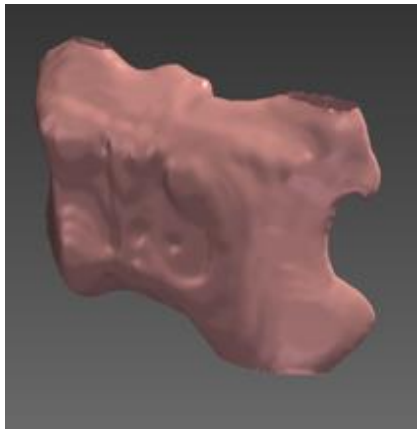
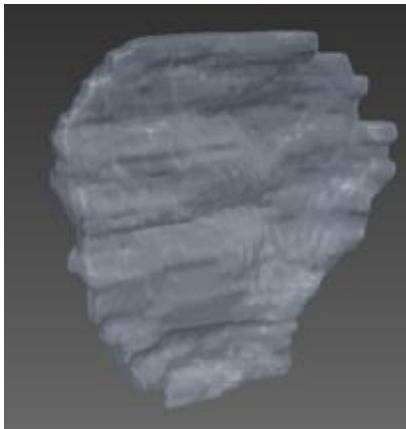
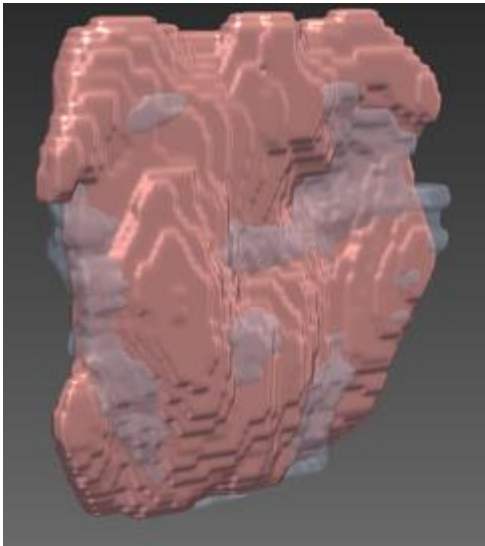
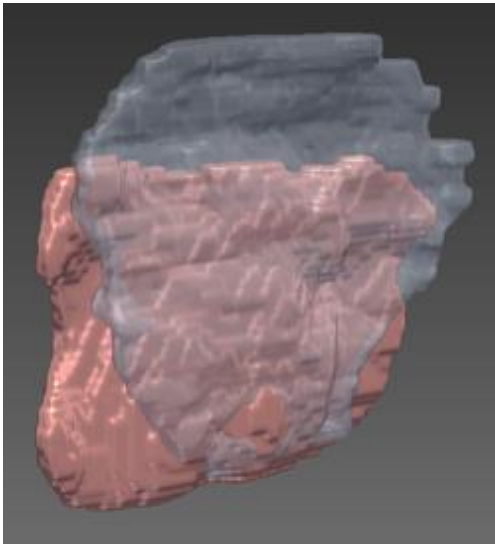
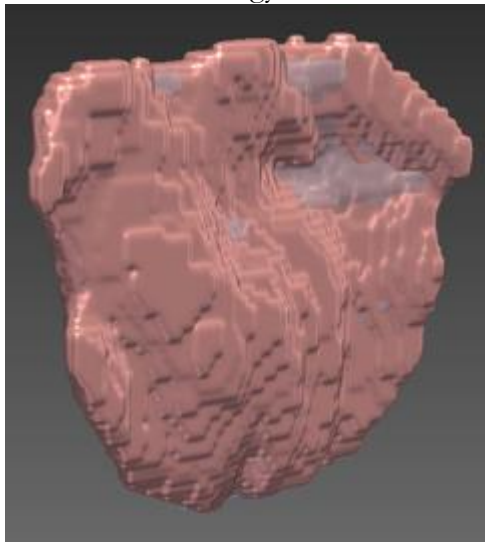
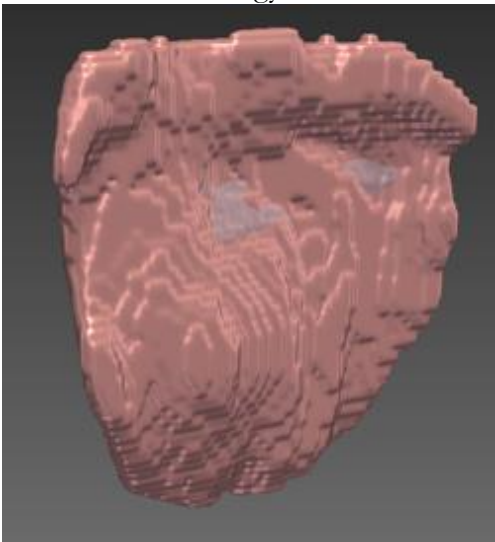
Strategy 3

Strategy 3a



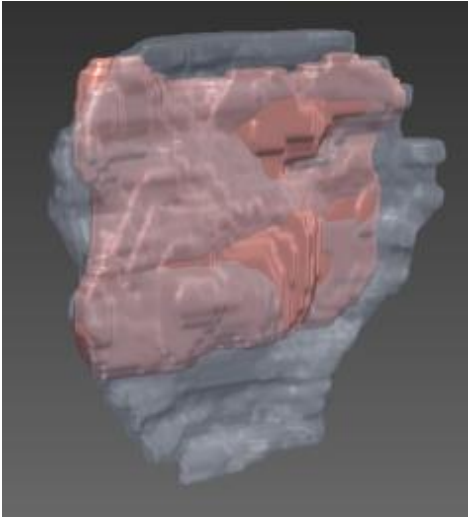
Strategy 3b



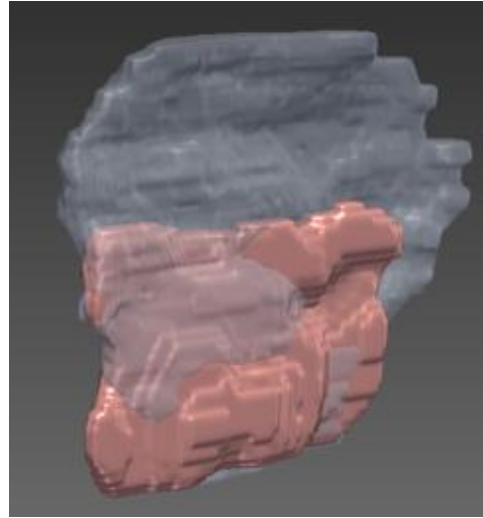
Patient 3	
Initial US 	Initial MR 
Strategy 1	
Strategy 1a 	Strategy 1b 
Strategy 1c 	Strategy 1c 

Strategy 2

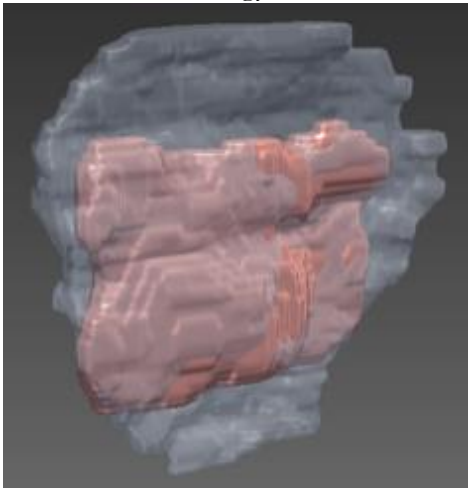
Strategy 2a



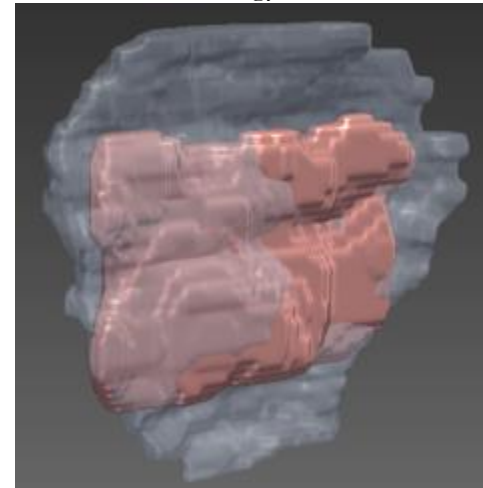
Strategy 2b



Strategy 2c

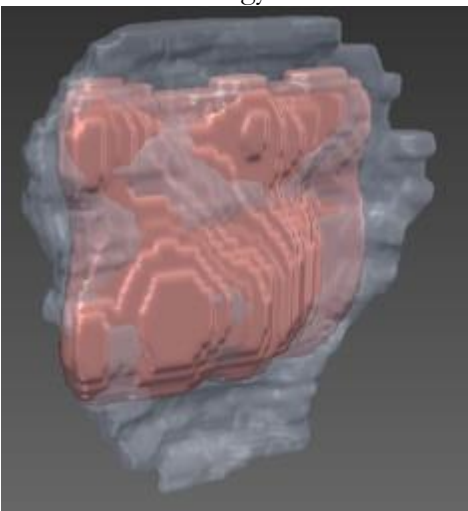


Strategy 2d

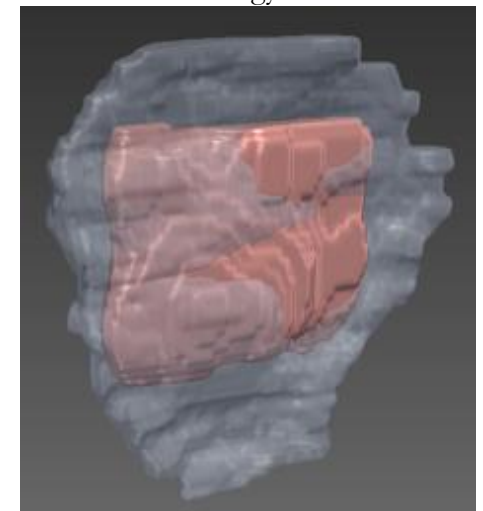


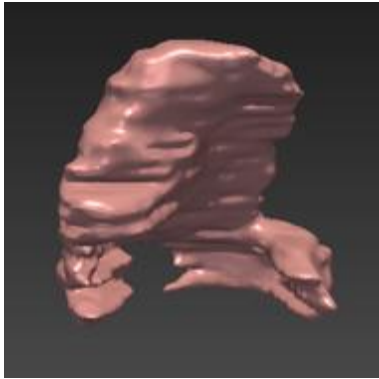
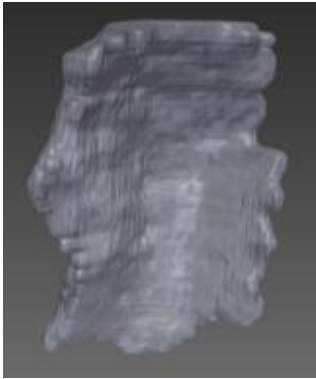
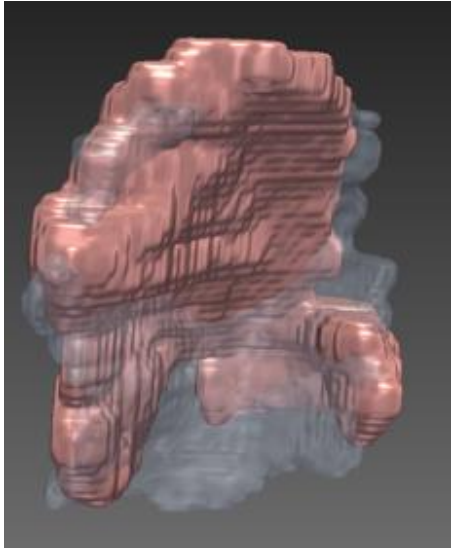
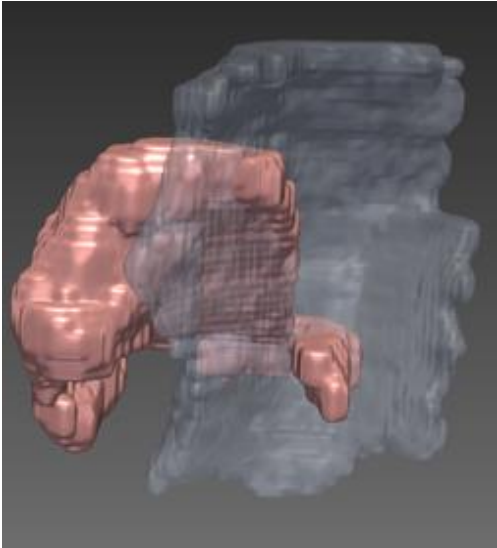
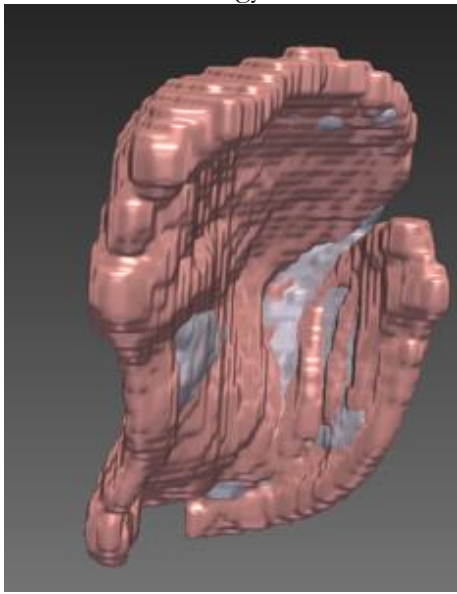
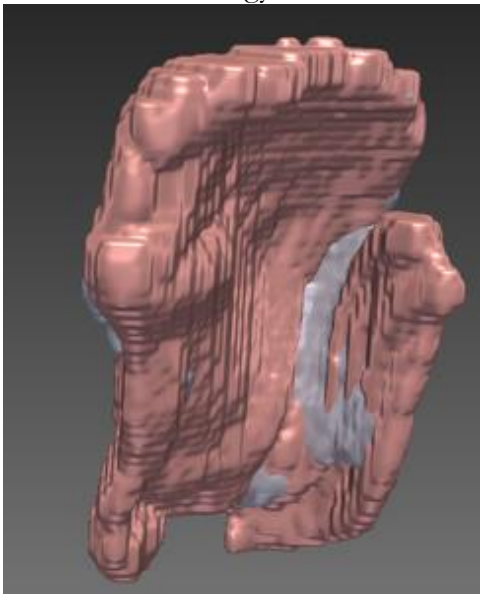
Strategy 3

Strategy 3a



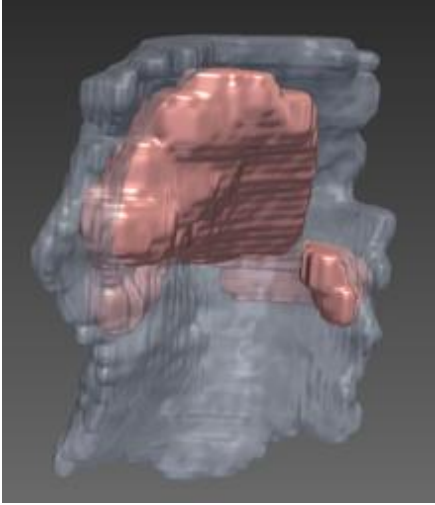
Strategy 3b



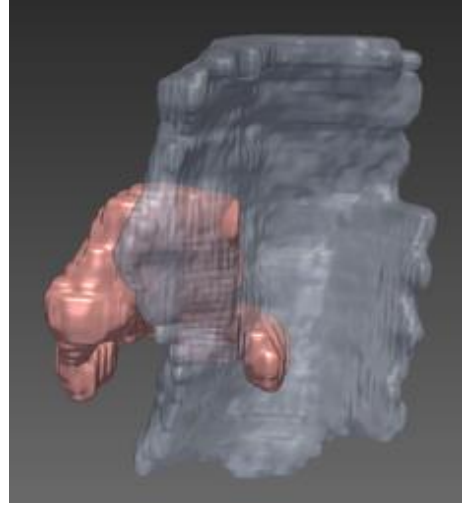
Patient 4	
<p>Initial US</p> 	<p>Initial MR</p> 
Strategy 1	
<p>Strategy 1a</p> 	<p>Strategy 1b</p> 
<p>Strategy 1c</p> 	<p>Strategy 1d</p> 

Strategy 2

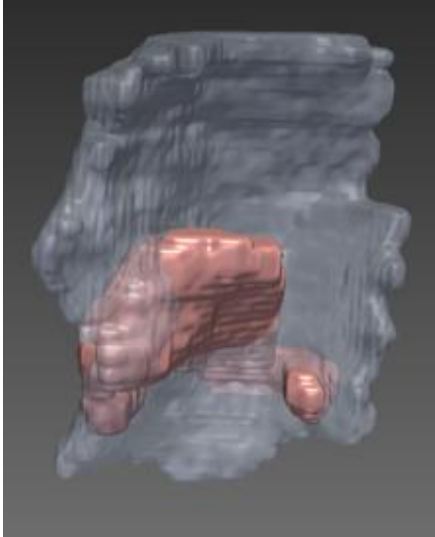
Strategy 2a



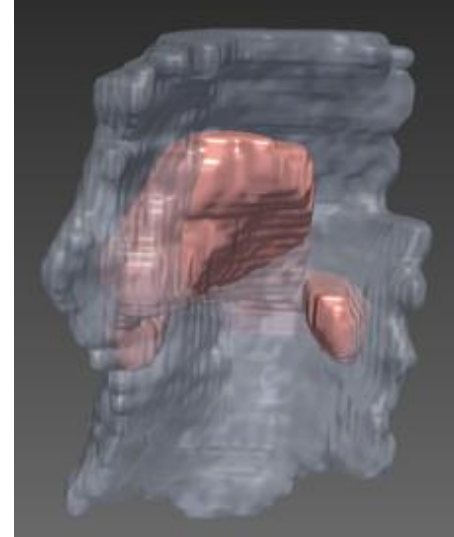
Strategy 2b



Strategy 2c

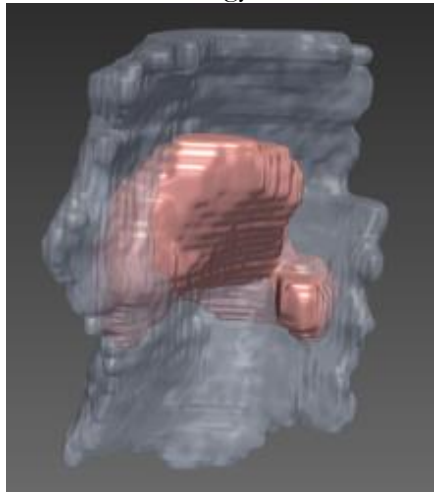


Strategy 2d

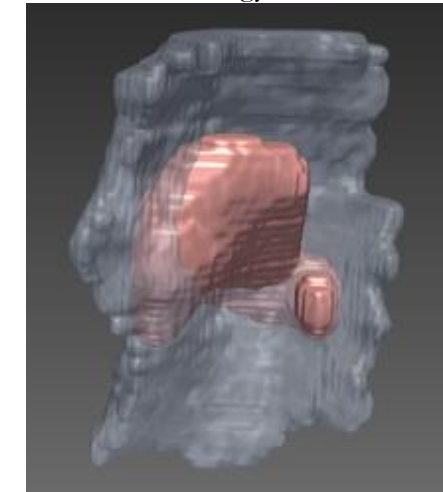


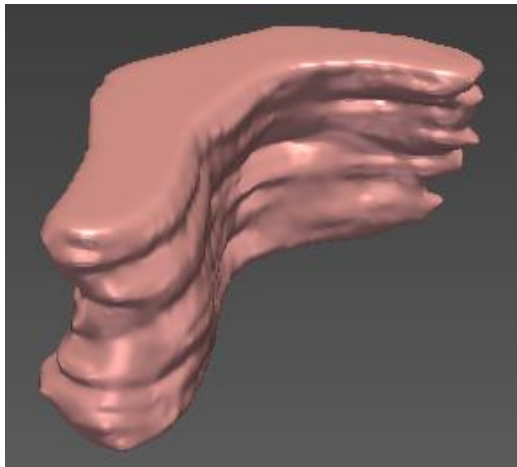
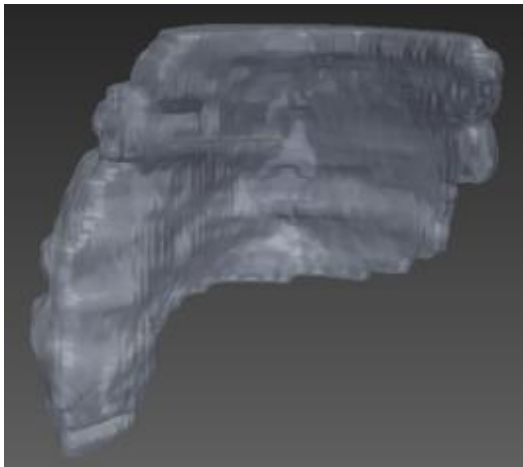
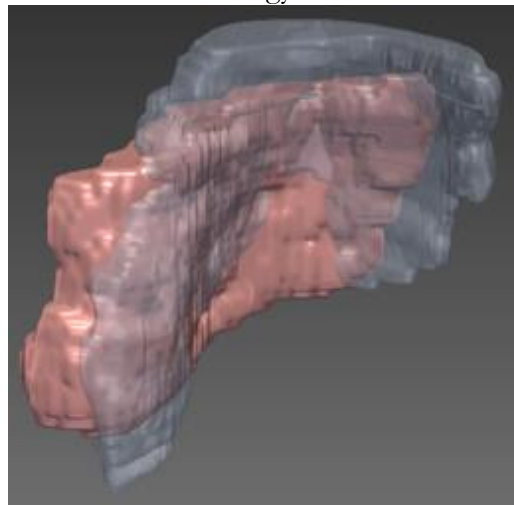
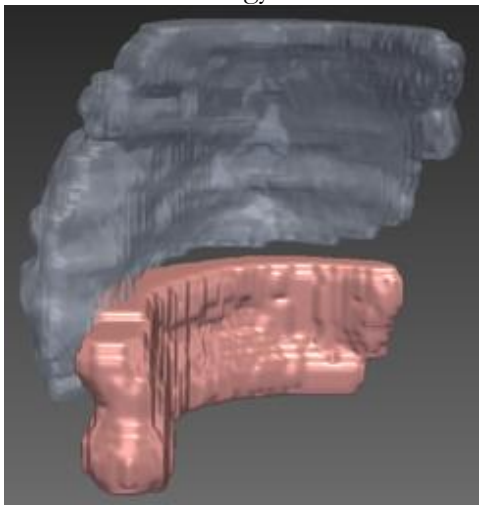
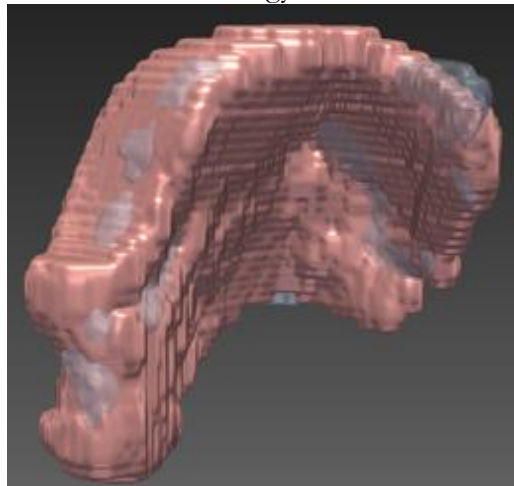
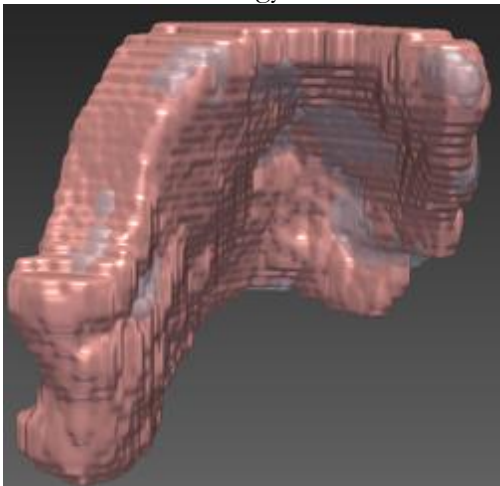
Strategy 3

Strategy 3a



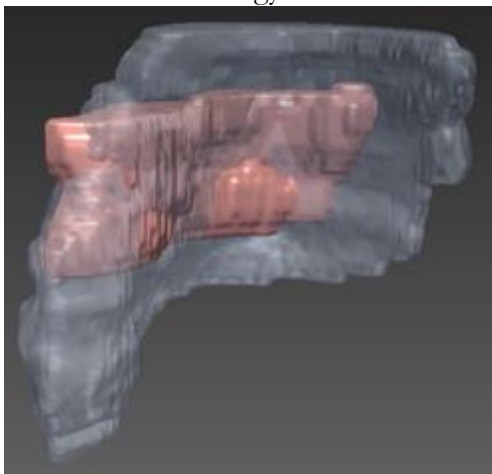
Strategy 3b



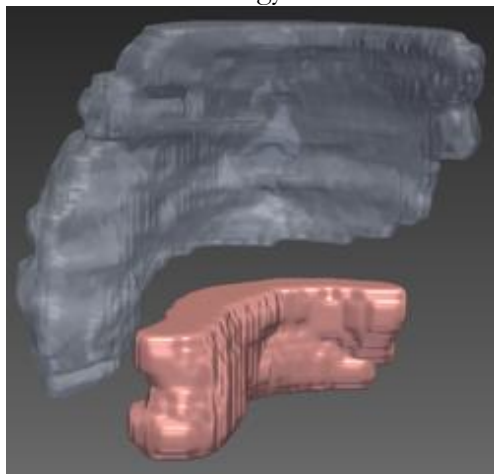
Patient 5	
Initial US 	Initial MR 
Strategy 1	
Strategy 1a 	Strategy 1b 
Strategy 1c 	Strategy 1c 

Strategy 2

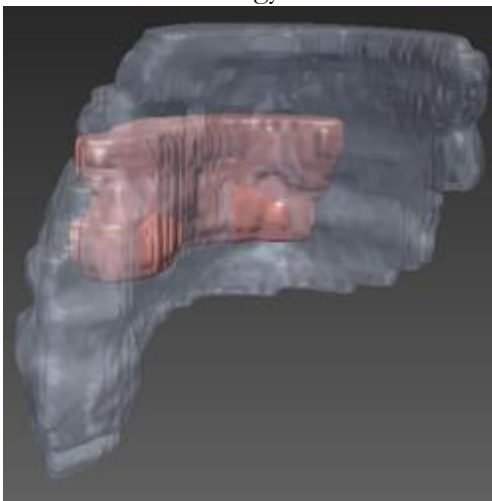
Strategy 2a



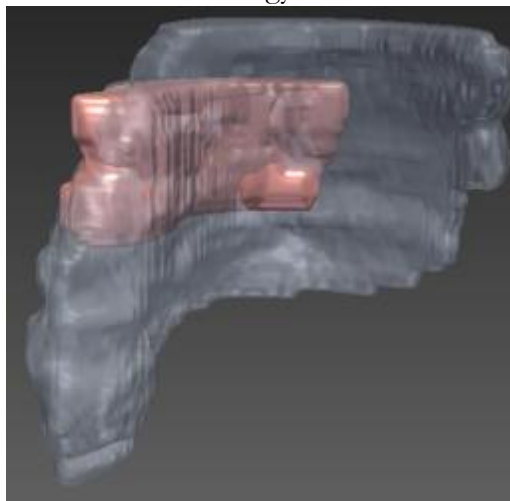
Strategy 2b



Strategy 2c

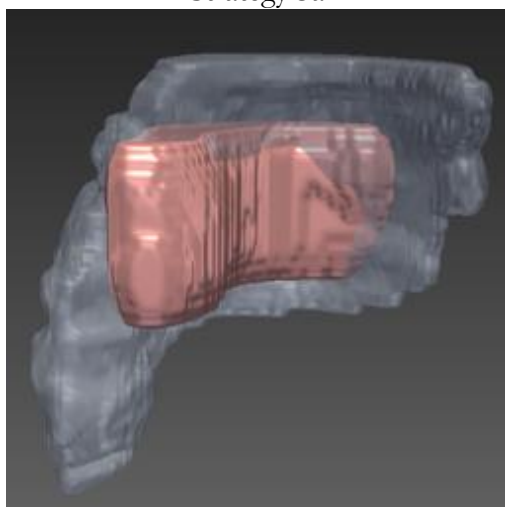


Strategy 2d

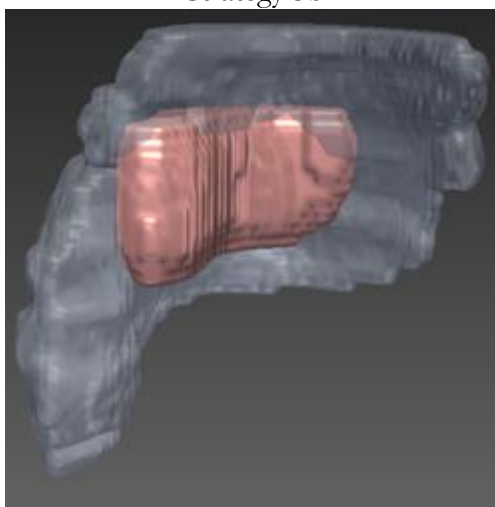


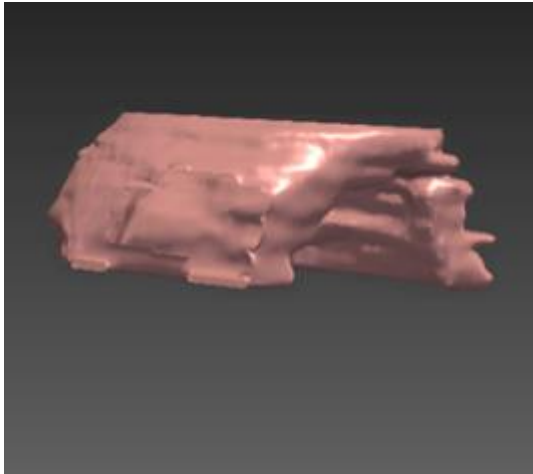
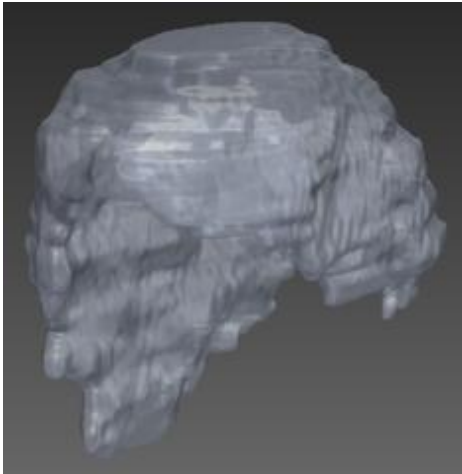
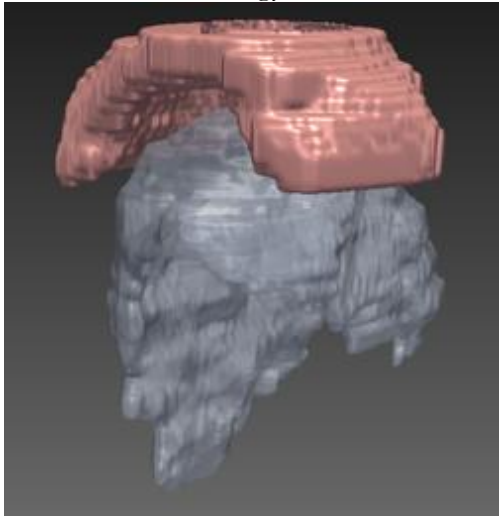
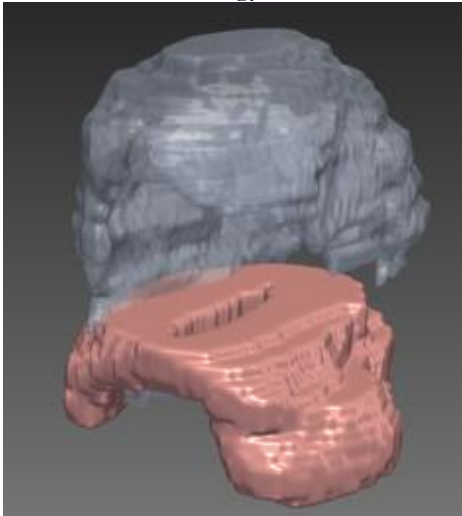
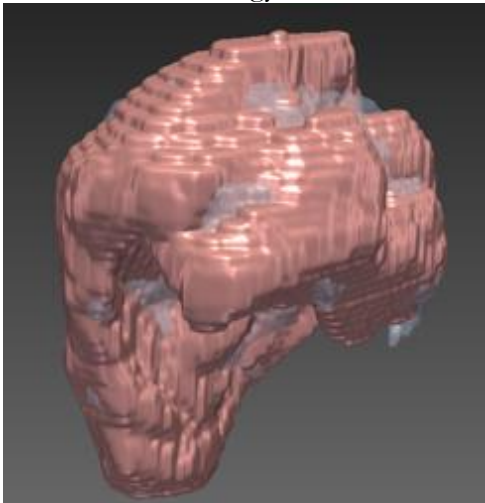
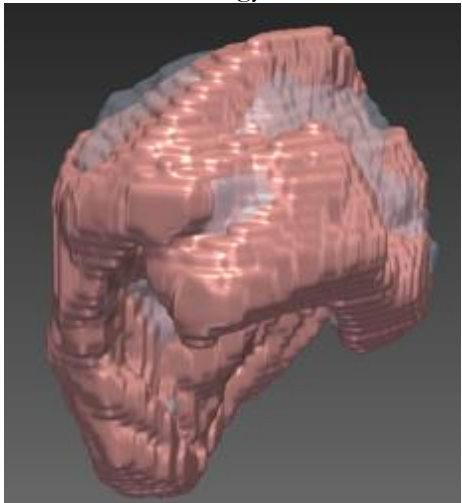
Strategy 3

Strategy 3a



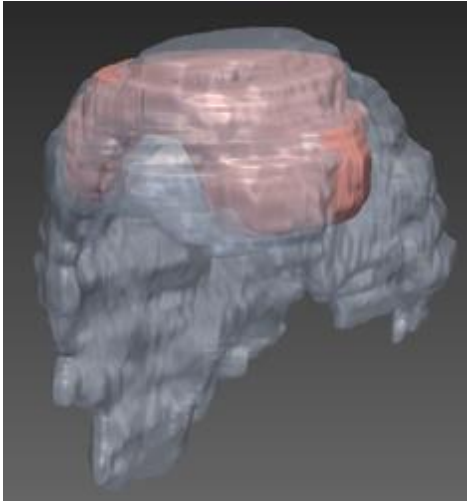
Strategy 3b



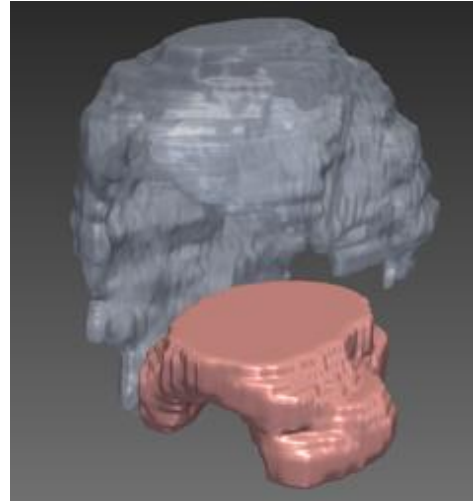
Patient 6	
Initial US 	Initial MR 
Strategy 1	
Strategy 1a 	Strategy 1b 
Strategy 1c 	Strategy 1c 

Strategy 2

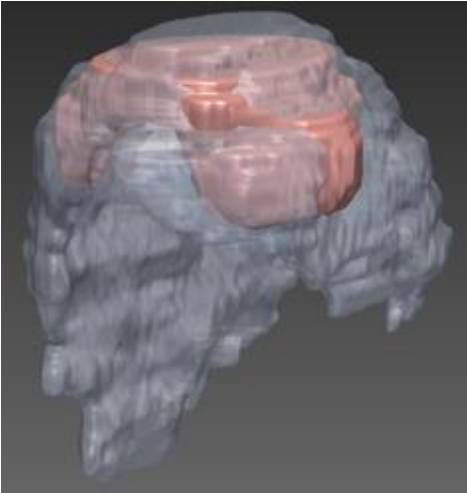
Strategy 2a



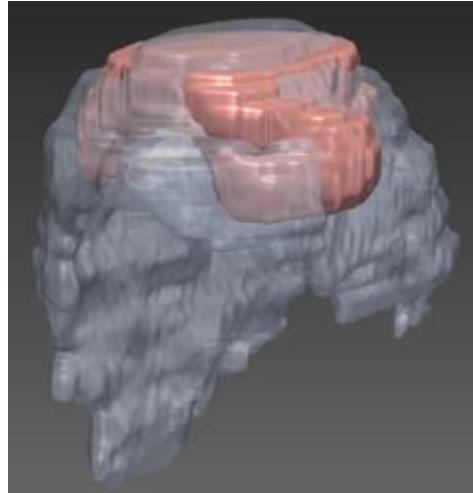
Strategy 2b



Strategy 2b

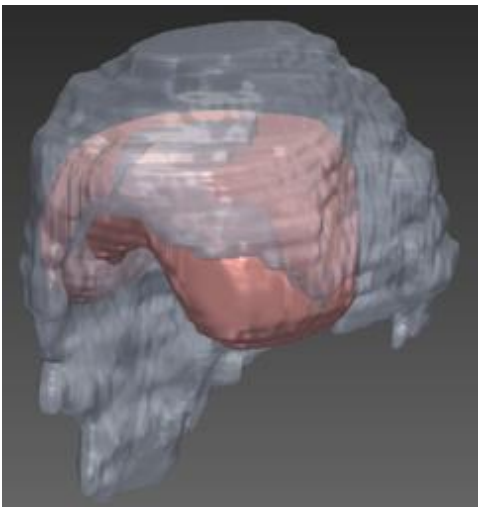


Strategy 2d

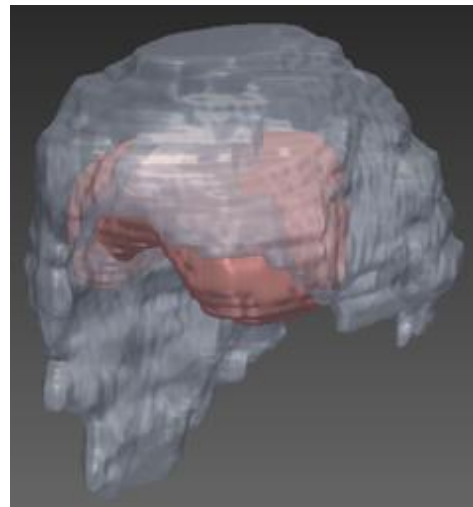


Strategy 3

Strategy 3a



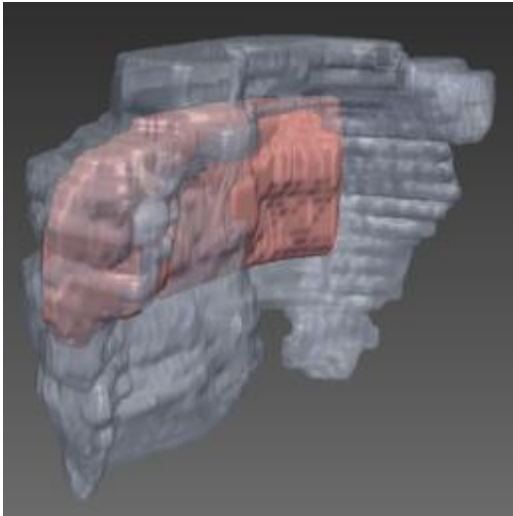
Strategy 3b



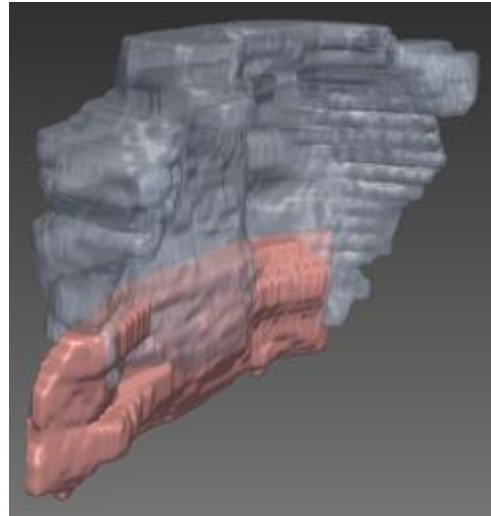
Patient 7	
Initial US	Initial MR
Strategy 1	
Strategy 1a	Strategy 1b
Strategy 1c	Strategy 1c

Strategy 2

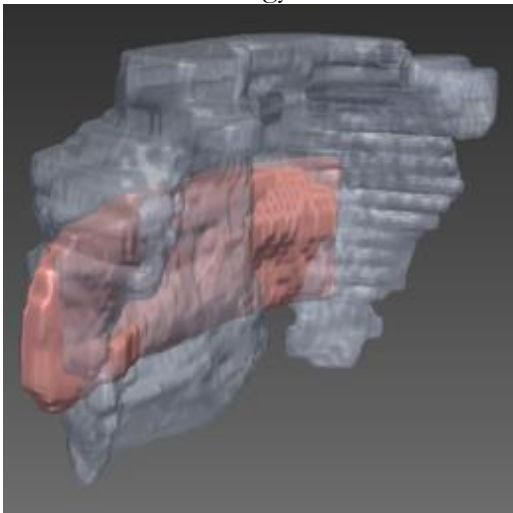
Strategy 2a



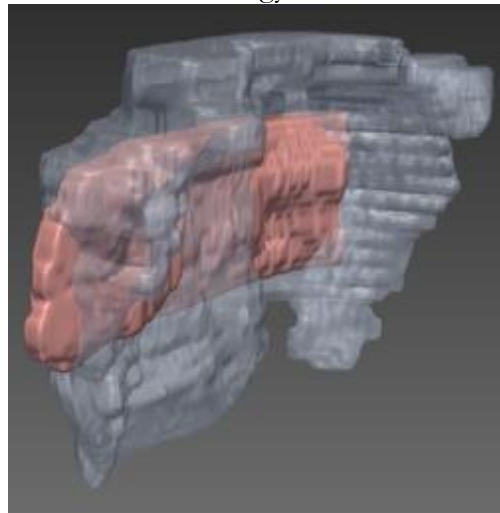
Strategy 2b



Strategy 2b

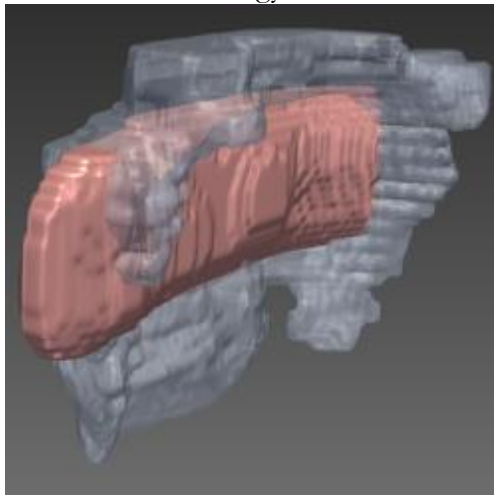


Strategy 2d

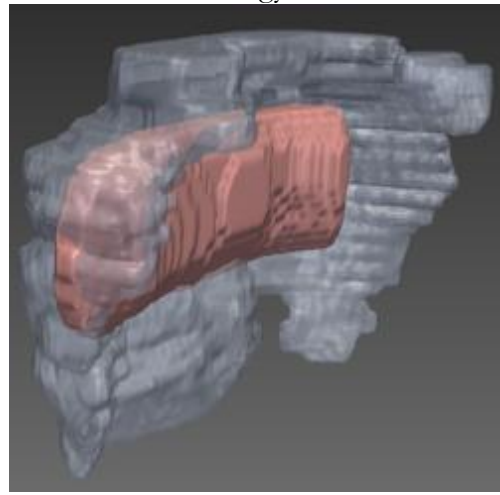


Strategy 3

Strategy 3a



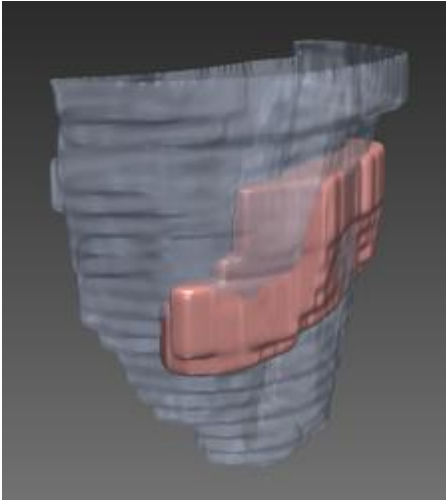
Strategy 3b



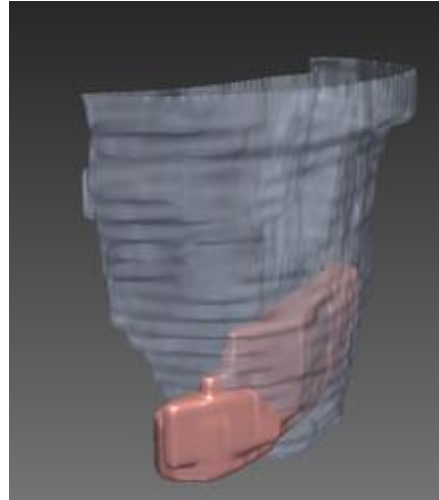
Patient 8	
Initial US	Initial MR
Strategy 1	
Strategy 1a	Strategy 1b
Strategy 1c	Strategy 1c

Strategy 2

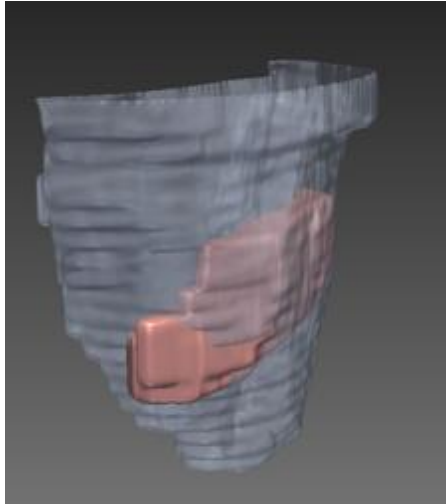
Strategy 2a



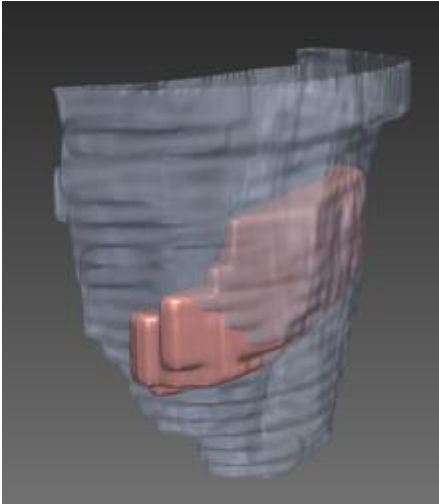
Strategy 2b



Strategy 2b

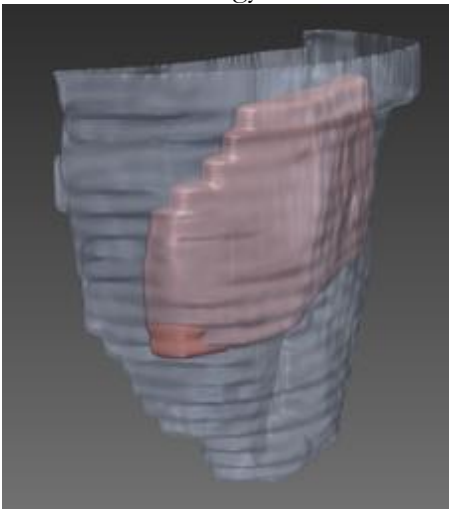


Strategy 2d

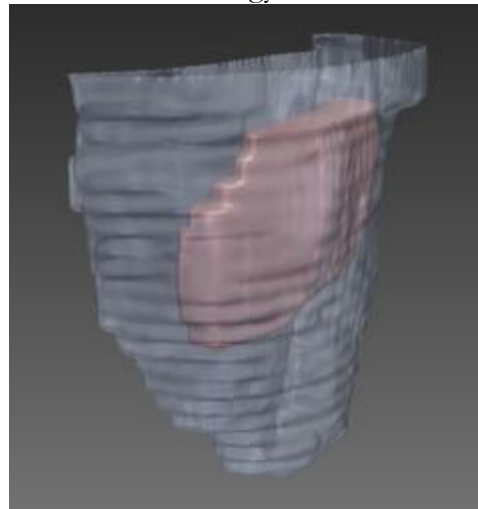


Strategy 3

Strategy 3a



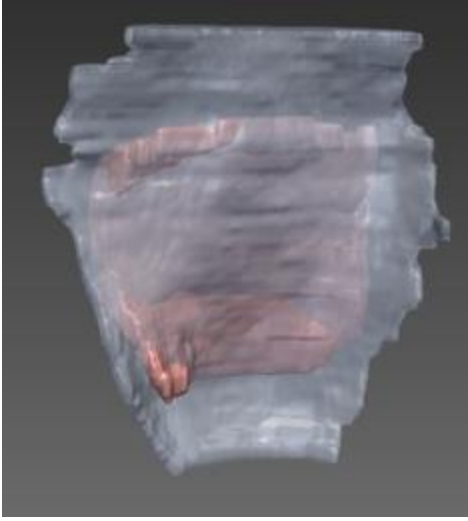
Strategy 3b



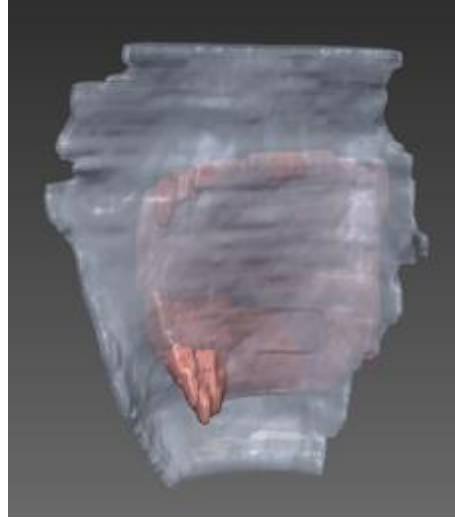
Patient 9	
Initial US	Initial MR
Strategy 1	
Strategy 1a	Strategy 1b
Strategy 1c	Strategy 1c

Strategy 2

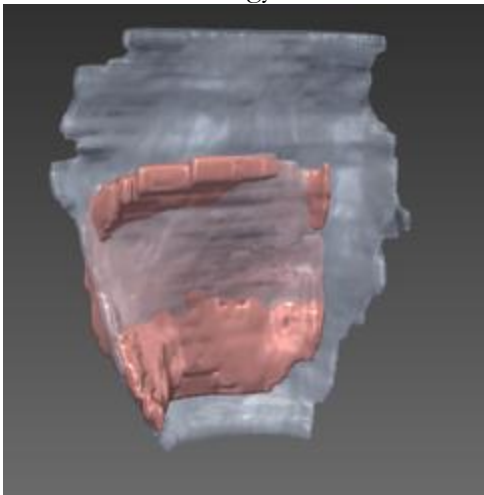
Strategy 2a



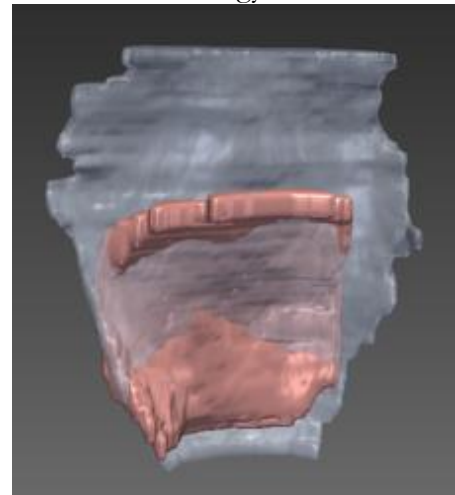
Strategy 2b



Strategy 2b

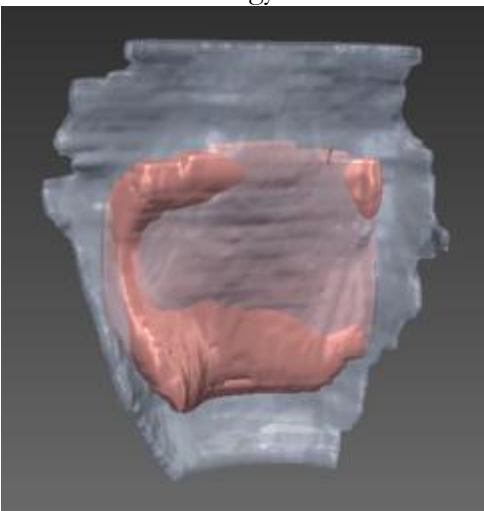


Strategy 2d

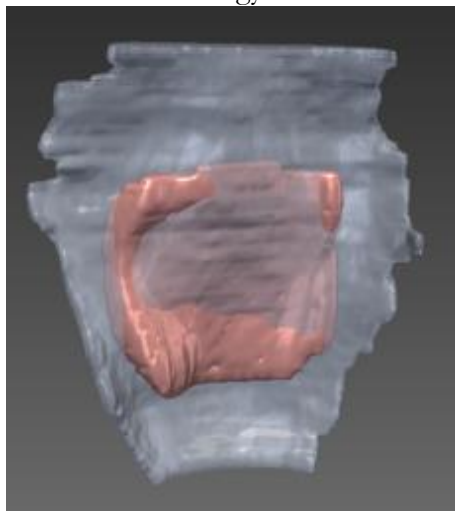


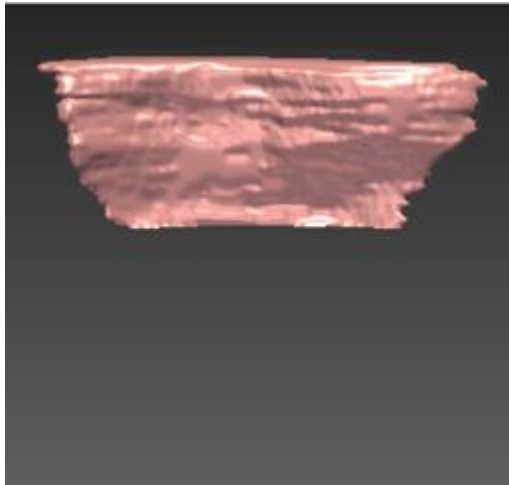
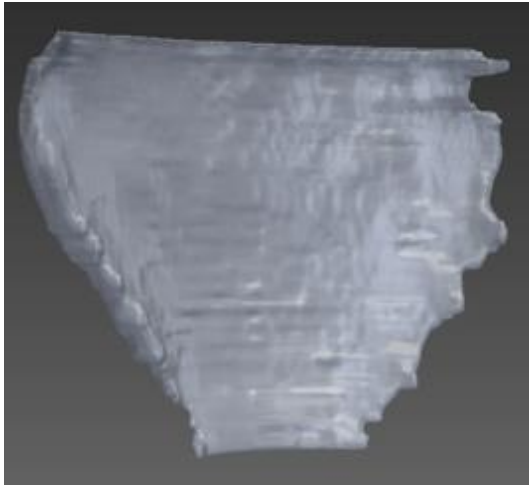
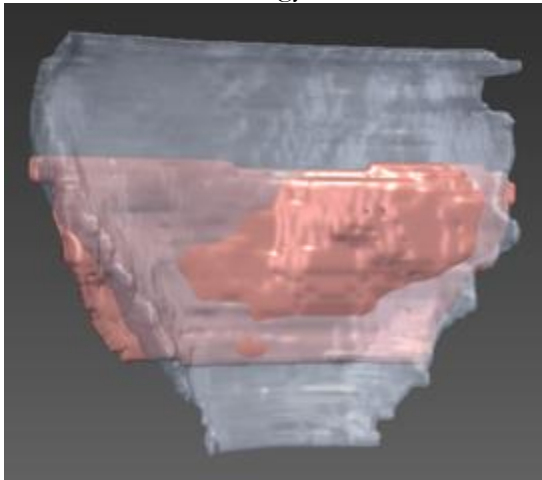
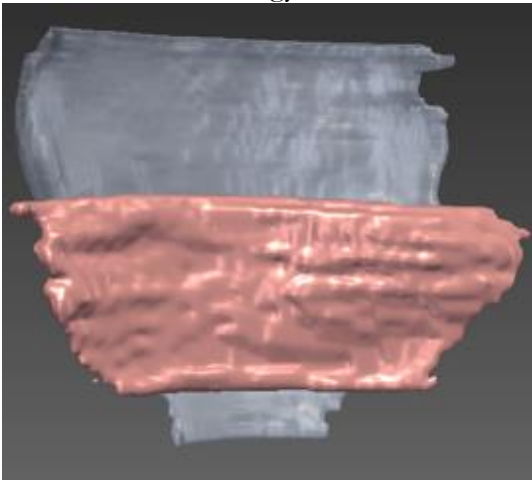
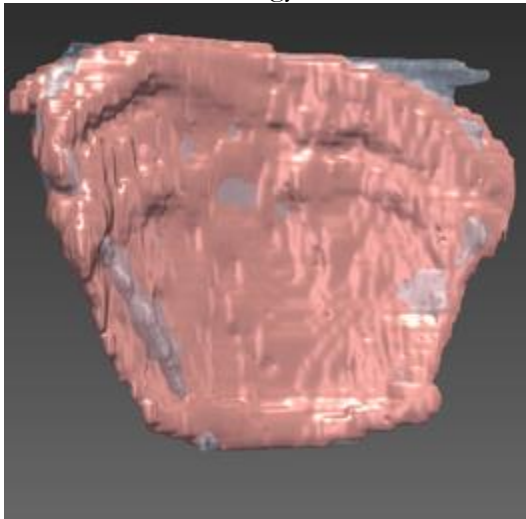
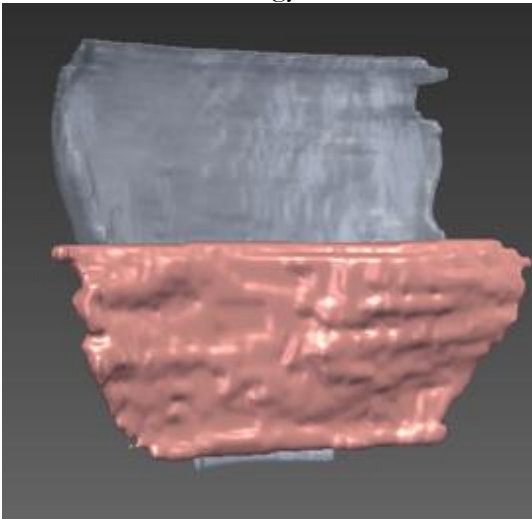
Strategy 3

Strategy 3a



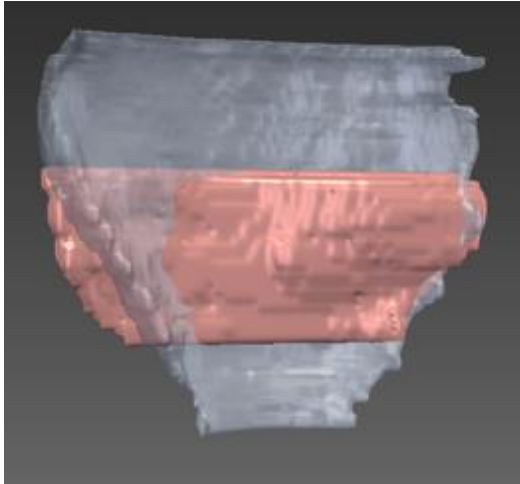
Strategy 3b



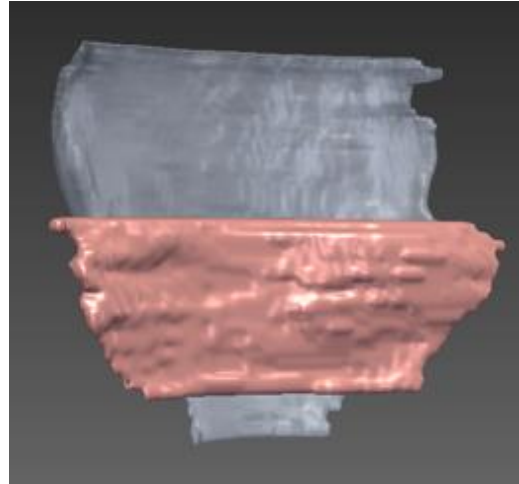
Patient 10	
Initial US 	Initial MR 
Strategy 1	
Strategy 1a 	Strategy 1b 
Strategy 1c 	Strategy 1c 

Strategy 2

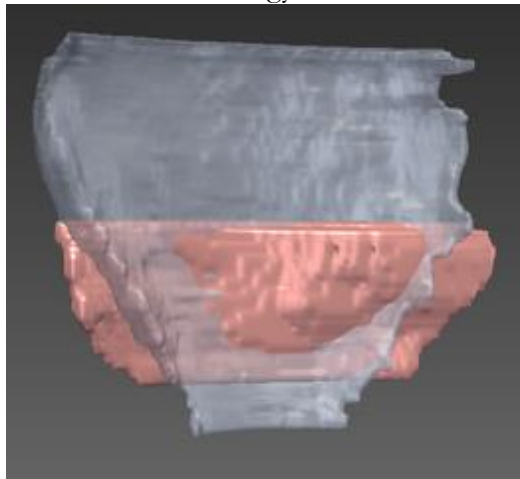
Strategy 2a



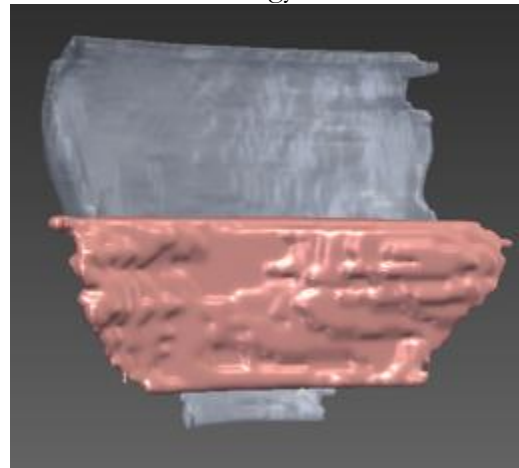
Strategy 2b



Strategy 2b

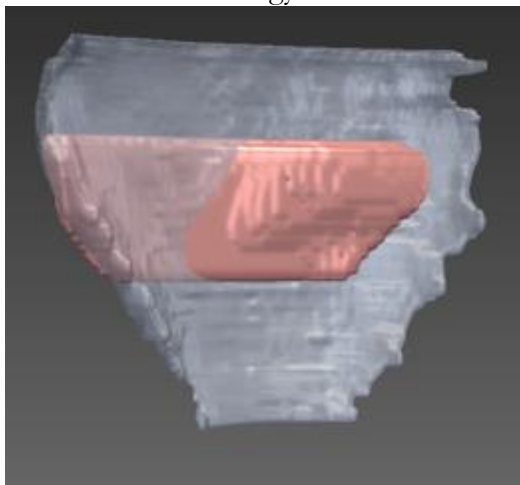


Strategy 2d



Strategy 3

Strategy 3a



Strategy 3b

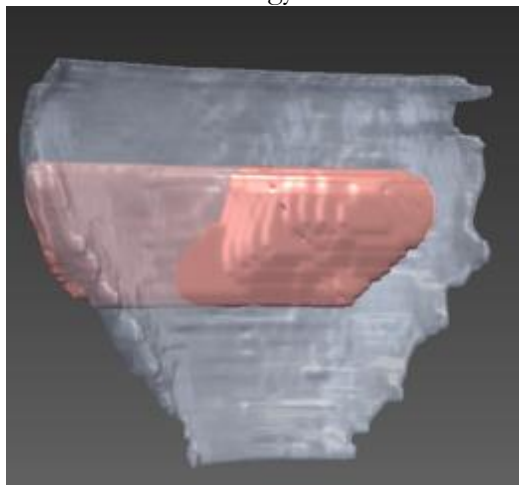
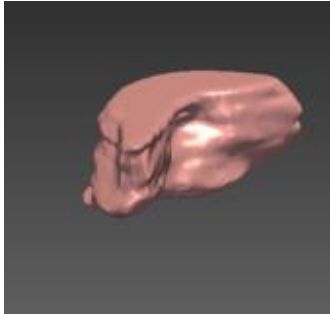
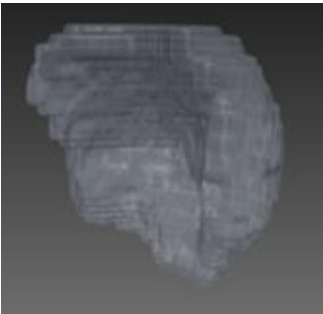
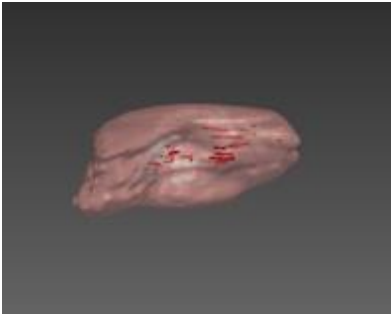
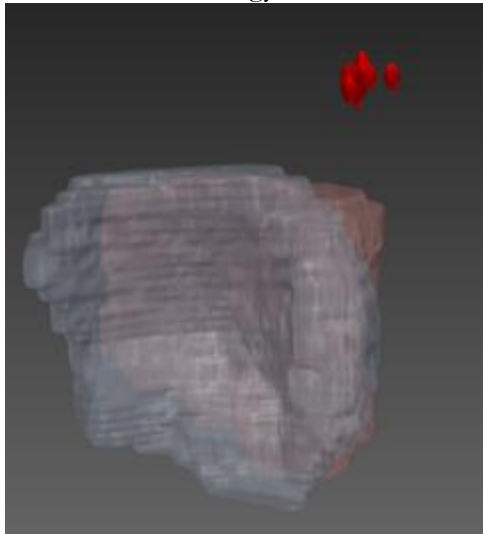
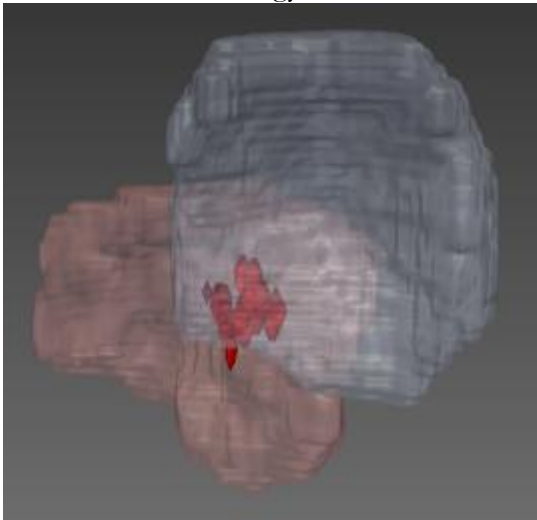
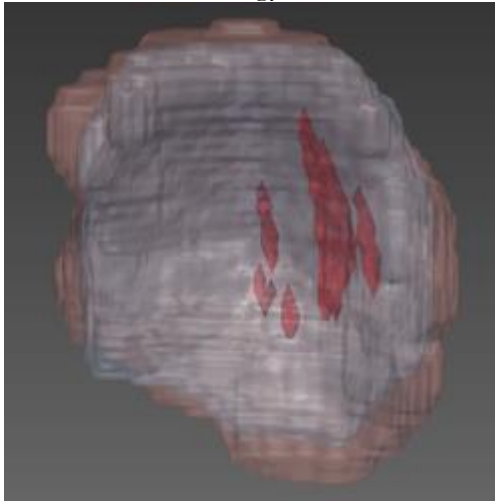
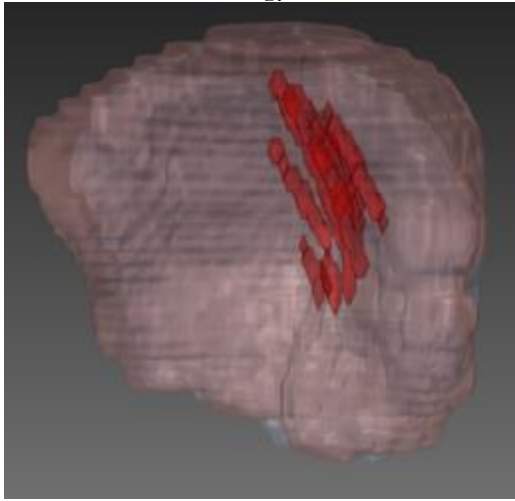
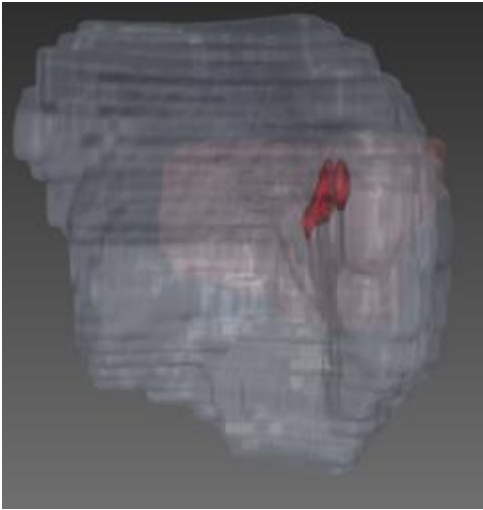


Table 6. Vessels results from all patient after applying each Registration Strategy (transformed US placenta in pink, MR placenta in grey and vessels in red). There are 10 patients, and each one of them has the initial information about the conformation of US placenta and vessels and results from each Strategy and Sub-strategy.

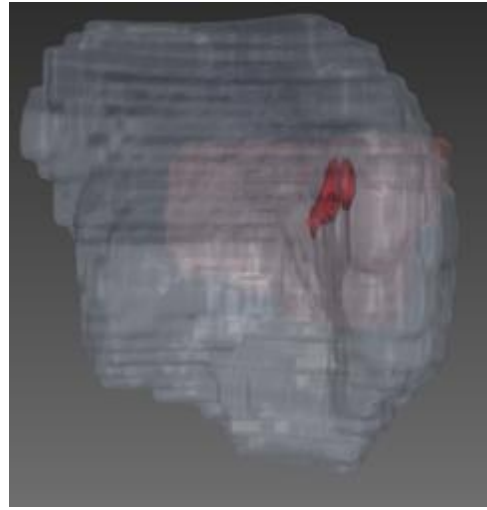
PATIENTS		
Patient 1		
Initial US	Initial MR	Initial US vessels
		
Strategy 1		
Strategy 1a	Strategy 1b	
		
Strategy 1c	Strategy 1d	
		

Strategy 2

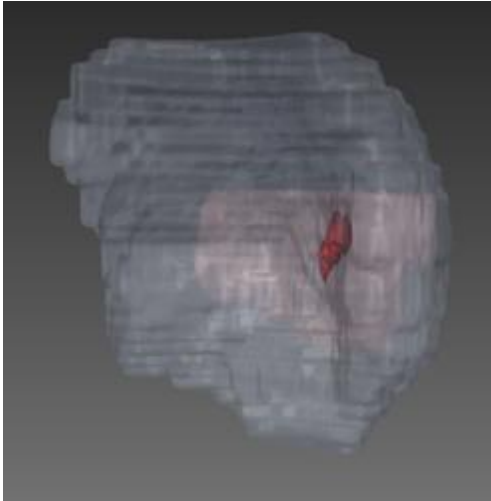
Strategy 2a



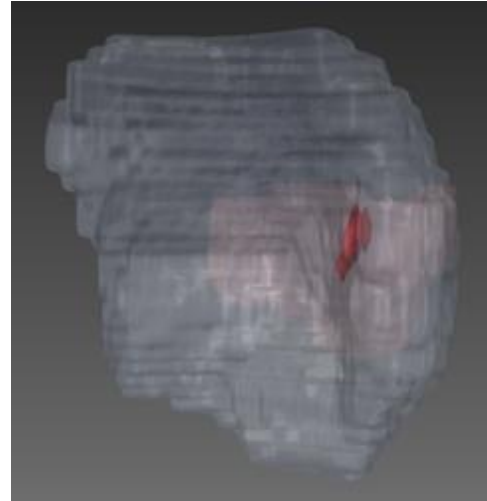
Strategy 2b



Strategy 2c

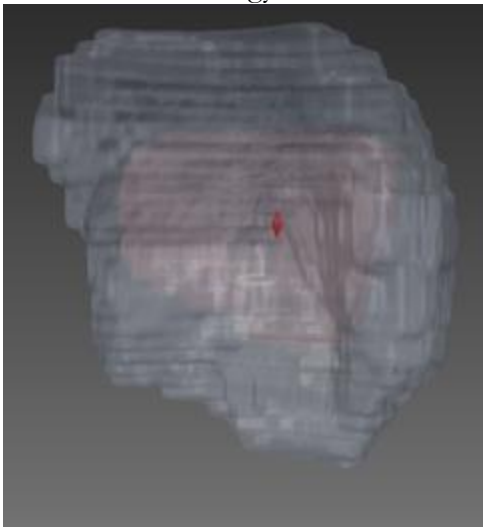


Strategy 2d

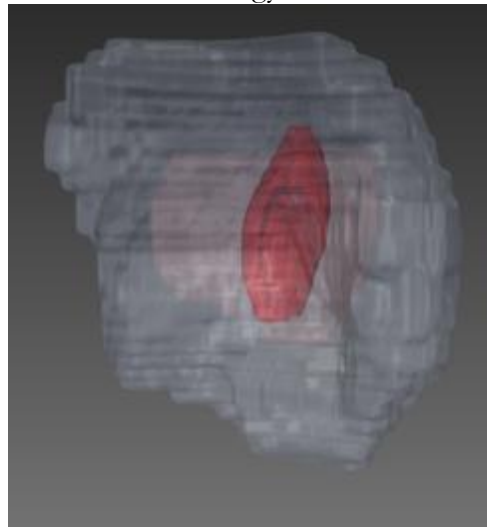


Strategy 3

Strategy 3a

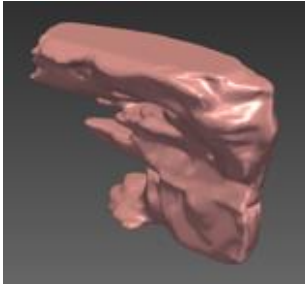


Strategy 3b

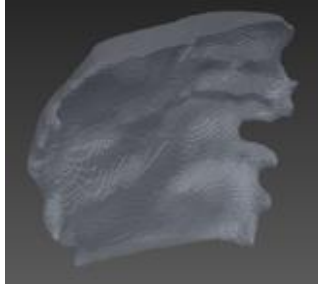


Patient 2

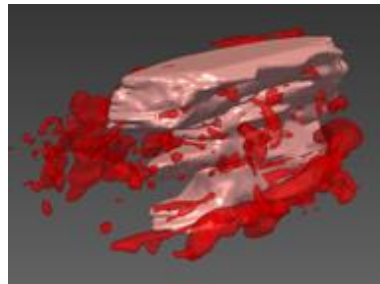
Initial US



Initial MR

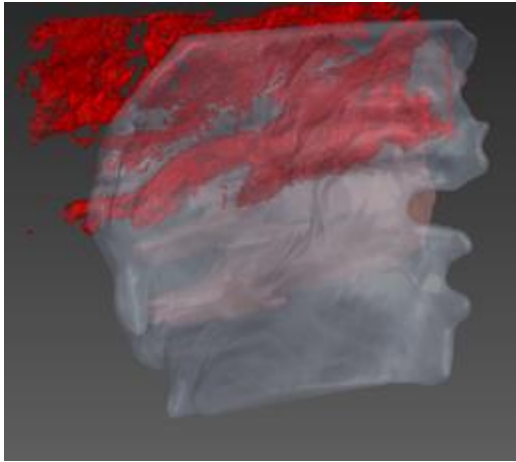


Initial US vessels

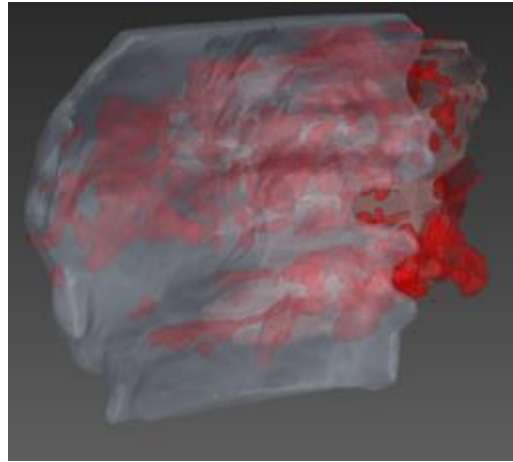


Strategy 1

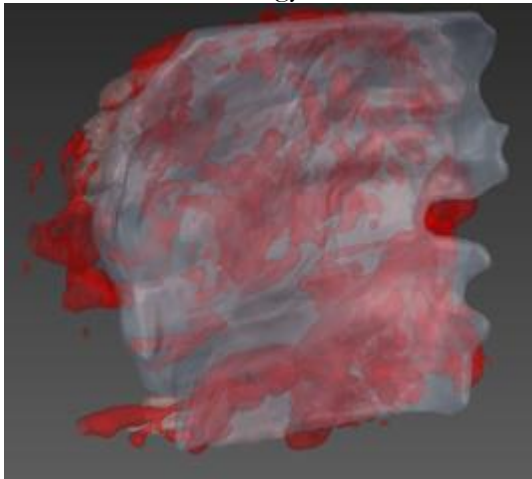
Strategy 1a



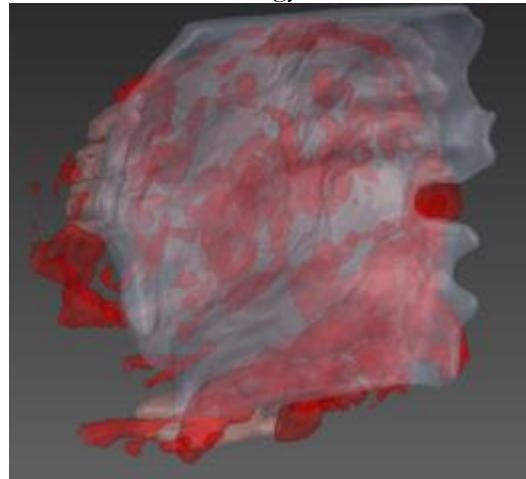
Strategy 1b



Strategy 1c

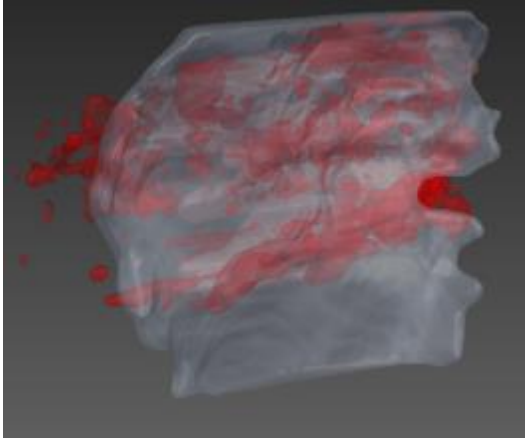


Strategy 1d

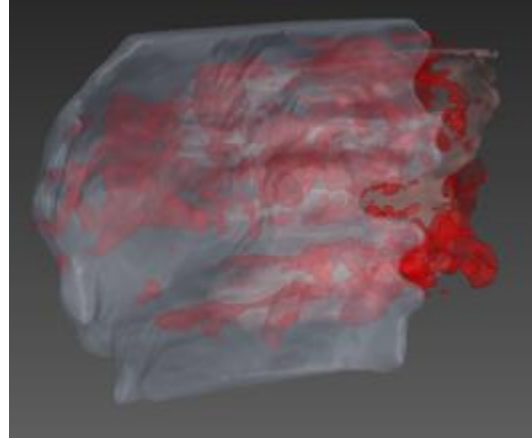


Strategy 2

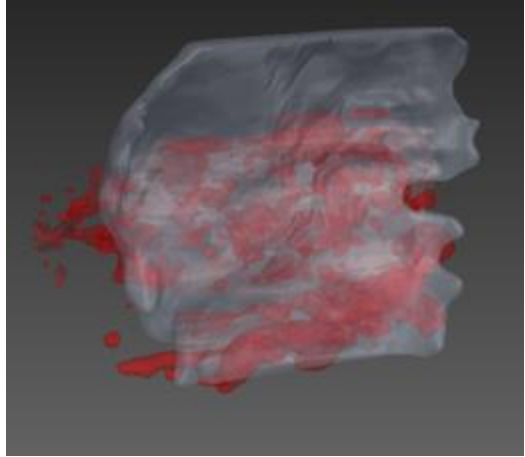
Strategy 2a



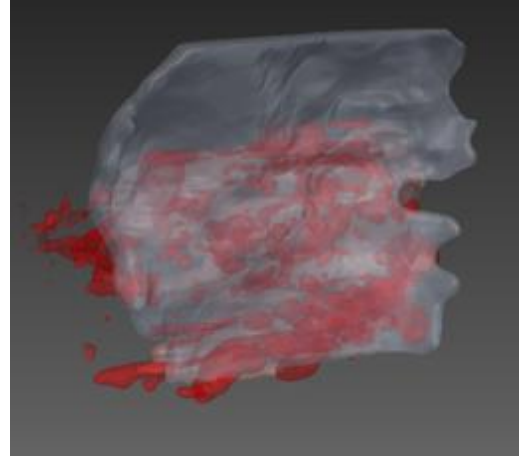
Strategy 2b



Strategy 2c

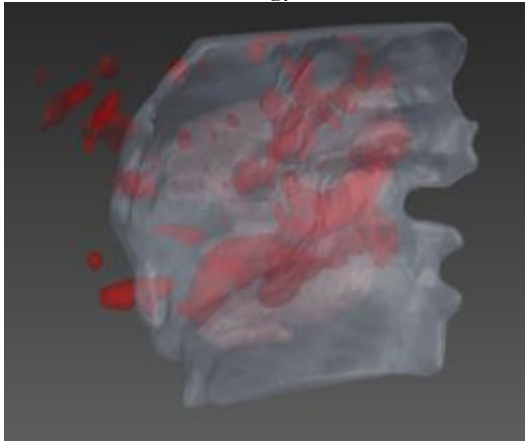


Strategy 2d

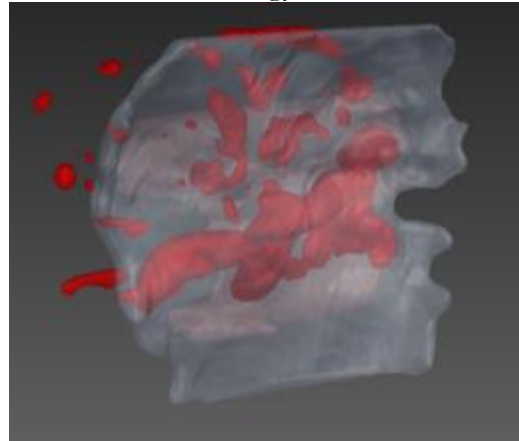


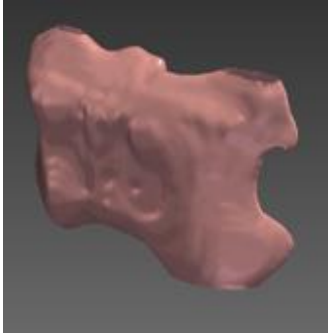
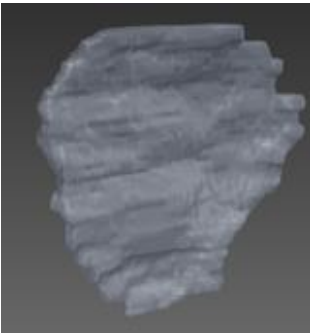
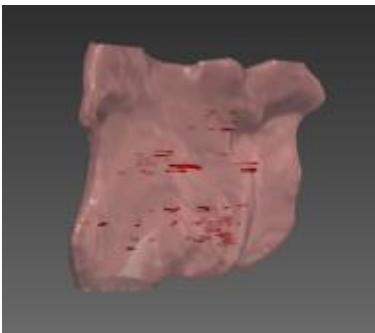
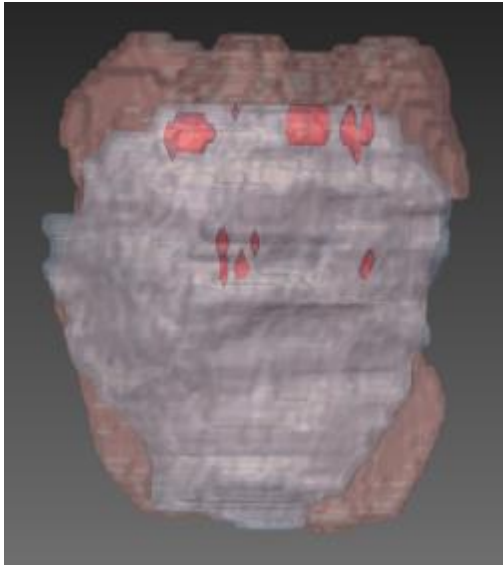
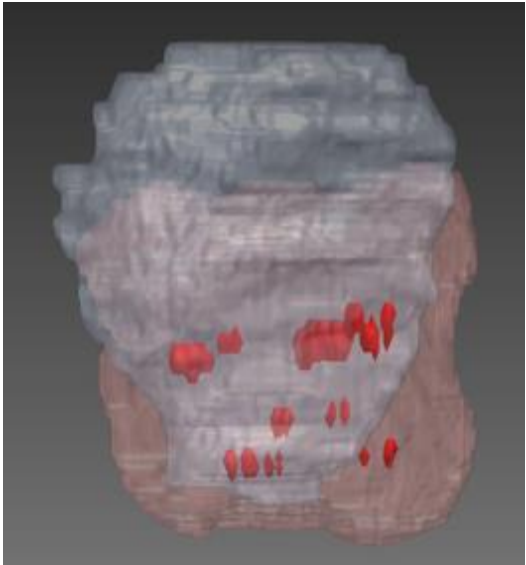
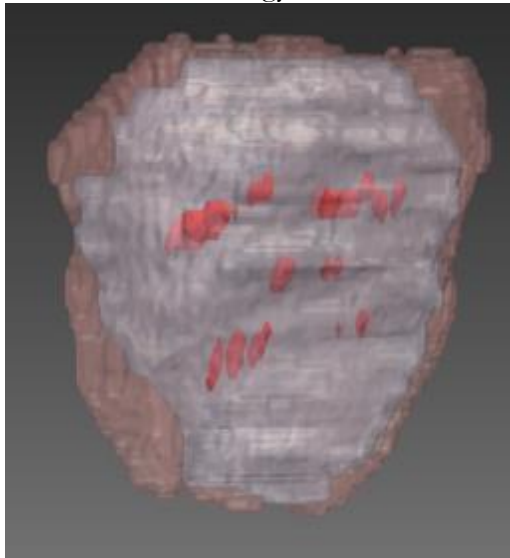
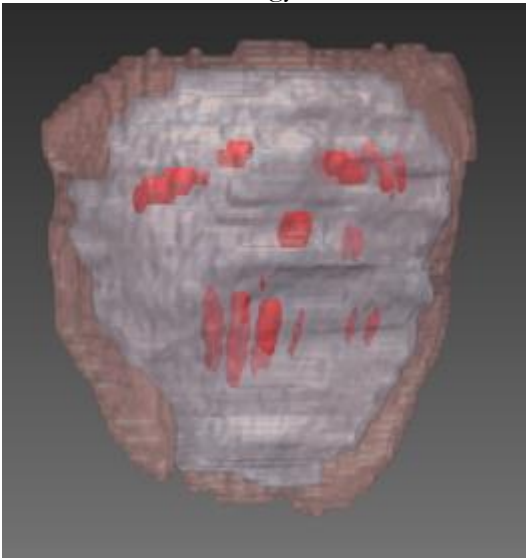
Strategy 3

Strategy 3a



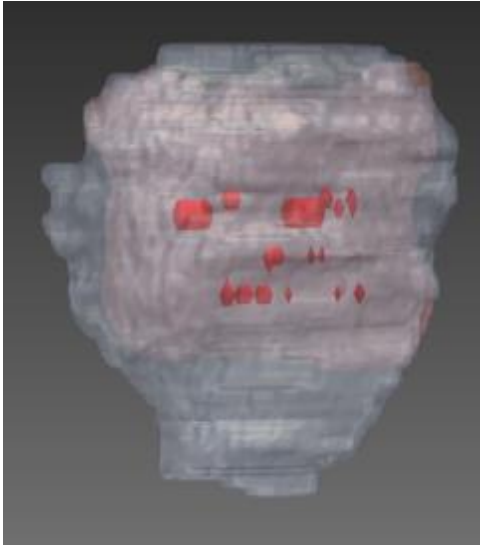
Strategy 3b



Patient 3		
Initial US	Initial MR	Initial US vessels
		
Strategy 1		
Strategy 1a	Strategy 1b	
		
Strategy 1c	Strategy 1c	
		

Strategy 2

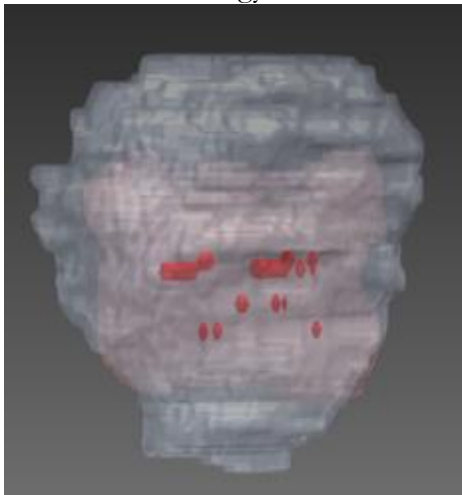
Strategy 2a



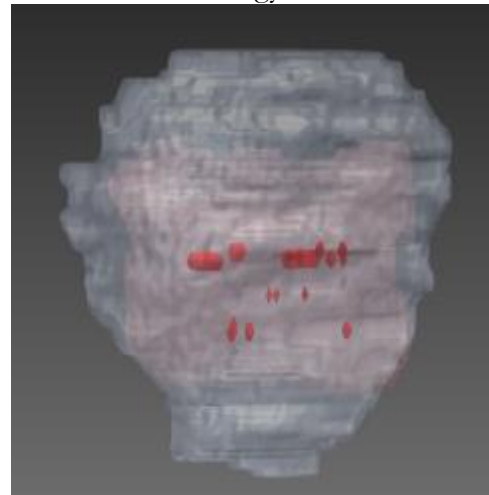
Strategy 2b



Strategy 2c

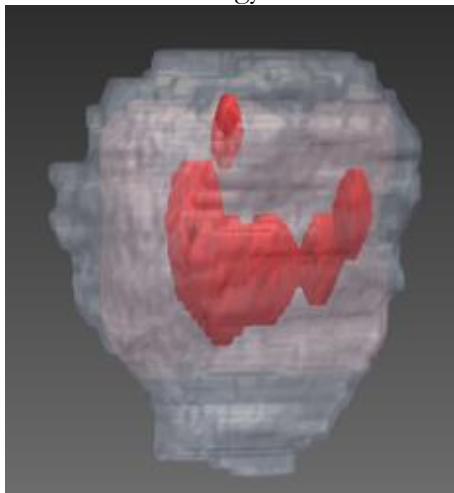


Strategy 2d

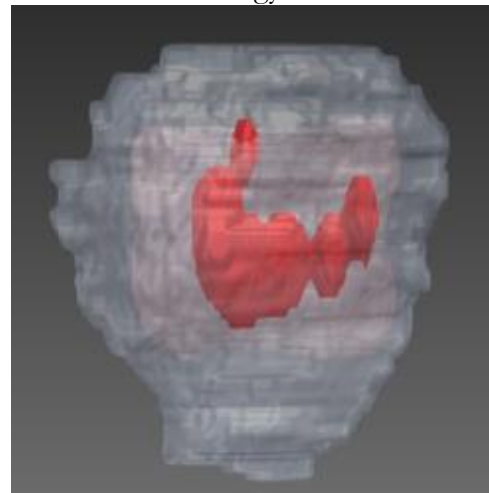


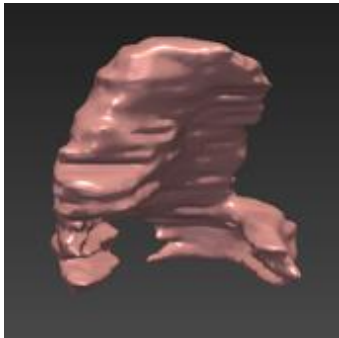
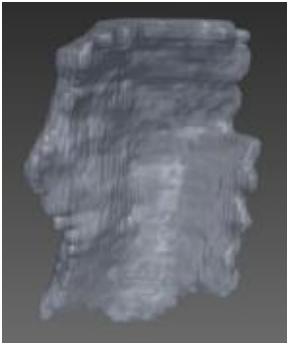
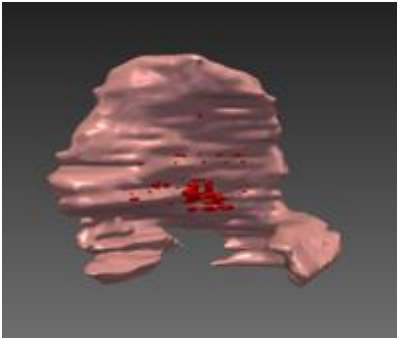
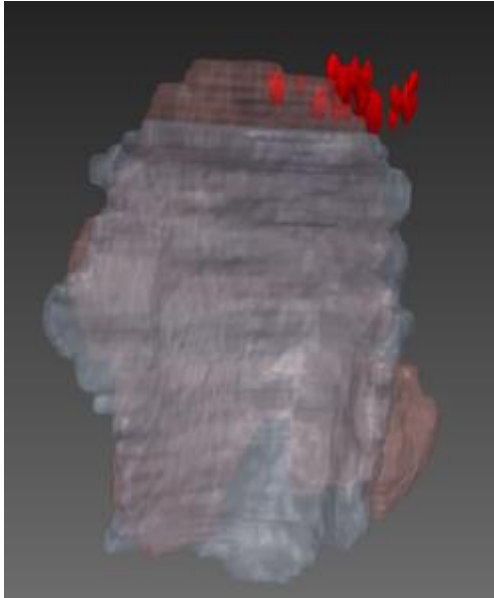
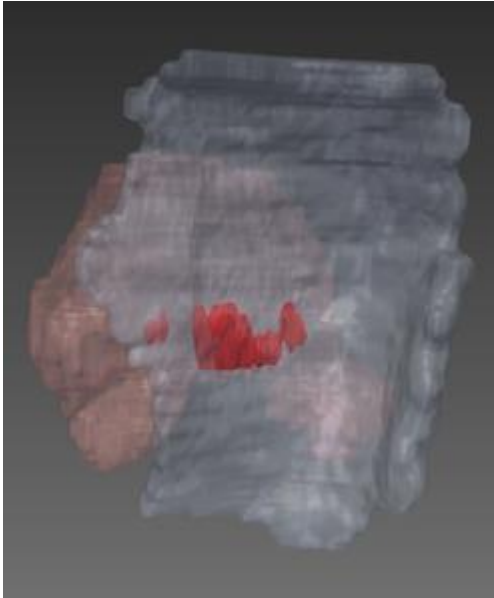

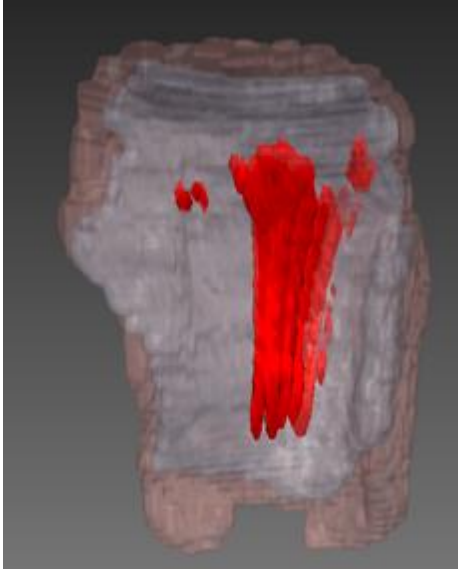
Strategy 3

Strategy 3a



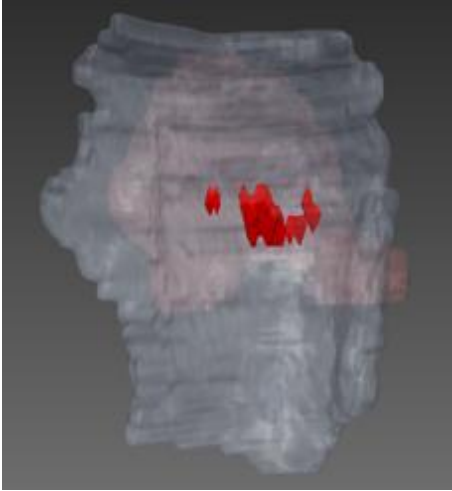
Strategy 3b



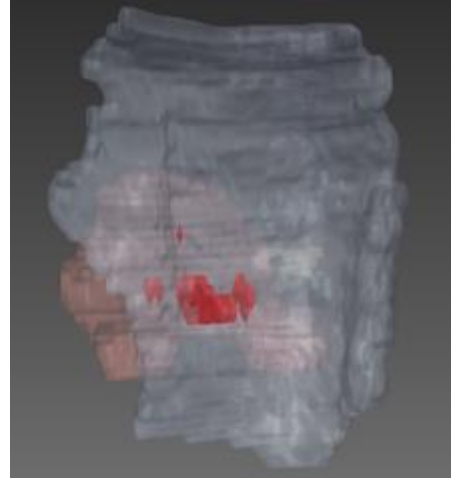
Patient 4		
Initial US	Initial MR	Initial US vessels
		
Strategy 1		
Strategy 1a	Strategy 1b	
		
Strategy 1c	Strategy 1d	
		

Strategy 2

Strategy 2a



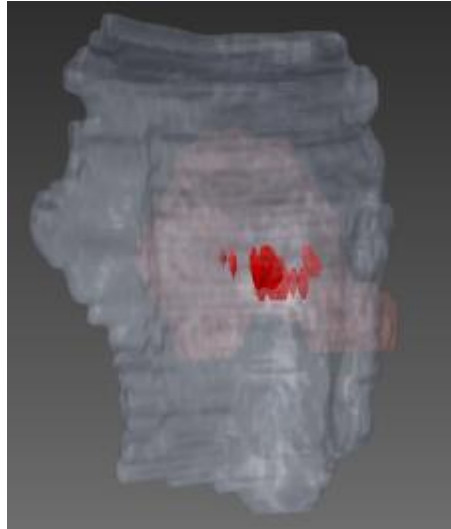
Strategy 2b



Strategy 2c



Strategy 2d

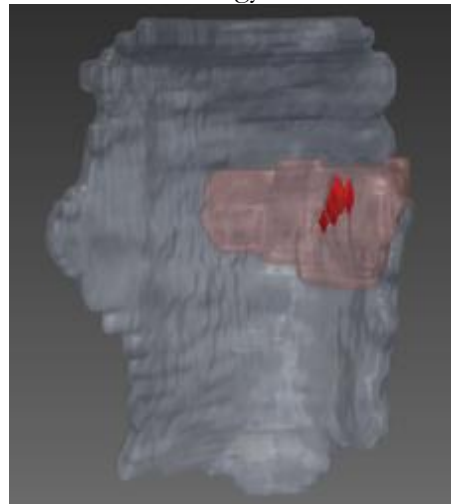


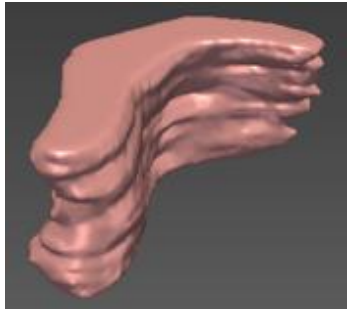
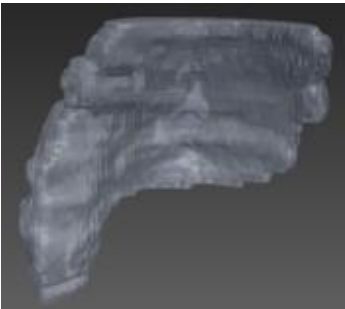
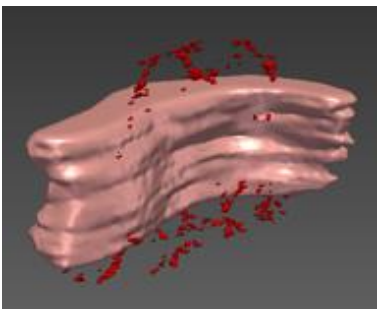
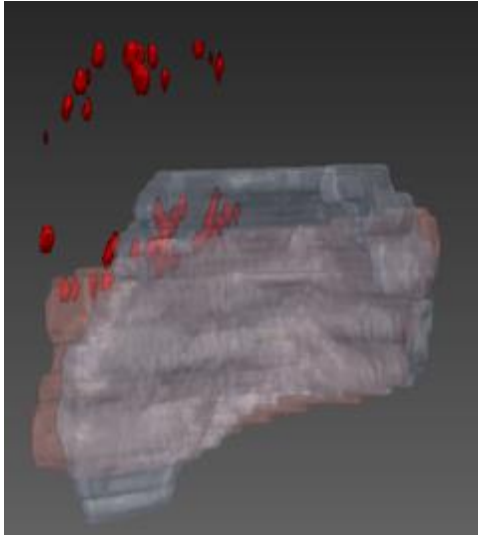
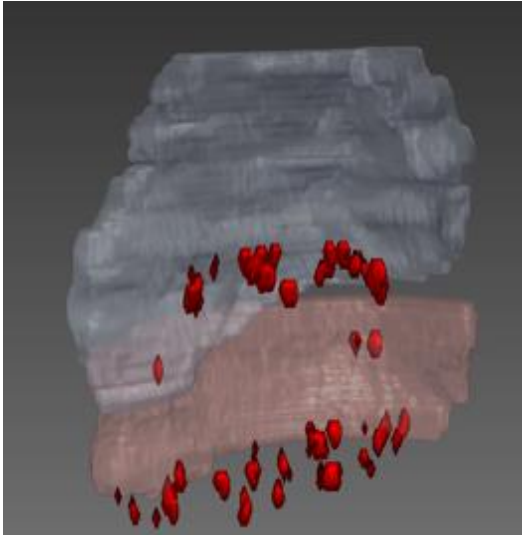

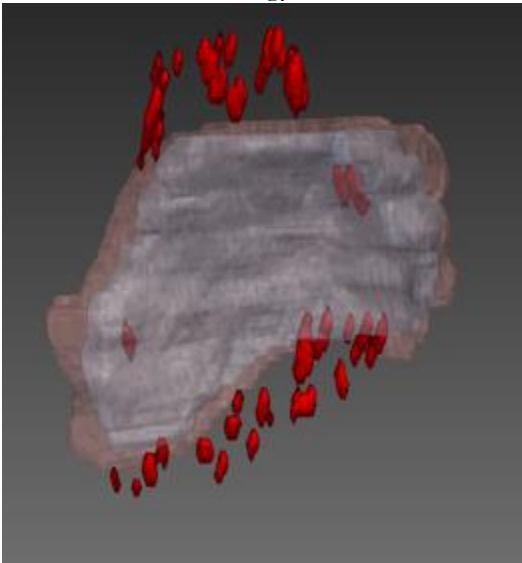
Strategy 3

Strategy 3a



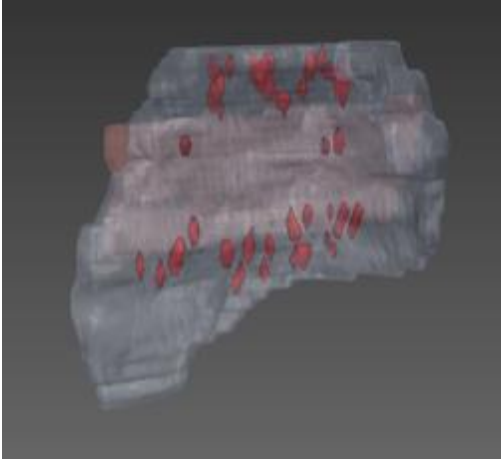
Strategy 3b



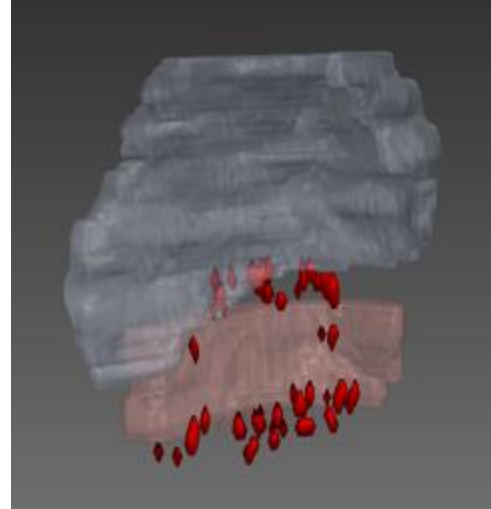
Patient 5		
Initial US	Initial MR	Initial US vessels
		
Strategy 1		
Strategy 1a	Strategy 1b	
		
Strategy 1c	Strategy 1d	
		

Strategy 2

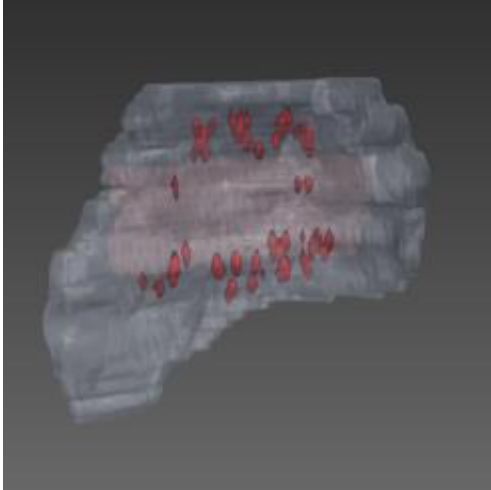
Strategy 2a



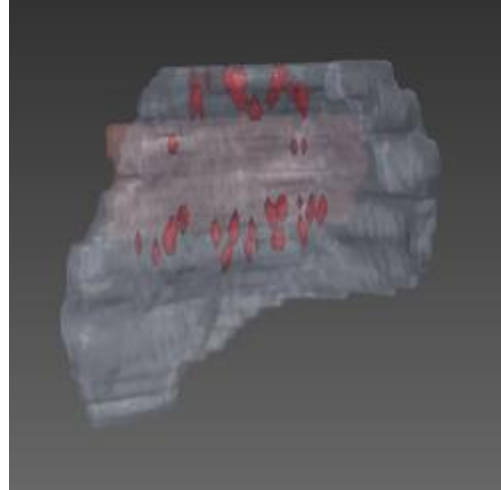
Strategy 2b



Strategy 2c

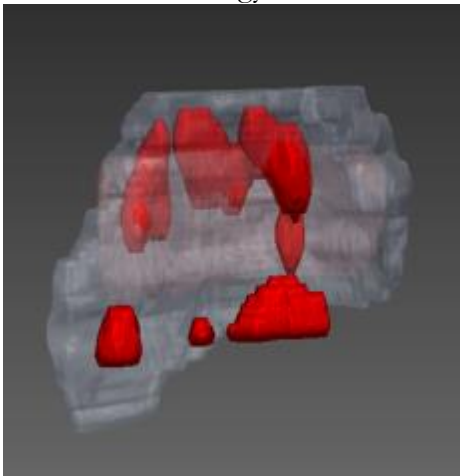


Strategy 2d

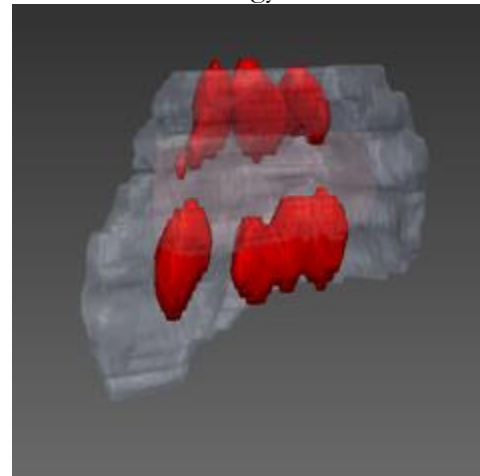


Strategy 3

Strategy 3a

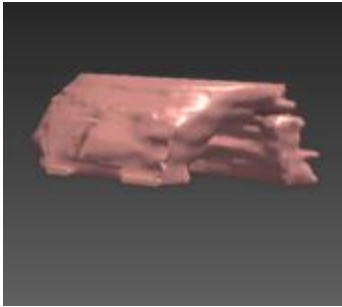


Strategy 3b

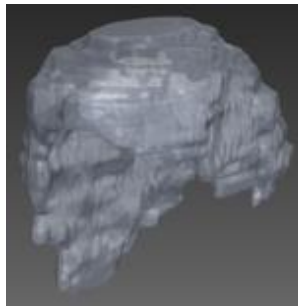


Patient 6

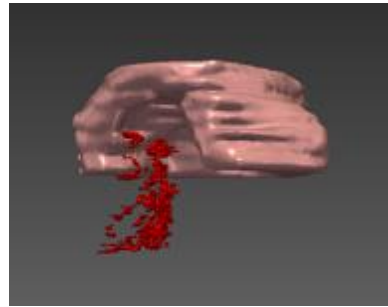
Initial US



Initial MR

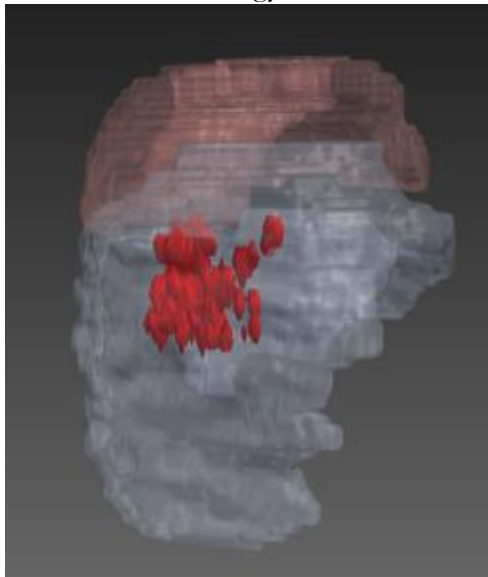


Initial US vessels

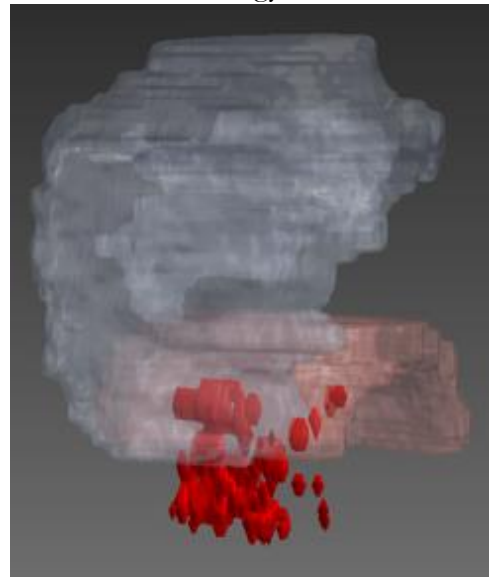


Strategy 1

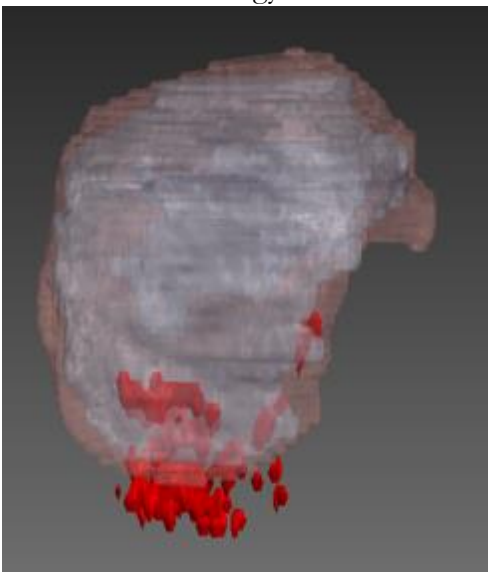
Strategy 1a



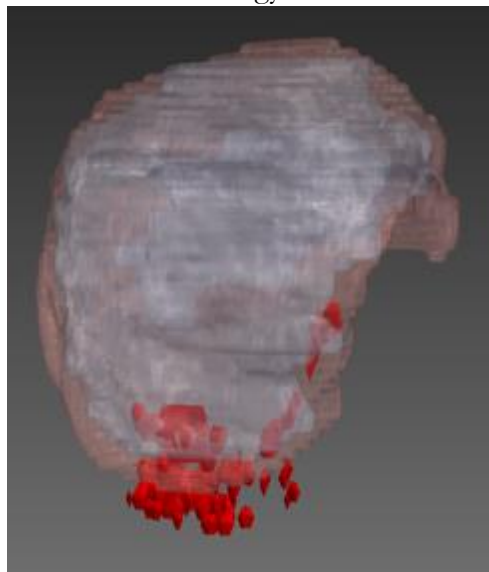
Strategy 1b



Strategy 1c

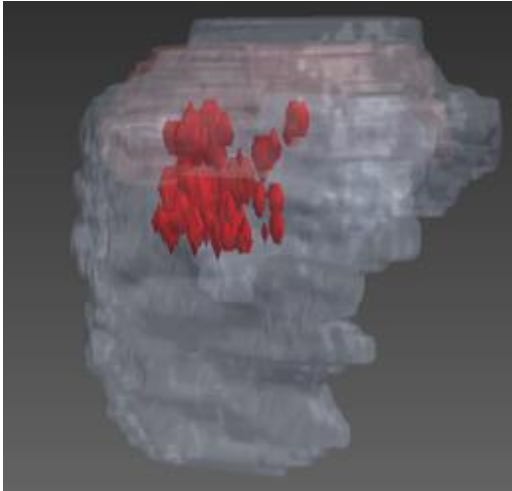


Strategy 1d

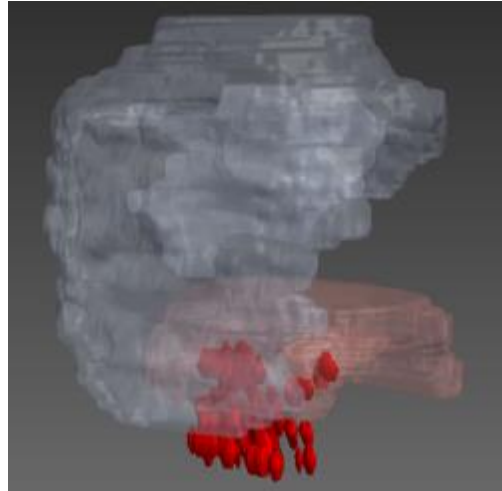


Strategy 2

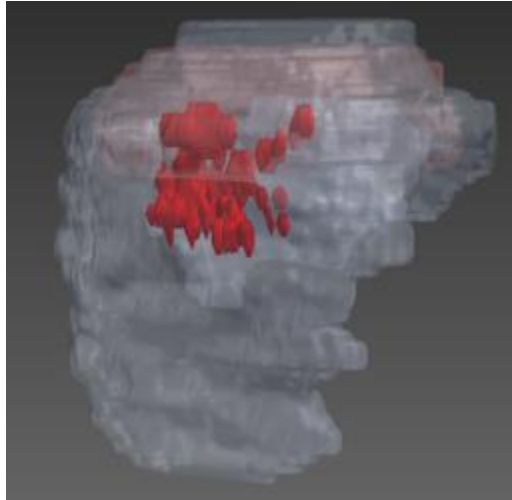
Strategy 2a



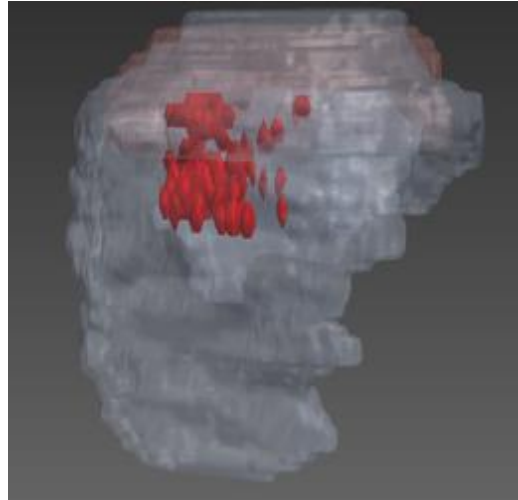
Strategy 2b



Strategy 2c

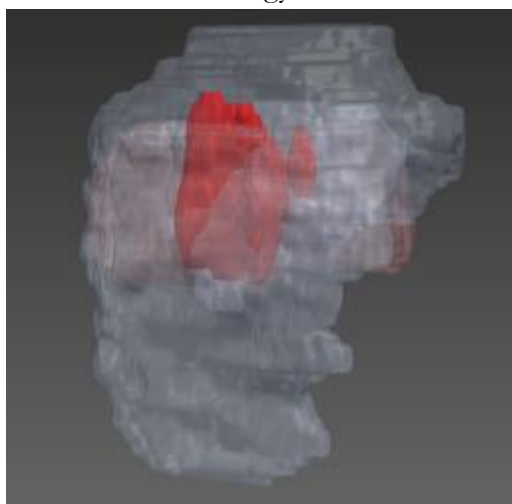


Strategy 2d

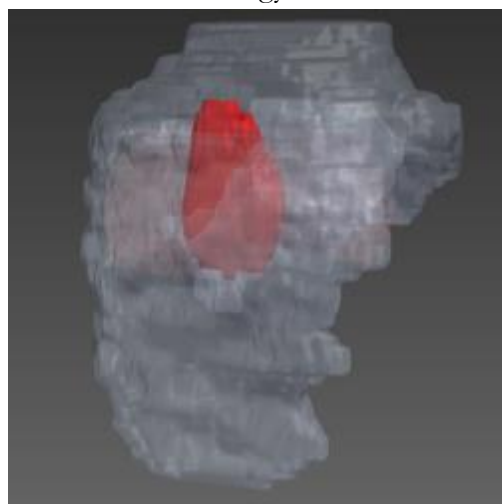


Strategy 3

Strategy 3a

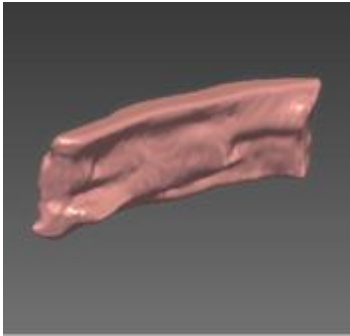


Strategy 3b

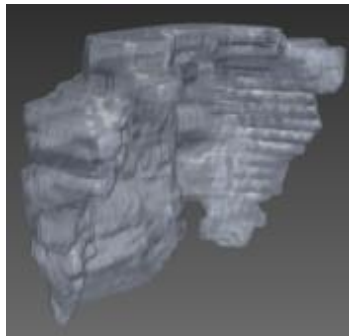


Patient 7

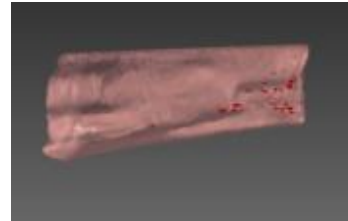
Initial US



Initial MR

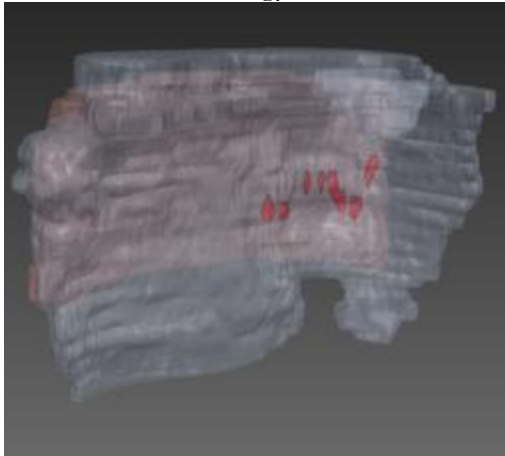


Initial US vessels

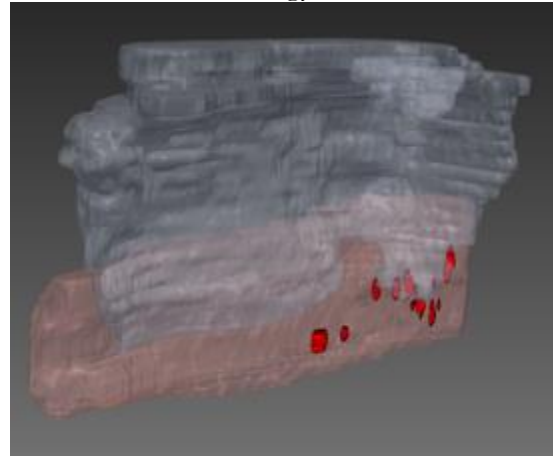


Strategy 1

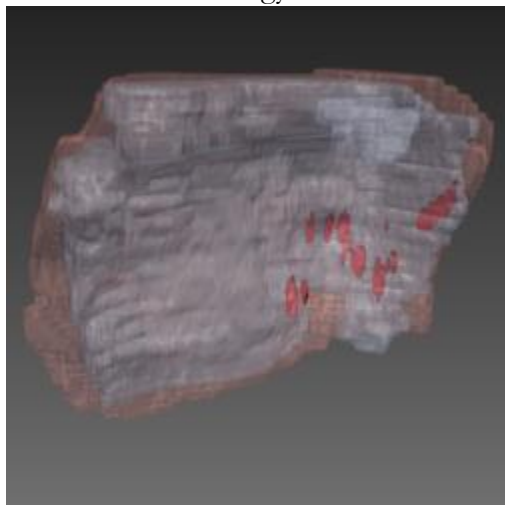
Strategy 1a



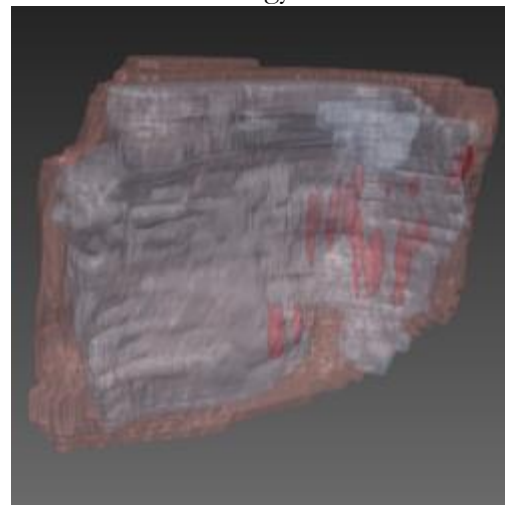
Strategy 1b



Strategy 1c

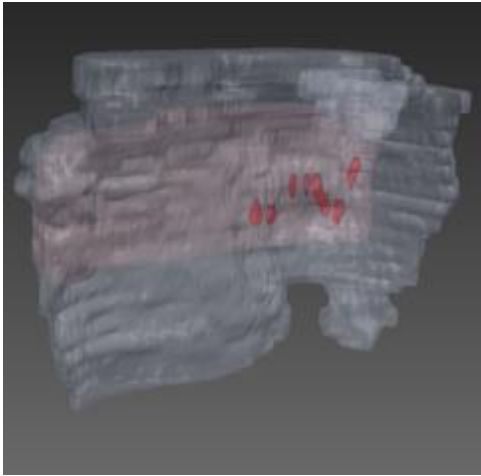


Strategy 1d

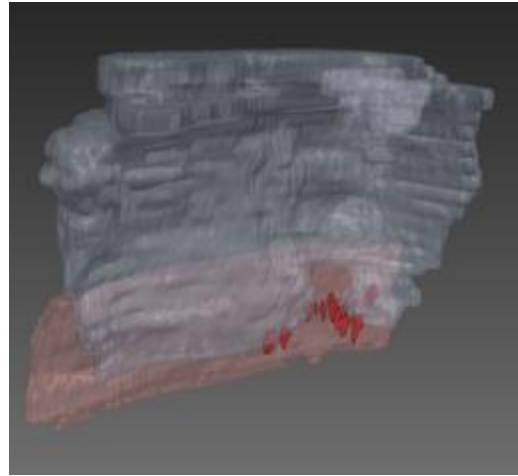


Strategy 2

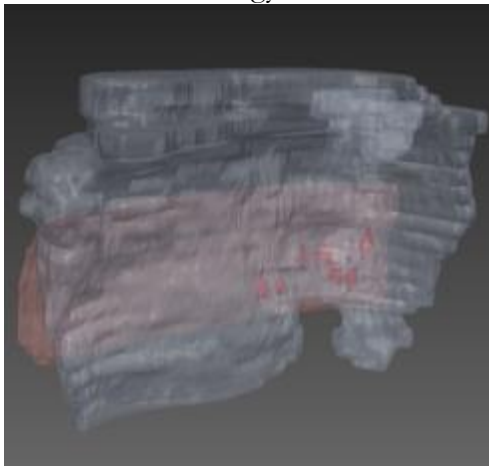
Strategy 2a



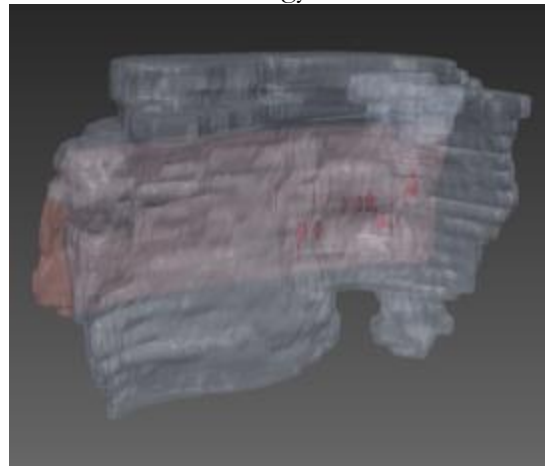
Strategy 2b



Strategy 2b

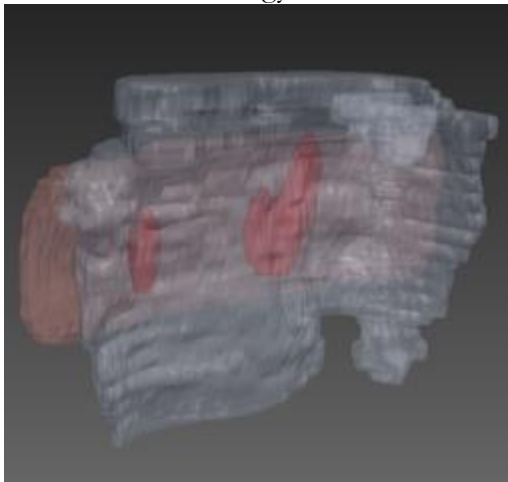


Strategy 2d

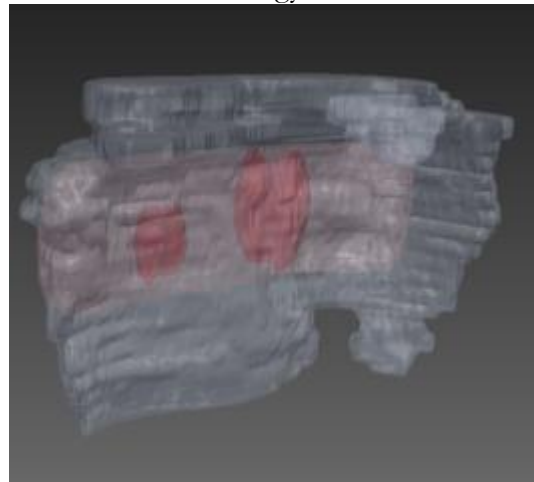


Strategy 3

Strategy 3a



Strategy 3b

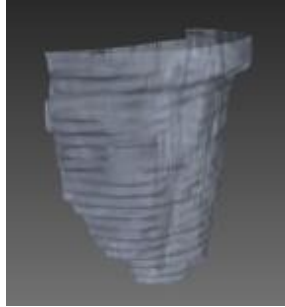


Patient 8

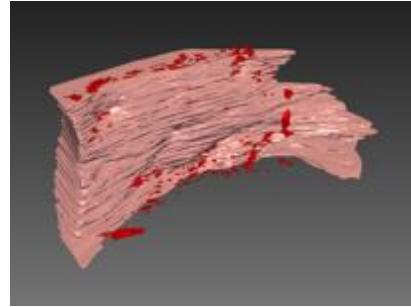
Initial US



Initial MR

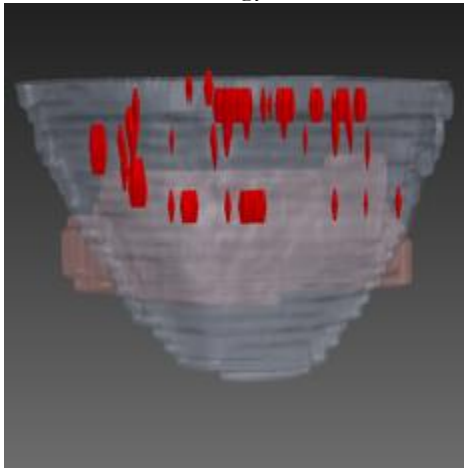


Initial US vessels

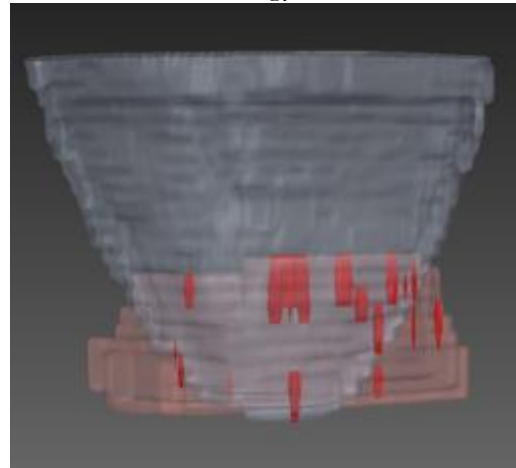


Strategy 1

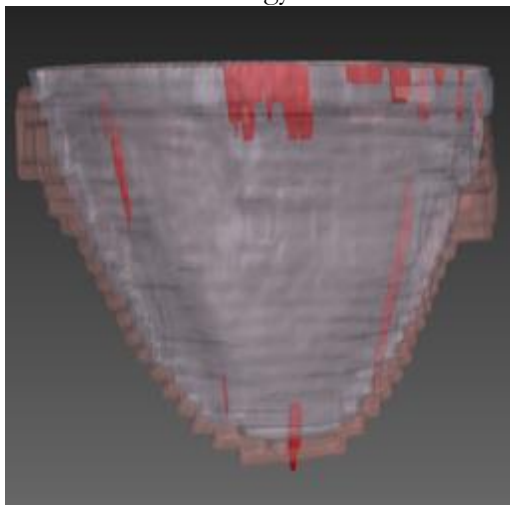
Strategy 1a



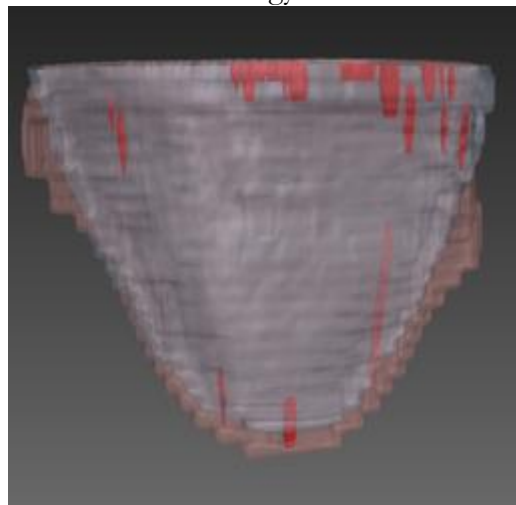
Strategy 1b



Strategy 1c

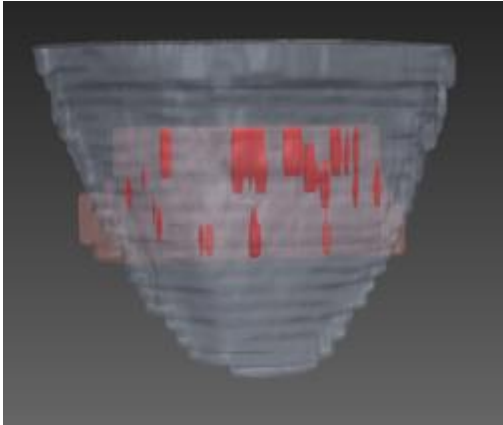


Strategy 1d

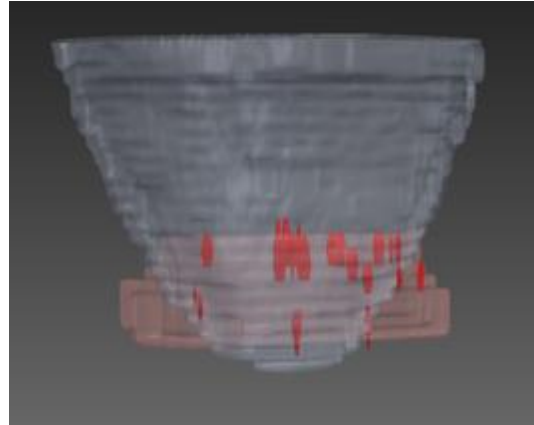


Strategy 2

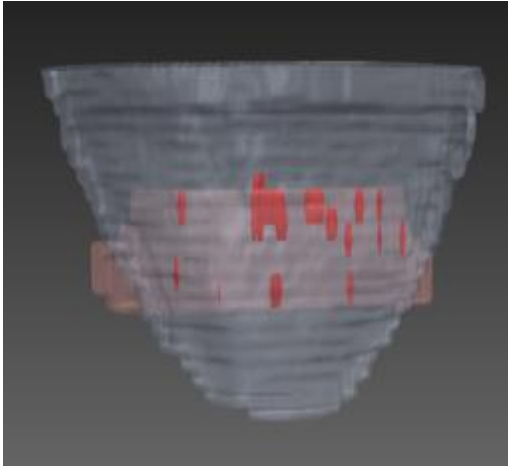
Strategy 2a



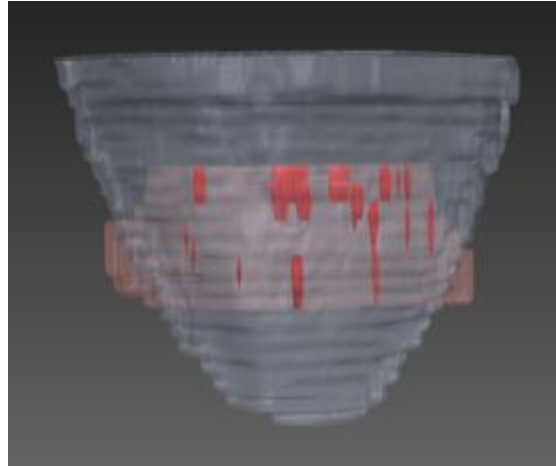
Strategy 2b



Strategy 2b

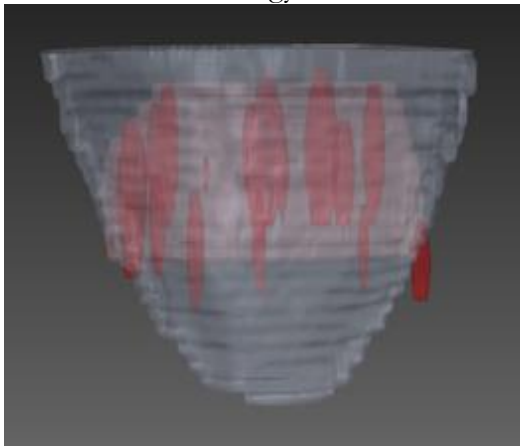


Strategy 2d

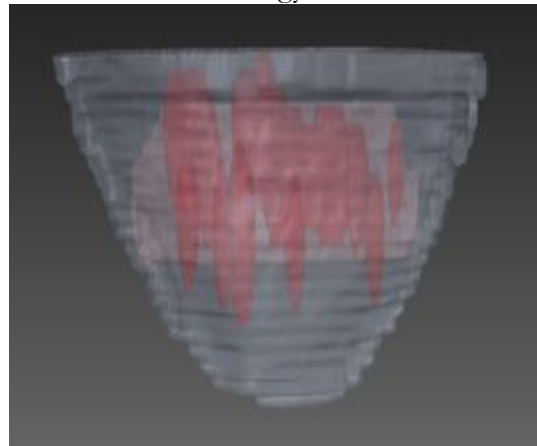


Strategy 3

Strategy 3a

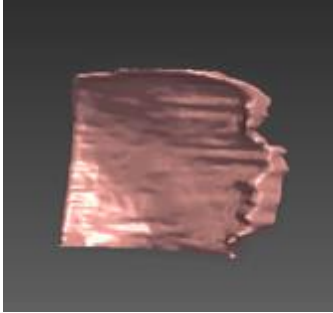


Strategy 3b



Patient 9

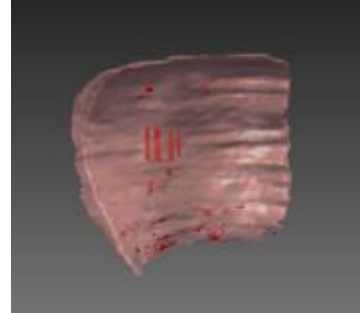
Initial US



Initial MR

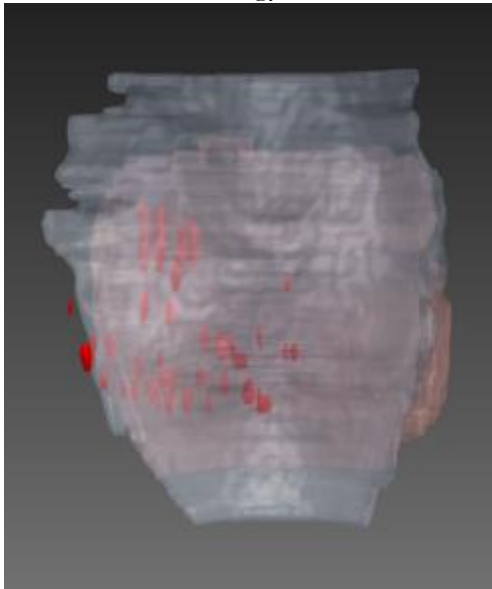


Initial US vessels

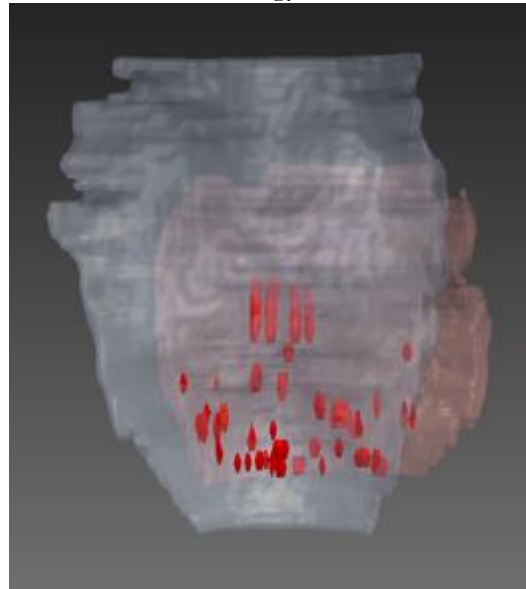


Strategy 1

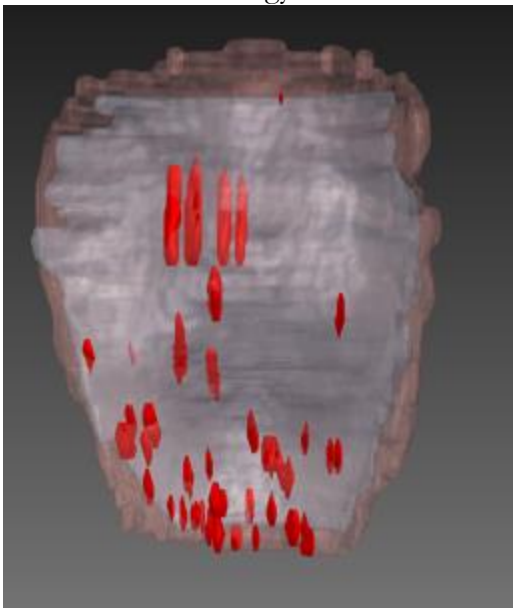
Strategy 1a



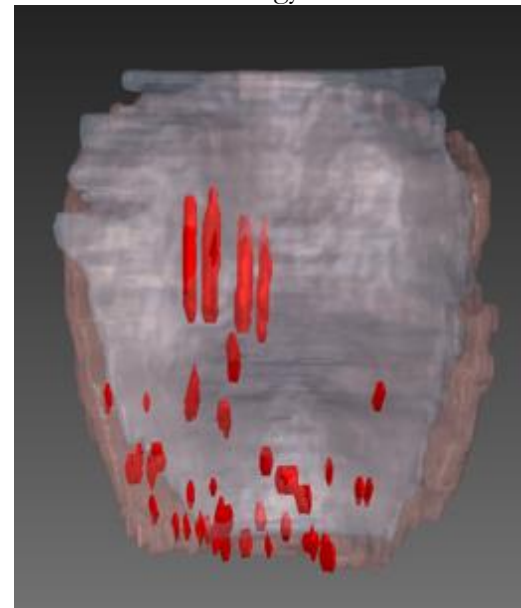
Strategy 1b



Strategy 1c

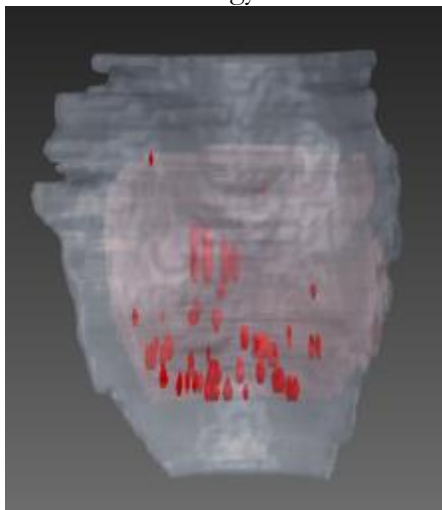


Strategy 1c

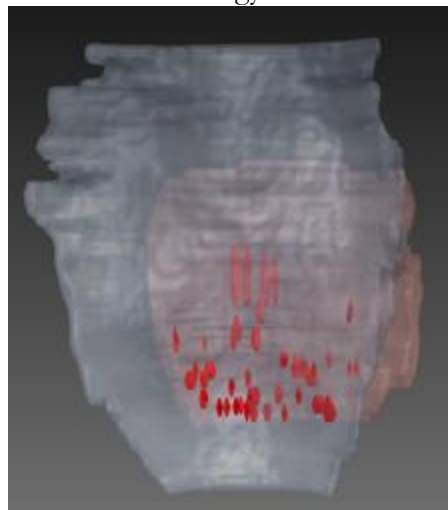


Strategy 2

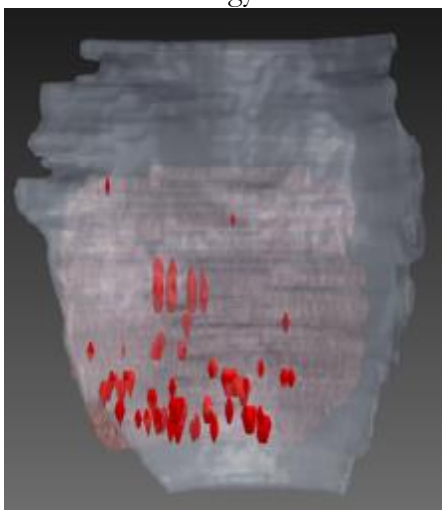
Strategy 2a



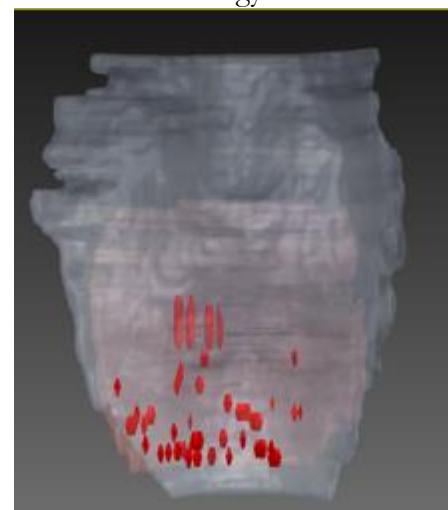
Strategy 2b



Strategy 2b

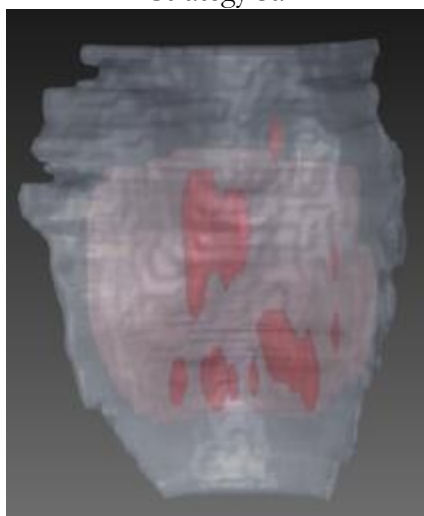


Strategy 2d

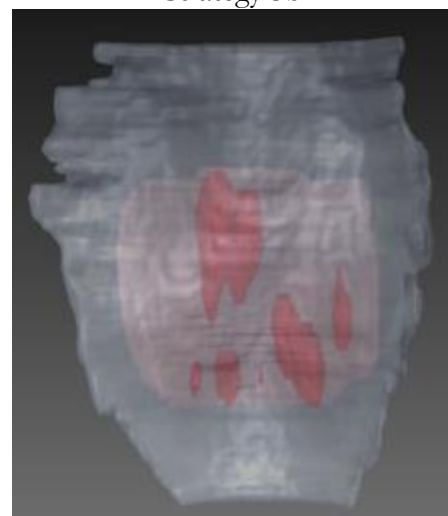


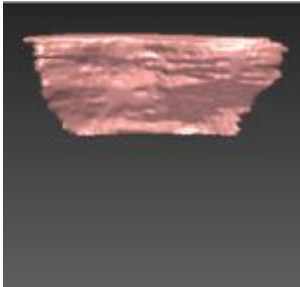
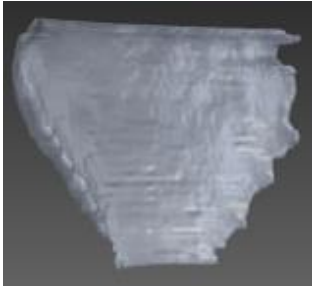
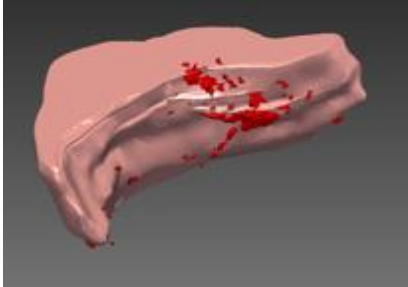
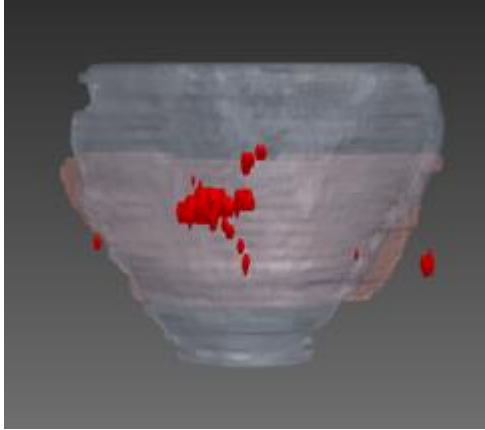
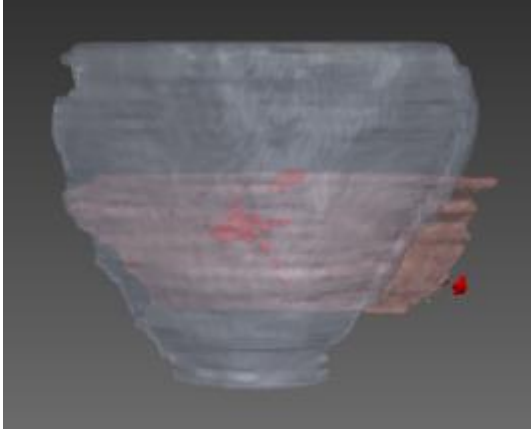
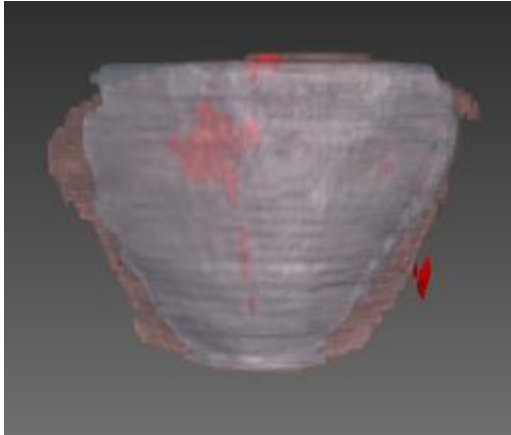
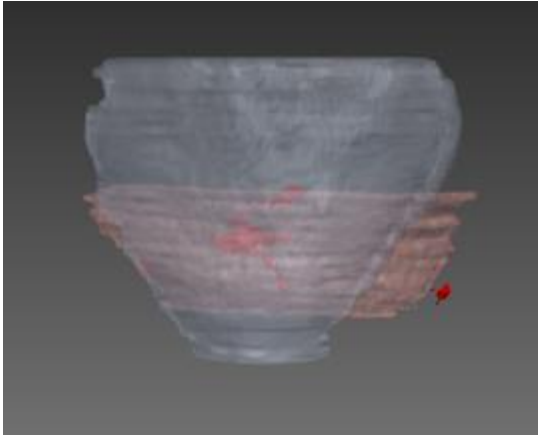
Strategy 3

Strategy 3a



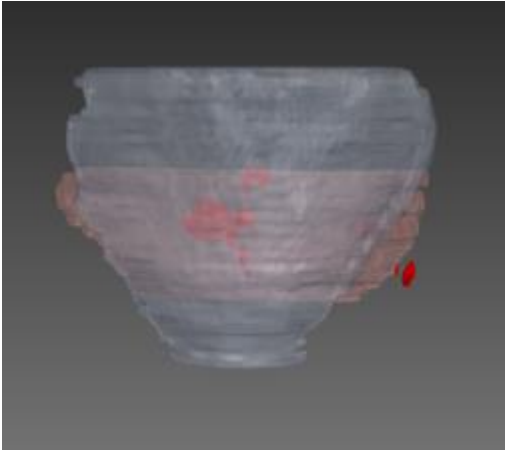
Strategy 3b



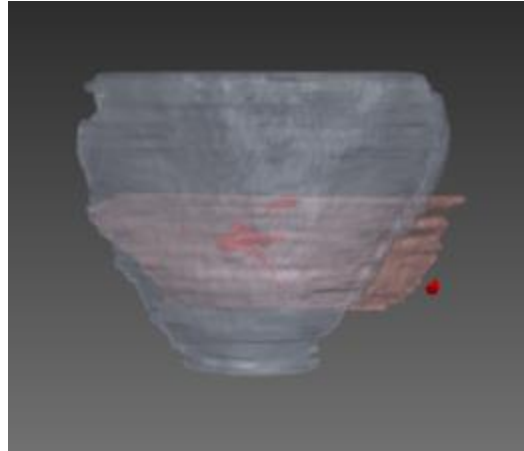
Patient 10		
Initial US	Initial MR	Initial US vessels
		
Strategy 1		
Strategy 1a	Strategy 1b	
		
Strategy 1c	Strategy 1c	
		

Strategy 2

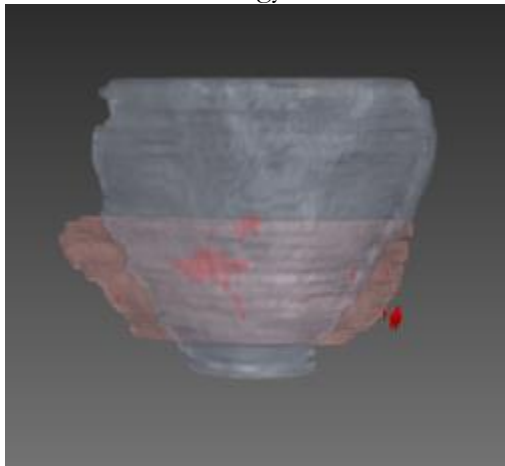
Strategy 2a



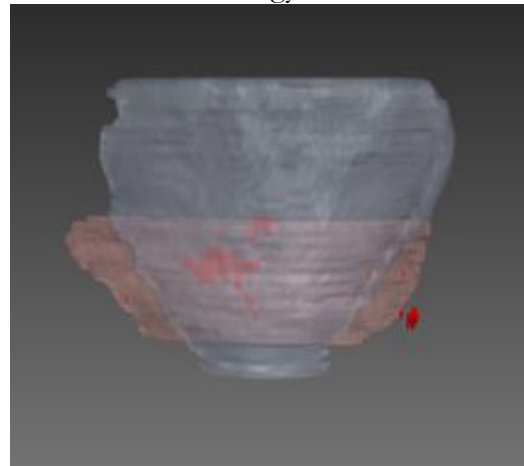
Strategy 2b



Strategy 2b

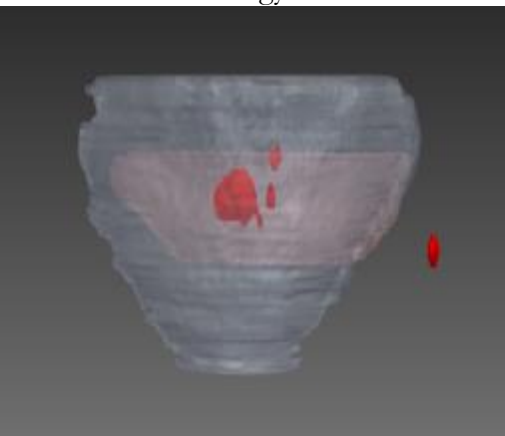


Strategy 2d



Strategy 3

Strategy 3a



Strategy 3b

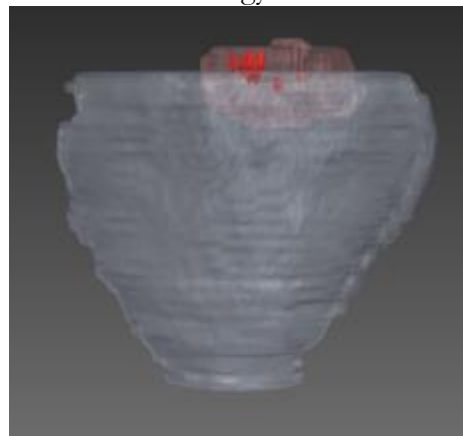


Table 7. Validation results from all patient. 40 percentiles for DC, VS, HD, ASD and UCID have been calculated for each Registration Strategy. Maximum distance is also used to transform HD into weighted Hausdorff Distance (wHD). In blue, numerical values of the non-registered structures, (original conformation), in red the higher values and in green the lowest values. ^[1] Some UCID could not be calculated because insertions were no appreciable due to image resolution, so real GS will be higher than GS calculated. Moreover, non-registered images have very high distances between US and MR placentas (outside possible region), so in cases where UCID or other metric were not possible to calculate, ^[2] GS can't have a numerical value.

Strategy 1									
Pat. ¹¹	Input Data	DC	VS	HD	Max Dist. ¹²	wHD	ASD	UCID ^[1]	GS ^[2]
1	Non-registered images	0,000	0,000	Requested region is (at least partially) outside the largest possible region				145,806	--
	Ddf	0,628	0,359	64,218	10510,827	0,006	3,817	24,996	-3,554
	Original Images	0,161	0,369	64,666	7688,155	0,008	10,067	71,765	-10,283
	Mask	0,791	-0,331	13,077	11188,079	0,001	1,211	17,950	-0,089
	Image Mask	0,749	-0,383	17,757	11132,728	0,002	1,525	98,392	-0,395
2	Non-registered images	0,000	0,000	Requested region is (at least partially) outside the largest possible region				--	--
	Ddf	0,552	0,554	64,218	17989,703	0,003	10,051	--	-9,498
	Original Images	0,000	0,501	64,666	20441,396	0,003	40,544	--	-40,046
	Mask	0,774	0,006	13,077	14768,001	0,002	4,569	--	-4,565
	Image Mask	0,757	-0,008	17,757	16766,129	0,001	5,171	--	-5,179

¹¹ Pat. refers to Patients.

¹² Max Dist. refers to Maximum Distance.

3	Non-registered images	0,000	0,000	Requested region is (at least partially) outside the largest possible region				166,392	--
	Ddf	0,721	-0,356	33,398	4182,311	0,008	2,336	90,955	-1,267
	Original Images	0,263	0,155	65,219	5385,271	0,012	6,972	119,626	-6,876
	Mask	0,781	-0,356	29,634	4064,031	0,007	1,748	41,183	-0,618
	Image Mask	0,736	-0,504	30,547	3975,056	0,008	2,258	63,445	-1,026
4	Non-registered images	0,000	0,000	Requested region is (at least partially) outside the largest possible region				156,933	--
	Ddf	0,548	0,211	50,713	8152,027	0,006	2,823	23,213	-2,492
	Original Images	0,136	0,604	71,738	11269,154	0,006	10,457	42,376	-10,931
	Mask	0,745	-0,370	30,966	11472,166	0,003	1,464	36,256	-0,352
	Image Mask	0,732	-0,432	32,456	12098,404	0,003	1,696	56,943	-0,535
5	Non-registered images	0,000	0,000	Requested region is (at least partially) outside the largest possible region				227,069	--
	Ddf	0,528	0,552	122,774	17526,498	0,007	7,891	83,463	-7,922
	Original Images	0,018	1,181	152,781	13887,554	0,011	1,771	41,417	-2,945
	Mask	0,796	-0,268	38,843	17654,031	0,002	1,418	65,371	-0,356
	Image Mask	0,804	-0,283	20,972	17786,135	0,001	1,285	123,465	-0,199

6	Non-registered images	0,0000	0,000	Requested region is (at least partially) outside the largest possible region				164,466	--
	Ddf	0,006	0,999	144,780	10194,000	0,014	12,180	67,402	-13,187
	Original Images	0,067	0,919	113,410	7359,710	0,015	13,870	91,687	-14,737
	Mask	0,752	-0,288	22,800	2710,732	0,008	1,418	87,318	-0,386
	Image Mask	0,740	-0,297	28,759	2896,245	0,009	1,520	83,177	-0,492
7	Non-registered images	0,000	0,000	Requested region is (at least partially) outside the largest possible region				--	--
	Ddf	0,374	0,827	117,151	17347,003	0,006		Ddf	0,374
	Original Images	0,180	0,734	133,012	1435,904	0,092		Original Images	0,180
	Mask	0,735	-0,418	78,363	11364,011	0,006		Mask	0,735
	Image Mask	0,698	-0,535	78,787	11338,001	0,006		Image Mask	0,698
8	Non-registered images	0,000	0,000	Requested region is (at least partially) outside the largest possible region				197,758	--
	Ddf	0,173	1,308	72,285	12814,002	0,005		Ddf	0,173
	Original Images	0,181	1,287	104,740	9462,501	0,011		Original Images	0,181
	Mask	0,832	-0,208	20,593	3514,903	0,058		Mask	0,832
	Image Mask	0,821	-0,097	20,825	4023,801	0,052		Image Mask	0,821

9	Non-registered images	0,0000	0,0000	Requested region is (at least partially) outside the largest possible region				--	--
	Ddf	0,1721	0,1461	44,7790	7641,5	0,0058		Ddf	0,1721
	Original Images	0,186	0,307	57,732	11557,210	0,005		Original Images	0,186
	Mask	0,707	-0,494	29,559	6002,010	0,004		Mask	0,707
	Image Mask	0,679	-0,492	33,914	6380,101	0,005		Image Mask	0,679
10	Non-registered images	0,000	0,000	Requested region is (at least partially) outside the largest possible region				202,241	--
	Ddf	0,497	0,806	56,760	10968,001	0,005		Ddf	0,497
	Original Images	0,000	0,928	95,075	19077,002	0,004		Original Images	0,000
	Mask	0,801	-0,283	34,886	6708,001	0,005		Mask	0,801
	Image Mask	0,000	-1,003	140,170	2043,301	0,068		Image Mask	0,000

Strategy 2									
Pat. ¹¹	Input Data	DC	VS	HD	Max Dist. ¹²	wHD	ASD	UCID ^[1]	GS ^[2]
1	Non-registered images	0,000	0,000	Requested region is (at least partially) outside the largest possible region				145,8058	--
	Ddf	0,346	1,228	74,786	10510,827	0,007	6,577	30,119	-7,466
	Original Images	0,038	1,254	82,171	7688,155	0,010	13,894	61,037	-15,120
	Mask	0,311	1,287	82,485	11188,071	0,007	7,515	30,193	-8,498
	Image Mask	0,277	1,381	82,097	11132,725	0,007	7,609	27,274	-8,720
2	Non-registered images	0,000	0,000	Requested region is (at least partially) outside the largest possible region				--	--
	Ddf	0,649	0,218	41,174	13999,476	0,002	0,649	0,218	41,174
	Original Images	0,000	-0,132	78,735	26770,142	0,003	0,000	-0,132	78,735
	Mask	0,606	-0,188	44,975	15291,497	0,010	0,606	-0,188	44,975
	Image Mask	0,613	-0,185	44,211	15032,028	0,002	0,613	-0,185	44,211
3	Non-registered images	0,000	0,000	Requested region is (at least partially) outside the largest possible region				145,805	--
	Ddf	0,607	0,689	63,046	4182,311	0,015	0,607	0,689	63,046
	Original Images	0,413	0,857	80,994	5385,271	0,015	0,413	0,857	80,994
	Mask	0,525	0,865	52,832	4064,031	0,012	0,525	0,865	52,832
	Image	0,537	0,836	48,343	3975,056	0,012	0,537	0,836	48,343

	Mask								
4	Non-registered images	0,000	0,000	Requested region is (at least partially) outside the largest possible region				156,938	--
	Ddf	0,210	1,084	75,365	8152,027	0,009	0,210	1,084	75,365
	Original Images	0,087	1,254	89,648	11269,154	0,008	0,087	1,254	89,648
	Mask	0,233	1,316	100,857	1147,166	0,087	0,233	1,316	100,857
	Image Mask	0,259	1,257	94,649	12098,400	0,007	0,259	1,257	94,649
5	Non-registered images	0,000	0,000	Requested region is (at least partially) outside the largest possible region				156,938	--
	Ddf	0,328	1,291	122,875	17526,498	0,007	0,328	1,291	122,875
	Original Images	0,000	1,457	139,759	13887,553	0,0100	0,000	1,457	139,759
	Mask	0,241	1,483	125,305	17654,031	0,007	0,241	1,483	125,305
	Image Mask	0,240	1,467	123,787	17786,134	0,006	0,240	1,467	123,787
6	Non-registered images	0,000	0,000	Requested region is (at least partially) outside the largest possible region				164,460	--
	Ddf	0,295	1,286	113,412	7112,626	0,015	0,295	1,286	113,412
	Original Images	0,008	1,301	118,251	8274,740	0,014	0,008	1,301	118,251
	Mask	0,308	1,298	113,867	7052,951	0,016	0,308	1,298	113,867
	Image Mask	0,321	1,273	117,800	7212,489	0,016	0,321	1,273	117,800

7	Non-registered images	0,000	0,000	Requested region is (at least partially) outside the largest possible region				--	--
	Ddf	0,331	1,196	110,320	15928,828	0,006	0,331	1,196	110,320
	Original Images	0,158	1,231	144,206	16612,226	0,008	0,158	1,231	144,206
	Mask	0,318	1,196	122,805	16853,164	0,007	0,318	1,196	122,805
	Image Mask	0,354	1,116	111,734	15983,842	0,006	0,354	1,116	111,734
8	Non-registered images	0,000	0,000	Requested region is (at least partially) outside the largest possible region				197,755	--
	Ddf	0,229	1,432	71,386	12567,645	0,005	0,229	1,432	71,386
	Original Images	0,159	1,479	104,474	9602,367	0,010	0,159	1,479	104,474
	Mask	0,229	1,489	75,794	10430,091	0,007	0,229	1,489	75,794
	Image Mask	0,250	1,448	70,950	10526,281	0,006	0,250	1,448	70,950
9	Non-registered images	0,000	0,000	Requested region is (at least partially) outside the largest possible region				--	--
	Ddf	0,127	0,649	49,382	10818,733	0,004	0,127	0,649	49,382
	Original Images	0,103	0,691	64,203	14027,318	0,004	0,103	0,691	64,203
	Mask	0,361	0,717	58,338	9469,396	0,006	0,361	0,717	58,338
	Image Mask	0,381	0,701	62,163	8522,495	0,007	0,381	0,701	62,163

10	Non-registered images	0,000	0,000	Requested region is (at least partially) outside the largest possible region				202,240	--
	Ddf	0,253	1,002	60,648	10405,125	0,005	0,253	1,002	60,648
	Original Images	0,000	0,987	98,638	19457,017	0,005	0,000	0,987	98,638
	Mask	0,306	1,078	80,972	11525,887	0,007	0,306	1,078	80,972
	Image Mask	0,000	1,015	101,722	19672,089	0,005	0,000	1,015	101,722
Strategy 3									
Pat. ¹¹	Input Data	DC	VS	HD	Max Dist. ¹²	wHD	ASD	UCID ^[1]	GS ^[2]
1	Non-registered images	0,000	0,000	Requested region is (at least partially) outside the largest possible region				145,805	--
	Ddf	0,339	0,891	63,303	9105,321	0,006	6,016	56,463	-6,574
	Image Mask	0,252	1,199	64,280	9183,541	0,006	7,232	30,228	-8,185
2	Non-registered images	0,000	0,000	Requested region is (at least partially) outside the largest possible region				--	--
	Ddf	0,407	0,802	44,805	15233,982	0,002	16,072	--	-16,469
	Image Mask	0,446	0,663	40,506	13772,361	0,002	14,043	--	-14,262
3	Non-registered images	0,000	0,000	Requested region is (at least partially) outside the largest possible region				166,392	--

	Ddf	0,684	0,468	51,127	4743,274	0,010	2,926	76,704	-2,720
	Image Mask	0,482	0,968	59,524	6082,699	0,009	5,190	34,527	-5,685
4	Non-registered images	0,000	0,000	Requested region is (at least partially) outside the largest possible region				156,938	--
	Ddf	0,272	1,079	84,176	10893,605	0,007	7,7056	60,770	-8,519
	Image Mask	0,244	1,200	88,654	11612,0039	0,007	8,636	22,435	-9,599
5	Non-registered images	0,000	0,000	Requested region is (at least partially) outside the largest possible region				227,906	--
	Ddf	0,266	1,078	105,094	14490,194	0,007	10,271	51,139	-11,090
	Image Mask	0,133	1,436	107,611	15027,701	0,007	12,796	45,482	-14,106
6	Non-registered images	0,000	0,000	Requested region is (at least partially) outside the largest possible region				164,460	--
	Ddf	0,245	0,874	77,529	5696,268	0,013	6,339	84,298	-6,981
	Image Mask	0,180	1,163	80,975	6380,098	0,012	7,877	39,422	-8,872
7	Non-registered images	0,000	0,000	Requested region is (at least partially) outside the largest possible region				--	--
	Ddf	0,357	0,810	100,218	14138,134	0,007	6,728	--	-7,188
	Image Mask	0,230	1,204	103,406	14463,244	0,007	8,531	--	-9,512
8	Non-registered images	0,000	0,000	Requested region is (at least partially) outside the largest possible region				197,755	--
	Ddf	0,377	1,205	65,372	11765,977	0,005	8,522	63,048	-9,355

	Image Mask	0,303	1,372	67,791	12632,155	0,005	10,269	80,935	-11,343
9	Non-registered images	0,000	0,000	Requested region is (at least partially) outside the largest possible region				--	--
	Ddf	0,384	0,581	51,618	9126,720	0,005	6,204	--	-6,406
	Image Mask	0,327	0,877	57,329	100074,159	0,000	8,177	--	-8,727
10	Non-registered images	0,000	0,000	Requested region is (at least partially) outside the largest possible region				202,240	--
	Ddf	0,256	1,253	67,798	12683,526	0,005	9,824	65,033	-10,826
	Image Mask	0,257	1,252	70,754	12727,029	0,005	9,852	57,731	-10,852